Ph.D. in Electronic and Computer Engineering
Dept. of Electrical and Electronic Engineering
University of Cagliari

Inkjet Printing of Organic Transistor Devices

Laura Basiricò

Advisor: Prof. Annalisa Bonfiglio
Co-Advisor: Dr. Piero Cosseddu
Curriculum: ING-INF/01 Electronics

XXIV Cycle
March 2012

Ph.D. in Electronic and Computer Engineering
Dept. of Electrical and Electronic Engineering
University of Cagliari

Inkjet Printing of Organic Transistor Devices

Laura Basiricò

Advisor: Prof. Annalisa Bonfiglio
Co-Advisor: Dr. Piero Cosseddu
Curriculum: ING-INF/01 Electronics

XXIV Cycle
March 2012

Dedicated to my family

Abstract

In the last two decades inkjet printing passed from the field of graphic art and newspaper industry to that of organic and flexible electronics, as a manufacturing tool, becoming a major topic in scientific research. The appeal of this kind of technology is mainly due to its low cost, non-contact and additive approach, which makes it surely the most promising technique over the other technologies of Printed Electronics.
The focus of this thesis is the optimization of the printing process, employing a piezoelectric Drop-on-Demand inkjet printer, for the realization of organic transistors on highly flexible plastic substrates, and their development in more complex systems for sensing applications. Indeed, all the devices realized have been investigated by means of electrical measures and spectroscopic techniques, in order to assess their performances and, consequently, to evaluate the reliability of inkjet printing as fabrication technique for such devices.
In the first chapter a general introduction to the field of Printed Electronics, with particular focus on inkjet printing technique, is given.
The second chapter provides informations concerning the fabrication/characterization procedure followed, including a detailed description of the inkjet printing technology used, a report about the main physical and chemical properties of the materials employed, the explanation of the inkjet printing procedure for each material used in this thesis (as the printing parameters optimization and the approach for the resolution of some technical issues); finally also a brief description of the experimental techniques employed in order to characterize the devices is given.
The third chapter is fully dedicated to the results concerning the fabrication and the characterization of all-Organic ElectroChemical Transistors (OECTs), while in the fourth chapter the results about inkjet printed Organic Field Effect Transistors (OFETs) are discussed.

Finally, a brief chapter reports a summary of the main results achieved.

Keywords: inkjet printing, Organic Electrochemical Transistors, Organic Thin Film Transistors, PEDOT:PSS, TIPS-pentacene.

Sommario

Negli ultimi due decenni la stampa a getto di inchiostro é passata dall'essere uno strumento di produzione nel campo dell'arte grafica e dell'industria editoriale, al rappresentare un'innovativa tecnologia per la realizzazione di dispositivi nel campo dell'elettronica organica e flessibile, diventando cosí un importante argomento di ricerca scientifica. L'appetibilitá di questa tecnologia consiste principalmente nell'essere una tecnica a basso costo, non-contact e additiva, caratteristiche che la rendono certamente la piú promettente tra le tecnologie del settore dell'elettronica stampata.
Il fulcro di questa tesi é l'ottimizzazione del processo di stampa, svolto tramite l'impiego di una stampante a getto di inchiostro piezoelettrica Drop-on-Demand, per la realizzazione di transistor organici su substrati plastici altamente flessibili, e il loro sviluppo in sistemi piú complessi per applicazioni sensoristiche. Tutti i dispositivi realizzati sono stati caratterizzati tramite misure elettriche e spettroscopiche, al fine di stimarne le prestazioni e, di conseguenza, di valutare l'affidabilitá della stampa a getto di inchiostro per la fabbricazione di tali dispositivi.
Nel primo capitolo viene fornita un'introduzione generale sull'elettronica stampata, con una particolare attenzione alla stampa a getto di inchiostro.
Il secondo capitolo fornisce informazioni sulle procedure di fabbricazione e caratterizzazione eseguite, includendo una spiegazione dettagliata della tecnologia di stampa usata, un report sulle principali proprietá fisiche e chimiche dei materiali impiegati, la descrizione della procedura di stampa per ciascun materiale utilizzato in questa tesi (l'ottimizzazione dei parametri di stampa e l'approccio seguito per la risoluzione di alcuni problemi tecnici); infine viene fornita una breve descrizione delle tecniche sperimentali impiegate per la caratterizzazione dei dispositivi.
Il terzo capitolo é completamente dedicato ai transistor elettrochimici organici (OECTs), mentre nel quarto capitolo vengono discussi i risultati riguardanti i transistor organici

ad effetto di campo (OFETs).
In ultimo, un breve capitolo finale riassume i principali risultati ottenuti.

Parole chiave: stampa a getto di inchiostro, transistor organici elettrochimici, transistor organici a film sottile, PEDOT:PSS, TIPS-pentacene.

List of Publications Related to the Thesis

Journal articles

- **Inkjet printing of transparent, flexible, organic transistors**
  L. Basiricó, P. Cosseddu, B. Fraboni, A. Bonfiglio.
  Thin Solid Films 520 (2011) 1291-1294.

- **Electrical characterisctics of ink-jet printed, all-polymer electrochemical transistors**
  L. Basiricó, P. Cosseddu, A. Scidá, B. Fraboni, G.G. Malliaras, A. Bonfiglio.
  Organic Electronics 13 (2012) 244-248.

- **Investigation of the working regime of ink-jet printed, all-PEDOT:PSS electrochemical transistors**
  L. Basiricó, M. Demelas, E. Scavetta, G. Malliaras, A. Bonfiglio.
  In preparation.

- **Investigation on inkjet printing conditions of TIPS-pentacene as active layer for organic thin film transistors**
  L. Basiricó, P. Cosseddu, B. Fraboni, A. Scidá, S. Milita, A. Bonfiglio.
  In preparation.

Proceedings of international conferences with acceptance based on full paper submission

- **Inkjet Printed Arrays of Pressure Sensors Based on All-Organic Field Effect Transistors**
  L. Basiricó, P. Cosseddu, A. Bonfiglio, R. Neelgund, H. Tyrer.
  EMBC 2010 Conference Proceeding.

- **Matrices of inkjet printed OFETs for the realization of artificial robotic skin**
  P. Cosseddu, **L. Basiricó**, A. Loi, S. Lai, P. Maiolino, E. Baglini, S. Denei, F. Mastrogiovanni, G. Cannata, M. Barbaro, A. Bonfiglio.
  Material Research Society (MRS) Fall Meeting 2011, Conference Proceeding. Submitted

Proceedings of international conferences with acceptance based on abstract submission

- **Ink jet printing of PEDOT:PSS aqueous suspension for the realization of Organic Electrochemical Transistors as biological and chemical sensors**
  L. Basiricó, A. Bonfiglio.
  III National School on molecolar materials for photonic and electronic applications Nanostructured Hybrid Systems based on organic, inorganic and biological molecules: materials and devices 2009, Abstract.

- **Flexible and transparent all organic Thin Film Transistors, realized by means of inkjet printing**
  L. Basiricó, P. Cosseddu, A. Bonfiglio.
  TCM 2010 3rd International Symposium on Transparent Conductive Materials, 2010, Abstract.

- **Matrices of Inkjet Printed OFETs for the Realization of Artificial Robotic Skin**
  A. Loi, **L. Basiricó**, P. Cosseddu, S. Lai, M. Barbaro, A. Bonfiglio, E. Baglini,

S. Denei, P. Maiolino, F. Mastrogiovanni, G. Cannata.
Human-Robot Interaction (HRI) 2012 Workshop on Advances in Tactile Sensing and Touch based HRI, Extended Abstract. Submitted

- **Design, fabrication and test of arrays of piezoelectric transducers for robotic tactile sensors**
  L. Seminara, L. Pinna, M. Valle, **L. Basiricó**, A. Loi, P. Cosseddu, A. Bonfiglio, A. Ascia, M. Biso, A. Ansaldo, D. Ricci, G. Metta.
  Human-Robot Interaction (HRI) 2012 Workshop on Advances in Tactile Sensing and Touch based HRI, Extended Abstract. Submitted

Contents

List of Figures

LIST OF FIGURES

List of Tables

LIST OF TABLES

1

Overview on printing techniques for electronics

In this first chapter a general introduction to the field of Printed Electronics, with particular attention on inkjet printing techniques, is given. The first section is focussed on the description of different kinds of printing techniques with the exception of inkjet printing, which is discussed in the second section. Finally the third section reports an overview of the printed electronics applications.

1.1 Printed Electronics

The term *Printed Electronics* (PE) refers to a set of printing technologies used to fabricate a wide range of electronic devices employing many materials. In last few years printing technologies, e.g. flexography, soft lithography, screen, gravure and inkjet printing, gained the attention of electronic manufacturing industries thanks above all to their low-cost, high volume and high-throughput production of electronic components or devices which are lightweight and small, thin and flexible, inexpensive and disposable. Generally printing methods consist of the patterning of thin or thick structures on flexible or rigid substrates, depositing ink layer by layer. The essential requirement for printed materials is their processability in liquid form (solution, dispersion or suspension) in order to constitute an "ink", which can be based both on organic and inorganic materials. Inorganic-based inks typically contain metallic (e.g. copper, gold, silver, aluminium) nano-particles dispersed in a retaining matrix and are employed for RFID

tags, passive components and transistor electrodes fabrication. On the other hand as organic materials (conductors, semiconductors and dielectrics) are easily processable in liquid phase, printing technology has become the most promising and interesting fabrication technique in the field of Organic Electronics. Organic inks based on high conductive polymers are typically used for the realization of batteries, electromagnetic shields, capacitors, resistors and inductors, while inks based on organic semiconductors are employed as active layers of active devices as Organic PhotoDiodes (OPDs), Organic Light Emitting Diodes (OLEDs), Organic Field-Effect Transistors (OFETs), organic solar cells, sensors and electrochromic displays. In section 1.3 a brief overview on PE applications in the Organic Electronics field is reported. It should be noted that PE is not a substitute for conventional silicon-based electronics, which concerns the so-called "high-end electronics", characterized by high density integration and high switching speed performances, but it paves the way for the developing of new low-cost and high volume production markets, which does not require the high performances reached by means of conventional electronics. In particular, the main advantages of PE compared to traditional inorganic electronic manufacturing techniques are: the low production costs (even if the developing of optimal inks is still a challenge and requires investments on research), the low temperature of the process, which allows the employment of flexible substrates as plastics foils or paper, the simpler fabrication technique and the possibility of easily covering large area surfaces (see Figure 1.1) [1][3]. The reduction in manufacturing costs in PE technologies is due to several features. First of all PE processes allow reduction in material waste: they are based on an additive process i.e. the inks are selectively deposited only on the areas of interest (especially in inkjet printing technology where only few picoliters of material are ejected), in contrast with more conventional fabrication techniques, as photolithography, which are subtracting processes. In subtracting processes, in fact, usually a homogeneous layer of material is deposited over the whole substrate and the final pattern is achieved by subtracting excess material. The photolitographic patterning process, for example, consists of the deposition of an uniform layer of material over the substrate (by means of sputtering, thermal evaporation or chemical vapour deposition), a subsequent deposition of a layer of photoresist all over the structure (usually by means of spin casting), then the patterning of the photoresist by photolithography, the selective etching for removing the excess material and finally the etching of the photoresist. As showed in Figure

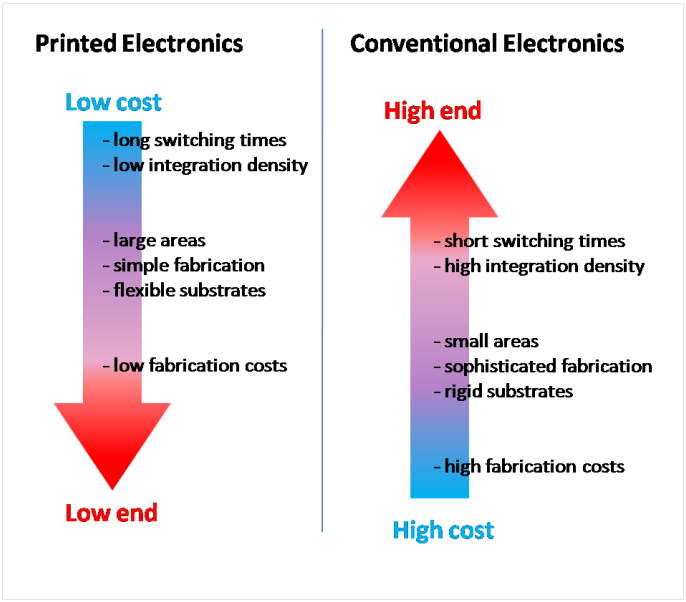

Figure 1.1: Comparison between the main features of printed electronics and conventional silicon-based electronics. They can be considered as complementary technologies. [1][2]

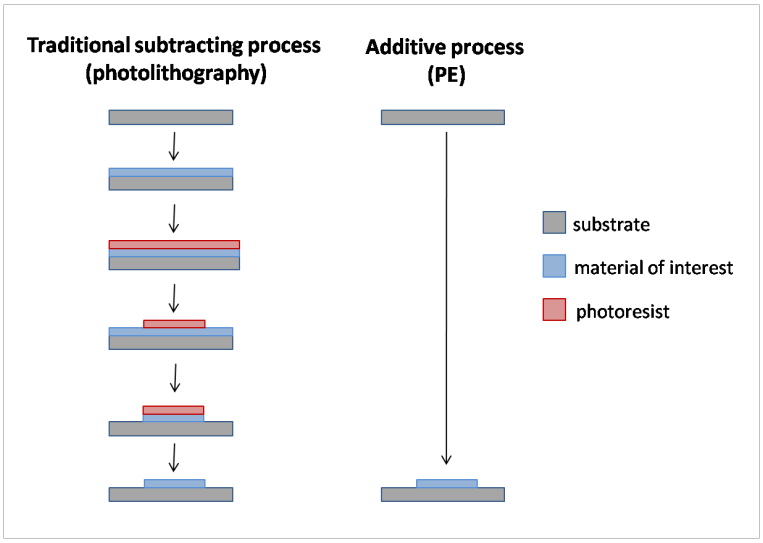

Figure 1.2: Traditional subtracting patterning technique steps compared to the additive printing ones.

1.2, compared to traditional techniques, printing not only allows limitation in material waste but also significantly reduces the manufacturing steps thanks to controlled direct printing of the desired pattern on the substrate. Moreover it doesn't require the employment of high resolution masks, generally very expensive, nor of special processing conditions as cleanroom or darkroom. A grater range of materials can be deposited by this technology, as, for example, bioactive fluids, which cannot tolerate exposure to photolithography and etching chemicals present in conventional techniques [4].
PE technologies can be divided in *contact techniques* (e.g. flexography, offset lithography, gravure and screen printing), in which the printing plate is in direct contact with the substrate, and in the *non-contact techniques*, as inkjet printing, where, conversely, the substrate gets in contact only with the inks. In this section the main features of some contact and non-contact printing techniques are discussed while a separate section is fully dedicated to inkjet printing.

1.1.1 Contact printing techniques

The main advantage presented by contact printing techniques is surely the high throughput and the ultra-low cost efficiency due also to possibility of employment in roll to roll (R2R) printing processes, which makes them suitable for mass customization and constitutes the reason why such technologies are actually the dominant printing processes in PE industries. However, the direct contact with the surface implies several limitations both in resolution and in the range of materials used (substrates, inks, solvents). Some of most diffused contact printing techniques are briefly described below, a more exhaustive review can be found in bibliography.

Flexography

A flexographic printing system is based on a set of rotary cylinders schematized in Figure 1.3. One of the cylinders is characterized by relieves (printing plate) that reproduce the positive image of the pattern to be transferred onto the substrate. Ink is applied on the printing plate by means of an engraved cylinder called anilox, in which the amount of released ink is controlled by the engravings i.e. a series of small cells or walls which can transfer a precise amount of ink to the printing plate, while the excess ink is removed by a doctor blade before printing. Finally, when the printing plate rolls over the substrate, the ink is deposited according to the desired pattern by the pressure of the

impression cylinder [1][5]. The main disadvantage of such technique is the low precision and the low resolution achievable mainly due to the *halo effect*, i.e. the spreading of the ink outside the image area, caused by the compressive pressure between the printing plate and the impression cylinder. On the other hand the flexography process allows the employment of a wide range of inks. Moreover, the softness of the printed plate and the fast-drying inks which can be used makes it suitable for printing on plastics and foils [3][5].

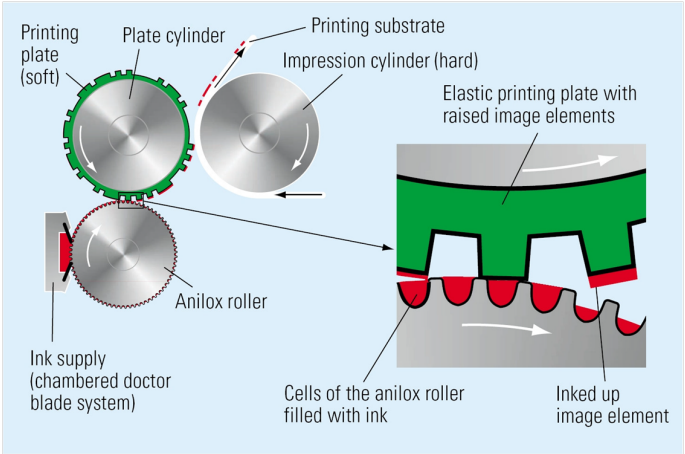

Figure 1.3: Schematic of flexographic printing system. [5]

Gravure printing

Gravure printing is based on the opposite principle respect to the flexography process in terms of wetting procedure of the printing plate, called in this case rotogravure plate. On the rotogravure plate the pattern is etched by laser or photolithography in order to hold the ink inside the grooves. The ink can be transferred to the rotogravure plate by means of an additional cylinder or directly from the ink supply. Finally the pattern is printed on the substrate through the pressure between the printing plate and the impression cylinder exactly as in flexography. This method allows very high printing speed and quality. Also, the wide range of materials and inks which can be used (e.g. toluene, xylene and alcohol based inks), makes it suitable for electronic application. In fact, despite the typical gravure printed output consists of small dots and thus it does not allow printing of conductive paths, by engraving linear structures

on the rotogravure plate it is possible to employ such technique or fabrication of RFID antennas and OLEDs; the term *intaglio* is used in this case. [3][5]

Soft lithography

Soft lithography indicates a group of contact printing techniques which utilize an elastomeric stamp, moulded from a master template, to transfer the desired pattern from the stamp to the substrate. Usually the master is prepared using either e-beam or photolithography; once it has been realized, several stamps can be moulded from it and each stamp can be used several times without degradation. The stamp is made of elastomeric polymers, as polyurethane, polyimide and most commonly of poly(dimethylsiloxane) (PDMS). Once PDMS (or, in general, the elastomer) is mixed with a catalyst or curing agent (i.e. a mixture of a platinum complex and copolymers of methylhydrosiloxane and dimethylsiloxane), the resulting compound is poured over the master. Then, it is heated at elevated temperatures and the liquid mixture becomes a solid, cross-linked elastomer in a few hours. After thermal treatment, the PDMS stamp can be pealed off from the master and will consist on a fully flexible and transparent elastic stamp reproducing the negative of the master pattern [7][8][9]. Finally the material of interest is deposited on the stamp and transferred on the substrate. The possibility to realize micro and nano-structures by means of this technique relies in the intrinsic property of PDMS elastomer to form a conformal contact with the surface which it has been brought into contact to. Conformal contact permits, in fact, the complete adaptation of a soft polymer layer to a rough surface (see Figure 1.4) [10]. Soft lithography printing techniques provide a cost-effective solution for patterning over large areas with a resolution capable to reach that of extreme ultraviolet lithography of about 20 nm. On the other hand, they cannot reach the economic advantage due to the rapid throughput of roll-to-roll printing techniques as flexography and gravure printing described above.

1.1.2 Non-contact printing techniques

As already mentioned, in non-contact printing techniques the substrate is in contact only with materials which make up the device and this lowers the risks of damage and contamination. The non-contact patterning method also permits to obtain accurate alignment with patterns already on the substrate, which is an indispensable functionality to pattern multilayered devices. Conversely contact techniques could encounter

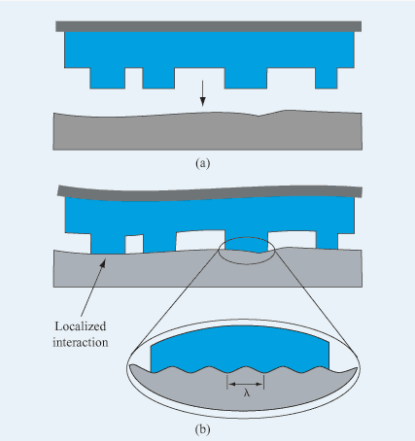

Figure 1.4: Conformal contact between a stamp and a hard substrate. (a) Stamp adapts its protruding zones to (b) the macroscopically uneven substrate and (b, inset) its microscopic roughness, whereas recessed zones do not touch the substrate. [11]

difficulties in completing multilayered devices [12]. In other words, even if some non-contact methods, as inkjet printing, are 2D deposition techniques, it is possible to easily build 3D structures additively by printing multiple layers of the same or different materials, after taking into consideration post processing and drying requirements of the deposited films and the compatibility between different solvents contained in the used inks [4]. Furthermore, the absence of direct contact between the printhead and the support together with the low processing temperature required by this kind of technologies, makes them compatible with various kinds of surfaces such as glass, silicon, metals, rubber, plastics (e.g. flexible polyester films, which can be irreversibly damaged and deformed if subjected to thermal stresses and high temperature processes) and, generally with contact-sensitive substrates. Also, non-contact techniques are typically digitally implemented i.e. a physical master of the to-be-printed image is not needed. Instead, the image is only represented as information in a digital form and every print can be different without an additional cost [1].

Laser Direct Writing

Laser Direct Writing is the name used to indicate a group of non-contact printing techniques (hereafter only the most common of these are shortly described but a wide review has been reported by Hon et al.[15]) which permits the realization of 1D to

3D structures by laser-induced deposition of metals, semiconductors, polymers, ceramics, without using masks of lithographic methods. Materials can be deposited from gaseous, liquid and solid precursors. *Laser Chemical Vapour Deposition* (LCVD), for example, employs an argon ion laser focussed by means of an optical microscope lens to a spot of less than 2 μm onto a substrate target. The process takes place in a reaction chamber filled with a gas precursor containing the element to be deposited. When the laser beam scans over the substrate, this is heated up causing the dissociation of gas precursor and, consequently, the deposition of a thin solid layer onto the surface. The repetition of scans permits the deposition of multilayered structures. This technique involves higher costs than other printing methods due to the employment of sophisticated equipments e.g. reaction chamber associated with vacuum equipment. Also, it is

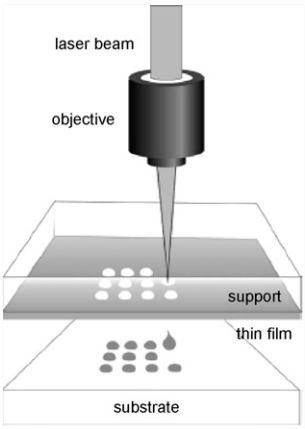

Figure 1.5: LIFT experimental setup.

limited by the gas phase because it allows the deposition only of volatile metal-organic and inorganic materials. Moreover it is no possible to deposit on organic substrates. In *Laser-Enhanced Electroless Plating* (LEEP), instead, the substrate is submerged in a chemical solution which contains the metallic ions required for the deposition. As in LCVD, a laser beam is focused onto the substrate causing a local temperature rise. The high temperature decomposes the liquid leading to the deposition of a metallic layer on the substrate surface. A subsequent electroplating o electroless plating process can be used to increase the thickness of the layer deposited. This technique does not allow the creation of 3D structures. Finally *Laser-induced forward transfer* (LIFT) is based on the transfer, by means of a laser beam, from an optically transparent support

onto a parallel substrate placed about 100 μm below it (see Figure 1.5). The laser beam vaporizes a small amount of material located on the support which recondenses on the substrate. Various kinds of materials can be deposited such as metals, oxides and polymers forming both 2D and 3D structures, but with the limitation of printing only on to flat substrates parallel to the material support.

Aerosol printing

Aerosol printing technology, also called spray printing, has been developed by Optomec [17] under the market name of M3D (Maskless Mesoscale Material Deposition). The Aerosol printing process, described schematically in Figure 1.6, consists of three different steps: first the ink is placed into an atomizer, where it aerosolizes in liquid particles. Particles with a diameter ranging between 20 nm and 5 μm can be created depending on the ink viscosity. The inks which can be employed using such techniques are solutions and nanoparticle suspensions and can be based on metals, alloys, ceramics, polymers, adhesives or even biomaterials. After a dense aerosol of particles is created in the atomizer, it is transported into the deposition head by a nitrogen flow. Finally the aerosol is focussed by means of a flow guidance deposition head and thus deposited on the substrate. This is a highly versatile technique because of the possibility of writing

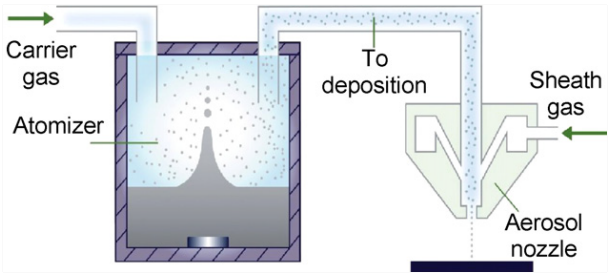

Figure 1.6: Schematic of aerosol jet printing system. [15]

feature size through three order of magnitude. In fact it has a wide range of application, e.g. the realization of displays, thin film transistors, dielectric passivation layer and solar cells [15][17]. Such kind of system can also print over complex conformal surfaces (3D Printed Electronics), since it is possible to control position in z-direction of the writing head over substrate during printing process, and will be thus used to develop integrated sensor, MID circuit and smart structure applications. An example of 3D

aerosol printing is shown in Figure 1.7: antennas or RFID, some conductive tracks and two interdigitated sensors have been printed onto a 3D plastic substrate [18].

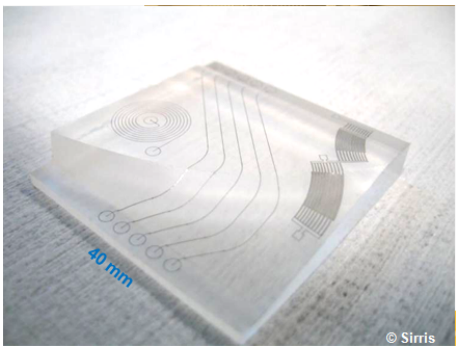

Figure 1.7: Antennas or RFID, some conductive tracks and two interdigitated sensors have been printed onto a 3D plastic substrate. [18]

1.2 Inkjet printing

The inkjet printing process involves the ejection of a fixed quantity of a liquid phase material, usually called ink, in form of droplets from a chamber through a nozzle. The ejected drops fall onto a substrate under the gravity force and air resistance to form a pattern. The solidification of the liquid may occur through the evaporation of a solvent, chemical changes (for example the cross-linking of polymers) or crystallization. Often some post-processing treatments are required, as thermal annealing or sintering, i.e. the melting of metallic nanoparticles in metallic inks, achieved by heating to elevated temperatures [13][15]. Inkjet printers usually work in two different most commonly used operation modes: *Continuous* or *Drop-on-Demand* (DOD). The differences between continuous and DOD inkjet technologies involves several features. First of all, the material throughput which a single nozzle can sustain is very different: in a continuous inkjet system a higher printing speed is achievable since the . On the contrary DOD technology allows higher placement accuracy and smaller drop size leading to higher resolution of printed patterns. Also, since the presence of a recirculation system in continuous inkjet (see Figure 1.8) constitutes a huge ink damage risk, such a technology is thus not suitable for applications that involve sensitive and/or expensive inks. More details on both the technologies are reported in the subsections 1.2.1, 1.2.2

and 1.2.3. Finally, some technical information about the inkjet printer employed in the manufacturing of the devices presented in this thesis are reported.

1.2.1 Continuous inkjet printing

In Figure 1.8 a typical continuous-mode inkjet system is shown: ink is pumped through a nozzle forming a continuous jet. Usually acoustic waves generated by the vibration of a piezoelectric crystal cause the breakdown of the flow of ink in single drops at regular intervals, but a stream of liquid emerging from an orifice is intrinsically unstable and will tend to break down into drops also under the only effect of surface tension [15] (Rayleigh instability phenomenon [19][20] showed in Figure 1.9). Once formed, the drops cross an electrostatic field acquiring an electrostatic charge as they leave the stream. The charged drops are then directed to the desired location on the substrate by an electrostatic deflection field. Uncharged drops are collected by a catcher and enter in a ink recirculation system. The name *continuous* refers to the continuous formation

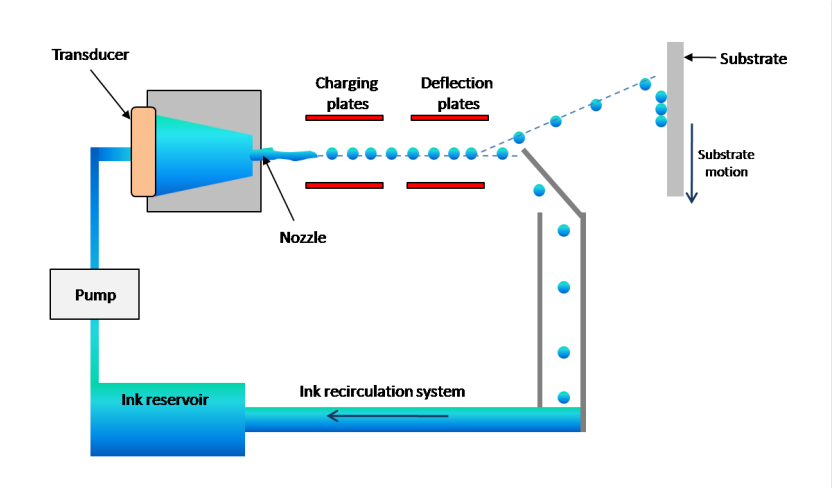

Figure 1.8: Schematic of continuous inkjet system.

of droplets, which are then directed along trajectories varied by the amount of charge applied [21][22]. The pattern is thus created by the impact of the deflected droplets on a moving substrate. Typically, a commercial continuous inkjet printing system requires high drive frequency (∼75 kHz), has a jet velocity of 20 m/s, a jet diameter of 60 μm and drop size of about 120 μm [15]. It is mainly employed in high-speed graphical

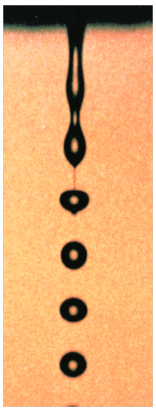

Figure 1.9: A jet of water breacking up due to Rayleigh instability. [22]

application, as textile printing [21].

1.2.2 Drop-on-Demand inkjet printing

In such technology the system ejects an ink droplet from a reservoir through a nozzle only when a voltage pulse is applied to a transducer, i.e. only when the ejection is required. The technology is thus called *Dop-on-Demand* (DOD). In Figure 1.10 a simple schematic of a DOD inkjet system is shown, while a digital photo of a DOD inkjet device is reported in Figure 1.11. The production of drops by means of an electromechanical pressure was observed for the first time by Hansell in 1950 [23]. Commonly, two different kinds of actuators are used, a thermal transducer and a piezoelectric transducer:

Thermal DOD inkjet printing

In a *thermal DOD* inkjet printer (also called bubble-jet), the ink droplet is ejected by means of a heating resistor located inside each nozzle. In more detail (see Figure 1.12), when a huge current is passed through the resistor, the Joule effect causes the heating of the resistor and subsequently of the ink surrounding it. Thus, the ink inside the nozzle starts to vaporize, a growing vapour bubble is generated and the increasing pressure forces the ink through the nozzle. As the current is suddenly cut off, the bubble breaks and the pressure decreases, causing the detachment of the droplet from the nozzle [24].

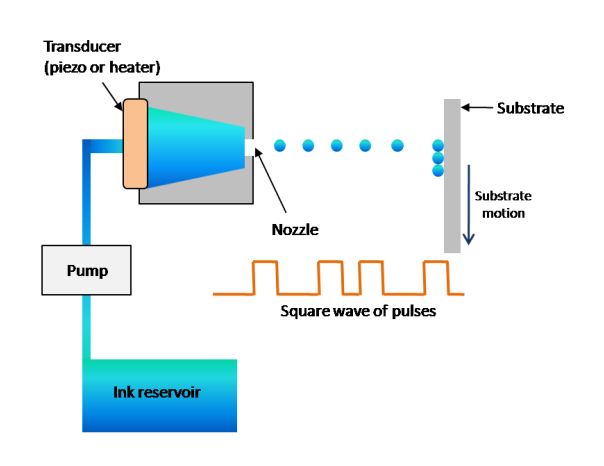

Figure 1.10: Schematic of Drop on Demand inkjet system.

Figure 1.11: Digital photo of a DOD inkjet device. [22]

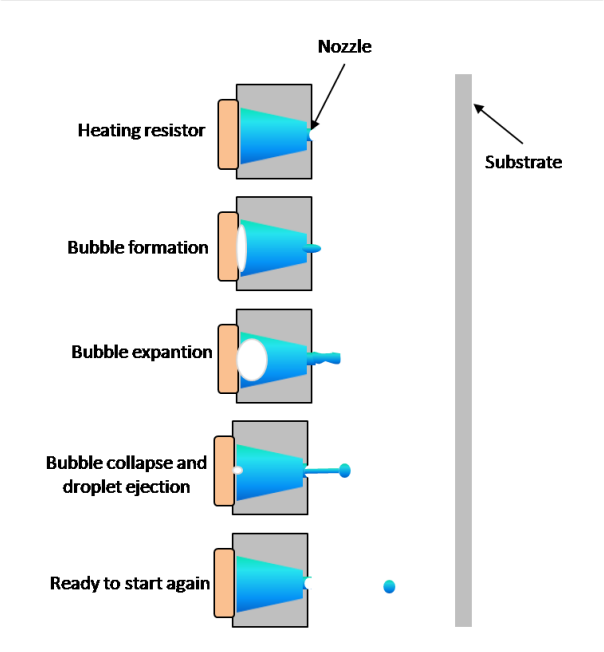

Figure 1.12: Schematic of the drop formation mechanism in a thermal DOD inkjet system.

Piezoelectric DOD inkjet printing

In *piezoelectric DOD* systems the ejection of the droplet is caused by the mechanical deformation of a piezoelectric material under the application of an electric field. The phases of the drop formation mechanism in such kind of system are shown in Figure 1.13: before the printing process starts, the ink chamber is depressed by applying an appropriate bias to the piezoelectric crystal in order to prevent the ink from falling down from the nozzle (Start or Standby phase). A zero voltage is then applied to the piezo, which is thus undeformed in its relaxed position, leading to a flow of fluid in the ink chamber from reservoir. In the next phase the chamber is strongly compressed causing the drop ejection from the nozzle. Finally the chamber is brought back to the initial decompressed condition to pull back the ink in the chamber and to prepare the system for the next ejection [25].
Since thermal DOD involves the vaporization of the ink inside the chamber, it requires the use of volatile solvent-based ink. This restriction is not present in piezoelectric DOD, that is therefore more versatile than the thermal one. It should be noted that

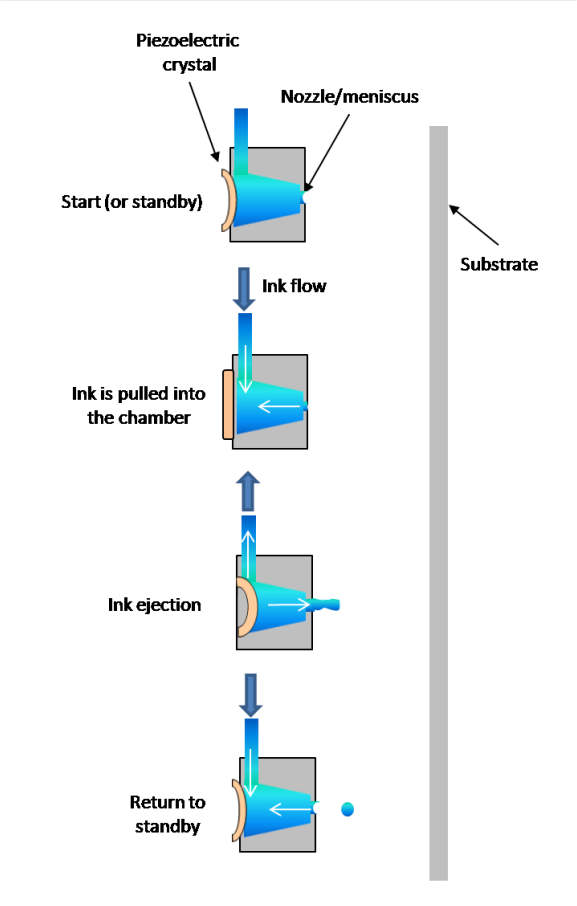

Figure 1.13: Schematic of the drop formation mechanism in a piezoelectric DOD inkjet system.

also other DOD techniques exist, as the *electrohydrodynamic DOD* jet printing (see bibliography for further informations [14][26]).

1.2.3 Drop formation and impact phenomena

The physical properties of ink, as its *viscosity* and *surface tension* constitute the most crucial features of inkjet printing technology. The surface tension of a fluid is strictly related to the shape of the drop as it is jetted from the nozzle. Typical values of surface tension span from 28 mNm^{-1} to 350 mNm^{-1} [21]. At the same time, viscosity values lower than 20 mPas are suitable in order to allow droplet ejection from the nozzle. The relation between the viscous forces to inertial and surface tension forces is expressed by the dimensionless *Ohnesorge number (Oh)* [27]:

$$Oh = \frac{\sqrt{We}}{Re} = \frac{\eta}{\sqrt{\rho D \sigma}} \tag{1.1}$$

where: η, ρ and σ are the viscosity, density and surface tension of the ink and D is a length parameter, usually the nozzle diameter. Re is the *Reynolds number* and We is the *Weber number*, defined respectively as:

$$Re = \frac{\rho V D}{\eta} \tag{1.2}$$

$$We = \frac{\rho V^2 D}{\sigma} \tag{1.3}$$

where V indicates the velocity. The Reynolds number is the ratio of the inertial force and the viscous force, while the Weber number is the ratio of inertial force to surface tension (both Re and We are dimensionless). Thus, the Ohnesorge number defines the ratio between viscous force and the square root of the product of inertial force and surface tension. Often, authors refer to the inverse of Ohnesorge number: $Z = Oh^{-1}$. In the earliest studies of *drop formation* in a DOD system, Fromm[28] predicted that the drop formation would have been guaranteed only for $Z > 2$. Later Reis and Derby[29] indicated the range $1 < Z < 10$, where the lower limit is controlled by ink viscosity i.e. for $Z < 1$ viscous dissipation in the fluid prevents drop ejection, and the upper limit is related to unwanted satellite drops formation rather than a single drop in ejection process [3][30]. In Figure 1.14 a typical satellite drop formation, reported by Kawase et al.[31], is shown. The Z range founded by Reis and Derby was later confirmed by subsequent studies [32]. It should be noted that the drop

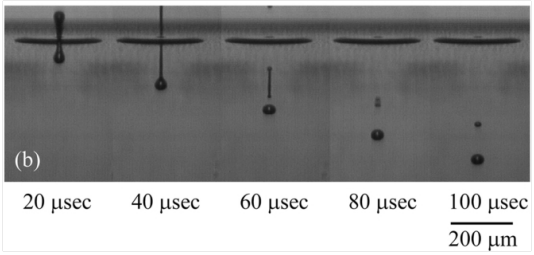

Figure 1.14: Stroboscopic image of satellite drop formation of poly(9,9'-dioctylfluorene) solution in xylene. [31]

formation dynamics for *polymer-based inks* differs from that of ordinary Newtonian fluid described above. Because of the increase of viscoelastic forces, when adding even a small amount of polymer to an ink, the ejection of a droplet involves the formation of a filament connecting the ejected droplet to the nozzle of a printer (Figure 1.15). The lifetime and the length of the filament increase with the concentration and the

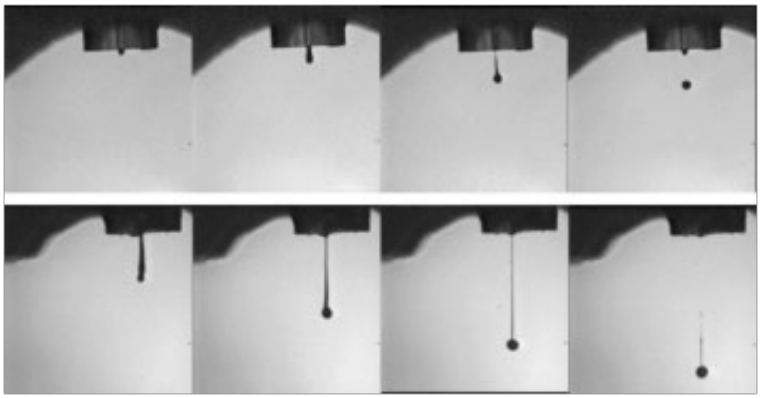

Figure 1.15: (top) Stroboscopic images of the formation of a Newtonian drop. (bottom) Effect of adding a small amount of polymer: the filament connecting the ejected drop and the nozzle is clearly visible and the time for the ejection strongly increases. [21]

molecular weight of the polymer as shown in Figure 1.15: normally the filament becomes a tail which breaks up from the main drop along its axis forming a satellite drop. As the concentration or molecular weight of polymer increase, only a few satellite drops occur; with a further increase, droplets without satellites are formed; finally if the concentration/molecular weight of polymer is higher than a certain value, the capillary force is not able to break the filament, which forced the drop to retract to the nozzle.

De Gans et al.[33] suggested that the micro-rheological explanation for the filament

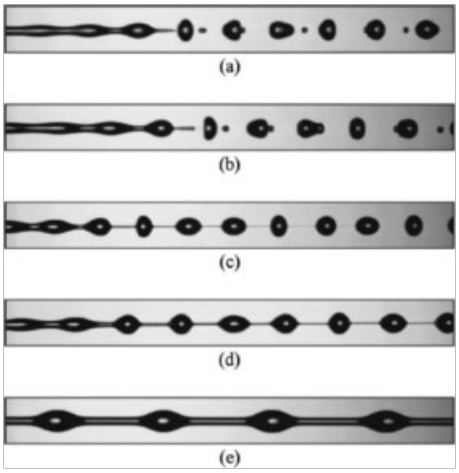

Figure 1.16: Pictures showing the influence of polymer concentration and molecular weight on the drop formation dynamics: (a) glycerol/water. (b) 0.3%100000 poly(ethylene oxide). (c) 0.1%300000 poly(ethylene oxide). (d) 0.05%1000000 poly(ethylene oxide). (e) 0.043%5000000 poly(ethylene oxide). [21]

formation is the sudden transition of the polymer chain from a coiled to a stretched structure (see Figure 1.17). This transition can be controlled by another dimensionless parameter, the *Weissemberg number*, defined as:

$$Wi = \dot{\xi}\tau \tag{1.4}$$

where ξ is the elongation rate and τ the elongation time of the filament. At $Wi = 0.5$ the transition occurs. Also the study of possible *drop impact effects* when the ink strikes on a dry surface becomes a key element in order to optimize printing performances, above all in electronic inkjet application, where usually the lateral resolution of printed structures represents a critical feature. The fluid impact phenomena, widely reported by Yarin [34] can be numerous, because the variables involved are numerous too: the drop velocity, its direction with respect to the substrate, the drop size, the ink properties mentioned above, the wettability and the roughness of the substrate and the nonisothermal effects (e.g. solidification and evaporation) may affect the drop impact on the substrate. Six possible drop impact phenomena, reported in Figure 1.18, have been investigated by Rioobo et al. [35] when a droplet strikes a solid dry surface. Four development phases of the diameter *spreading* of a drop onto a substrate (top line of

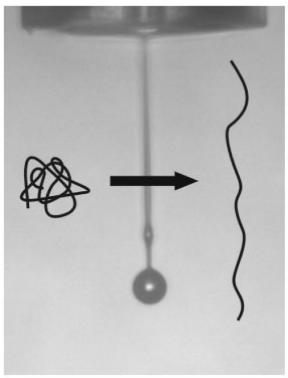

Figure 1.17: Coil to stretch transition of the polymer chain suggested as an explanation for the formation of filament in polymer-based inkjet by de Gans et al.. [33]

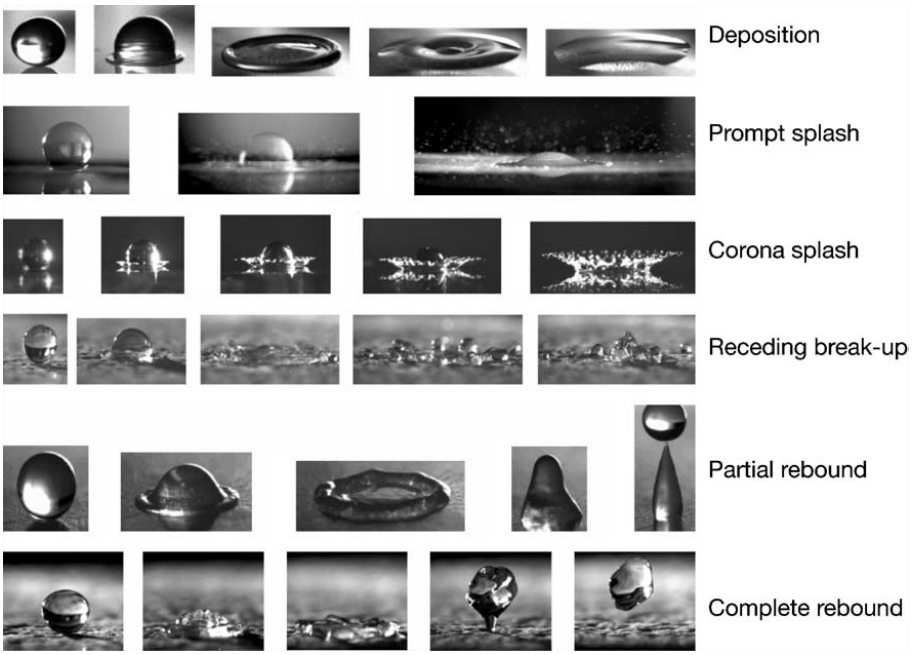

Figure 1.18: Morphology of drop impact on a dry surface. [34]

Figure 1.18) can be identified as reported in Figure 1.19, where in the axis t^* represents the time after impact, found using the drop velocity V and the drop initial diameter D ($t^* = Vt/D$), while d^* is the drop diameter (*spreading factor*), defined as the ratio between the contact zone diameter and D. Both t^* and d^* are non-dimensional parameters. In the first phase, the *kinematic phase*, the spreading factor increases according

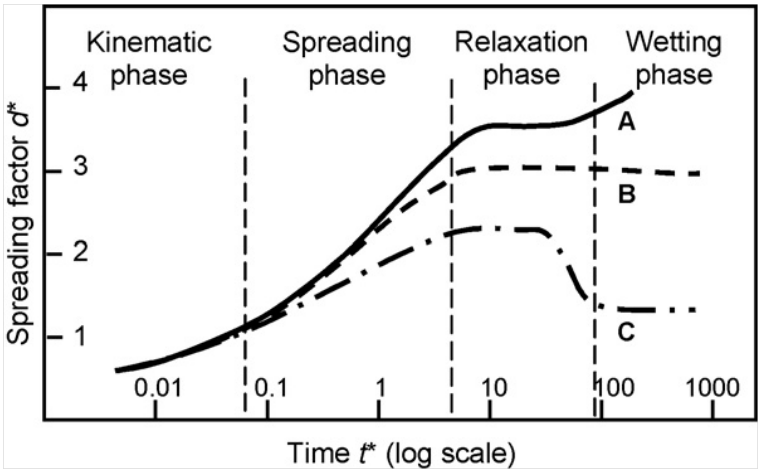

Figure 1.19: Phases of the drop spreading with time on to a solid surface. Curve A refers to a wet surface, curve C to a poorly wet substrate and curve B represents an intermediate case. [15][35]

to the power law $d^* \sim t^{*1/2}$, depending only by the drop velocity and the drop initial diameter. The next phase, called the *spreading phase*, is characterized by a constant increase of d^* with t^*. At the beginning of this phase ($t^* \sim 0.1$) the viscosity of the fluid strongly affects the spreading: the lower is the viscosity the larger is d^*, while the surface tension has moderate effect. Conversely, at the end of the phase ($t^* \sim 1$) the surface tension begins to affect the spreading becoming crucial in the *relaxation phase*, where the wettability of the surface and the balance between the inertial and viscous forces determine the equilibrium contact angle, thus the drop continues to expand or retract. Finally, for $t^* > 10$, if the surface is well wetted by the liquid, the drop continues to expand according to the power law $t^{*1/10}$ [15][35]. *Splashing*, showed in the second line of Figure 1.18, is generally an unwanted effect, especially in inkjet electronic applications, where a high precision in drop placement is required. The threshold for spreading on a dry surface can be expressed in terms of another dimensionless group $K = WeOh^{-2/5}$,

depending on the roughness of the surface $R = (roughness\ amplitude)/D$. It has been found [36] that splashing occurs if:

$$K > 649 + 3.76R^{-0.63} \tag{1.5}$$

Qualitatively, splashing is favoured by large drops size, high velocity, low surface tension and viscosity and high roughness of the substrate [15]. If the drop impacts very fast on a rough surface, tiny droplets may detach from the main drop resulting in the *corona splashing*, shown in the third line of Figure 1.18. Finally, if the surface is nonwettable the *receding breakup* scenario occurs (fourth line in Figure 1.18), where the drop after the impact breaks up into a number of fingers, each of them capable to further breakup, while if the surface is superhydrophobic, *partial* or *total rebound* may occur (fifth and sixth lines in Figure 1.18) [34].

1.2.4 Advantages and challenges

Inkjet technology has recently proliferated into the area of mass production thanks to the possibility of increasing printing speed by increasing both jetting frequency to values higher than 50 kHz and the number of nozzles on a printing head. High nozzle density of nearly 200 nozzles per inch has been achieved due to the recent development of microelectromechanical systems [12][14]. Furthermore it presents all the advantages already mentioned for non-contact printing techniques, with the peculiarity of lower cost of the equipment compared to other direct writing processes. For these reasons it is surely considered the most promising technique in PE technology. Nevertheless, like every kind of microfabrication technique, inkjet printing presents some limitations and critical issues which have to be taken into consideration during deposition process in order to achieve the best printing performances. The first limit consists of the typical resolution of conventional inkjet printers, lower than the resolution required for high-performance electronic devices, as transistors. The minimum achievable resolution is determined, first of all, by the droplets size, which is limited by the diameter of the jetting nozzle and by the surface tension of the ink used. For most of the commercially available inkjet printers for electronics application, as the printer used in this work (Fujifilm Dimatix Materials Printer 2800), it is difficult to reduce the droplet volume below 1 pL [14]. Another feature which strongly affects resolution is the interaction between the ink and the substrate, in particular the *spreading* phenomena, whose theory is de-

scribed in subsection 1.2.3, and the formation of *coffee-ring-like structures* (an example is shown in Figure 1.20), an effect of the surface-tension-driven transport of solutions along a surface with an evaporating solvent [13][37]. The choice of the processing of

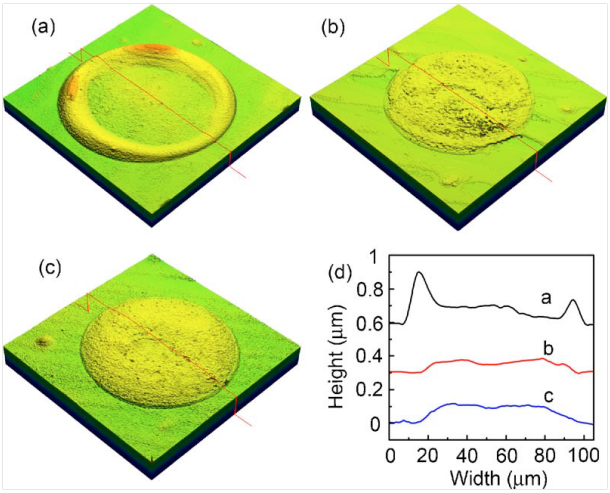

Figure 1.20: Threedimensional images reported by Kim et al.[37] for inkjet printed single dots obtained from conductive inks with varying solvent compositions: (a) 0, (b)16, and (c) 32 wt% Ethylene Glycol. (d) Corresponding two-dimensional profiles. The coffee-ring effect, clearly visible in (a), is reduced in (b) and (c) by varying the ink composition.

the ink is crucial because its physical properties, as density, viscosity, surface tension, volatility and shelf life, strongly affect the quality of printed films and the probability that undesired effects as nozzle clogging occur. In order to unclog nozzles some cleaning actions may be required (see paragraph named *Jets control* in subsection 2.1), which may cause material and time waste and sometimes permanent damage of nozzles. Also the compatibility of different inks used in multilayered structures must be considered in order to avoid redissolution, resuspension, or remelting of each previously deposited layer of ink in the new printed layer and thus to obtain uniform and uncontaminated layers [6]. In addition, different inks require different post-processing treatments as sintering, annealing or simply drying in air, which could change the morphology and the uniformity of the printed pattern and extend manufacturing time [4]. The optimization of the inks and of the substrate treatment processes thus constitutes the main research challenge in order to achieve improvements in resolution and repeatability of inkjet printed patterns and devices.

1.3 Applications of printed electronics

This section consists of a review of the most common applications of printed electronics technologies, with special attention to inkjet printing. These are very numerous and this section does not have to be considered complete nor exhaustive. The interested reader may refer to the bibliography for further informations. It should also be noted that a review about the employment of printing techniques for the realization of Organic Thin Film Transistors will be reported in chapter 4, where the results achieved in the course of my research activity regarding such devices are discussed.

1.3.1 Solar Cells

Despite the technical improvements in silicon photovoltaic solar cells industry has lowered the cost for the power generation from $\$80/W$ to $\$3/W$ so far, it is still ten times high as that of traditional fossil fuel-based energy sources. For this reason in recent years the employment of more cost effective solution processable materials such as organic small molecules and polymers in photovoltaic devices has become very attractive. By using roll-to-roll printing techniques as gravure printing, or non-contact printing, printed photo voltaic (PV) cells can be realised onto flexible and soft substrate. With such methods not only organic, but also Cu-In-Ga-Se (CIGS), and CdTe PV cells have been already realized. In Figure 1.21 the digital photos of two different kinds of flexible solar cells produced by Nanosolar, a global leader company in solar power innovation, by means of roll-to-roll printing techniques are shown. Several studies, where non-

Figure 1.21: Digital photos of two kind of printed photovoltaic cells produced by Nanosolar.[1]

contact printing methods have been used, are described in literature. Steirer et al.[40] reported above the investigation of the critical parameters for both inkjet (drop spacing

and substrate temperature) and aerosol (solution flow rate and substrate temperature) deposition of PEDOT:PSS thin film as a hole transport layer on indium tin oxide (ITO) coated glass substrate. They found that after optimization of printing parameters both inkjet and spray coated devices presents efficiency values comparable to those of spin coated devices. In Figure 1.22 AFM images and local rms roughness (Ra) of a) ITO b) PEDOT:PSS spin cast on ITO c) PEDOT:PSS inkjet on ITO, and d) PEDOT:PSS sprayed on ITO are repoted. In particular inkjet printing can be also used to deposit materials for inorganic and hybrid organic-inorganic PV cells (for example CIGS-based inks are used) [13]. The present efficiency values achieved are not high enough for commercial applications but progresses made in research pave the way for the spreading of such printed PV cells.

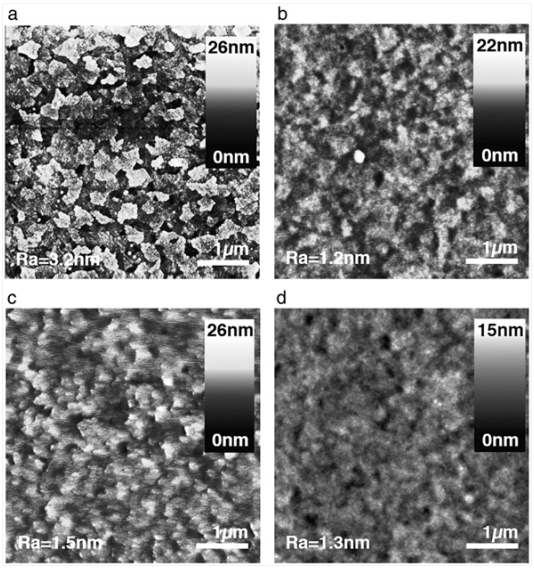

Figure 1.22: AFM images and local rms roughness (Ra) of a) ITO b) PEDOT:PSS spin cast on ITO c) PEDOT:PSS inkjet on ITO, and d) PEDOT:PSS sprayed on ITO. [40]

1.3.2 Light emitting devices

The capability of PE techniques of manufacturing devices with high throughput, low-cost on transparent and flexible substrates represents the most appealing feature for the fabrication of printed opto-electronic devices, as light emitting devices. Inkjet, screen and gravure printing are the most used technologies in fabrication of Organic Light

Emitting Diodes (OLEDs), which are Light Emitting Diodes which have an emissive electroluminescent layer composed of a film of organic compounds, already commercialized in display technology, e.g., cell phones, MP3 players and car audio systems [41]. In Figure 1.23 a digital photo of an all-printed flexible OLED demonstrator is reported. In such device the hole injection layer, made of PEDOT:PSS, was gravure printed on the top of an ITO coated PET substrate; yellow light-emitting polymer layer, poly(fluorene-alt-benzothiadiazole) (PFBT), was then gravure printed on the top of PEDOT:PSS using 2.5 wt% p-xylene solution. Finally an aluminium based ink was screen printed in order to achieve thick cathode layer on top of OLED structure [42]. Even if gravure printing is optimal for processing large, uniform areas required

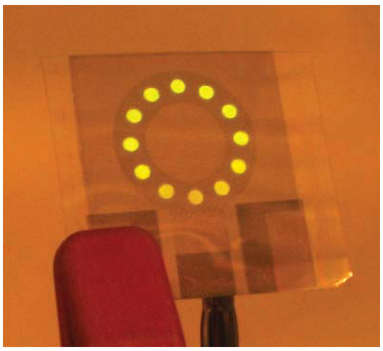

Figure 1.23: Digital photo of an all-printed flexible OLED demonstrator.[42]

for lighting applications, it is only able to fabricate monochromatic OLED displays since the realization of multicolour displays requires a micro-patterning technique, as for example inkjet printing, in order to locally deposit three differently coloured electroluminescent polymers. A schematic of an RGB multicolour display is shown in Figure 1.24 : green, blue, and red light emitting polymers are deposited by means of inkjet printing between polymer barriers (usually made of polyimide), which can be realized by means of photolithography or inkjet printing itself, on top af a conducting polymeric PEDOT:PSS layer. Both Seiko-Epson and Philips have realized OLED full-colour 130 ppi display using such kind of inkjet printed structure and nowadays, many companies invest a large amount of money in the development of printed OLEDs, including SONY, which developed several prototypes of OLED TV in 2007 and 2008 [1]. Inkjet technology is applied also in another display-related application, i.e. the realization of colour filters for liquid-crystal displays (LCDs), where every pixel is printed employing

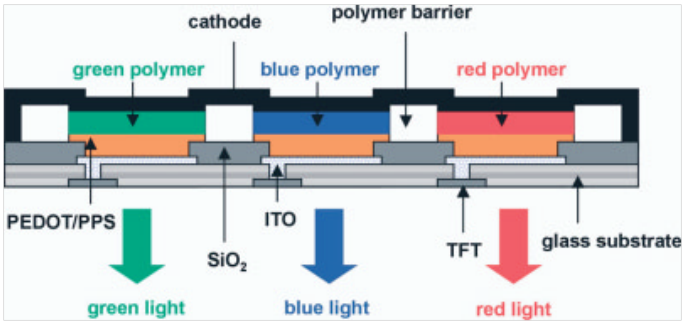

Figure 1.24: Schematic of a multicolour OLED display. [21]

inks which contain dyes and pigments of different colours [21]. Furthermore, different studies exist on the employment of single-wall and multi-wall carbon nanotubes (SWCNTs and MWCNTs) dispersed in organic solvents as inks for the realization of inkjet printed electrochromic devices [13].

1.3.3 Conductive Structures

The maskless additive property of printing processes can be exploited for the realization of metallic contacts and interconnections in electronic circuits, traditionally defined by means of lithography techniques. Both DOD and continuous inkjet have been used in order to achieve solder bumps onto circuit boards (some examples are reported in Figure 1.25). Microfab Inc. developed a drop on demand inkjet printing technology capable of accurately placing molten solder droplets, 25-125 μm in diameter, at rates up to 400 per second [43]. Several kinds of metallic-ink formulations have been also applied for the realization of conductive lines. Azucena et al.[45] used drop on demand piezoelectric inkjet process to print coplanar waveguides transmission lines on a glass substrate, employing an ink containing silver nano-particles capped with a polymer coating which keeps the particles in a colloidal suspension. They optimized printing process parameters (e.g. substrate temperature, number of superimposed printed layers) in order to achieve good resolution together with good conductivity reaching values comparable to those of plated copper. The minimum achievable width of printed line interconnections has been fully studied, since it strongly affects high density integration of conduction lines for some applications, as for example in backplanes. Osch et al.[46] achieved 40 μm width lines by inkjet printing of silver nanoparticles-based ink

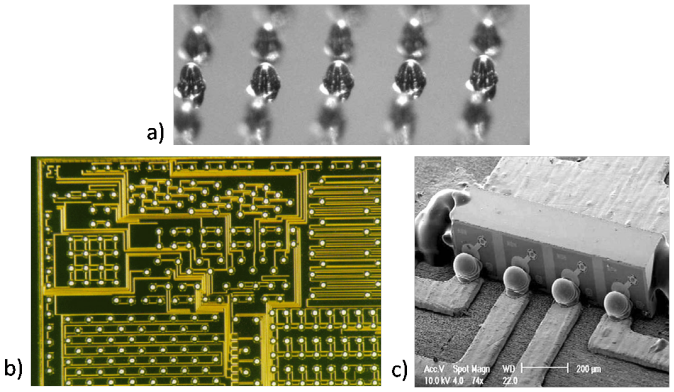

Figure 1.25: a) Solder drops (100 μm diameter) placed onto pitch pads at a rate of $400s^{-1}$ [43]. b) Solder bumps (70 μm diameter) deposited by DOD inkjet printing on to an integrated circuit test substrate [15]. c) 3-D deposition of solder joints to a right angle interface between conductors and a VCSEL array [43].

onto different polymeric substrates (see Figure 1.26) reaching conductivity of $13 - 23\%$ of bulk conductivity. Also, some passive microelectronics components, as capacitors, resistors and inductors can be realized by means of printed techniques. As an example in Figure 1.27 two photographs of (a) embedded resistors and (b) an inductor realized by means of piezoelectric DOD inkjet technology are reported [15][43].

1.3.4 Detectors and Sensors

The range of the sensors classes which can be manufactured by means of printing techniques is very wide. It includes gas and humidity sensors, photodetectors and mechanical stress sensors, which find their application above all in smart packaging of food and drug industry. Some examples are discussed in the following. Fully printable polyaniline (PANI)-copper (II) chloride sensor for the detection of hydrogen sulfide gas has been recently realized [47]. The device is composed of interdigitated silver and carbon electrodes screen printed onto a flexible PET substrate and polyaniline and copper (II) chloride (active layer) deposited by means of inkjet printing. The sensing behaviour of such device is based on the protonation of the PANI film when exposed to H_2S, leading to formation of emeraldine salt and to a corresponding increase in conductivity. Further details are beyond the scope of this thesis, but they can be found in literature. Figure 1.28 reports optical images of interdigitated electrodes with inkjet

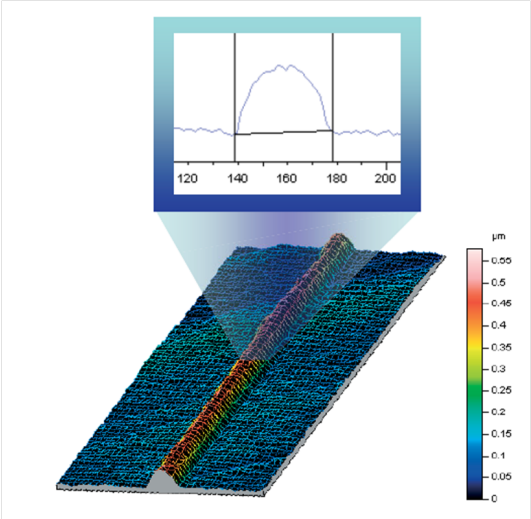

Figure 1.26: Cross-section nd 3D image of inkjet-printed silver line printed on a polyarylate film by means of DOD inkjet printing. [46]

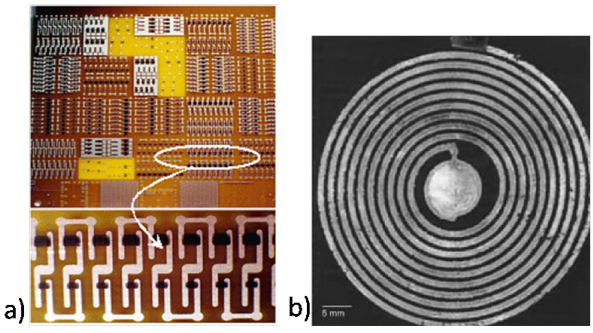

Figure 1.27: Photos of (a) embedded resistors [43] and (b) an inductor [15] inkjet printed.

printed films of (a) PANI, (b) PANI-$CuCl_2$ pre H_2S exposure, and (c) PANI-$CuCl_2$ post H_2S exposure (top), and the current-time transient obtained for a PANI-$CuCl_2$ sensor on exposure to increasing concentrations of hydrogen sulfide gas. Also printed pho-

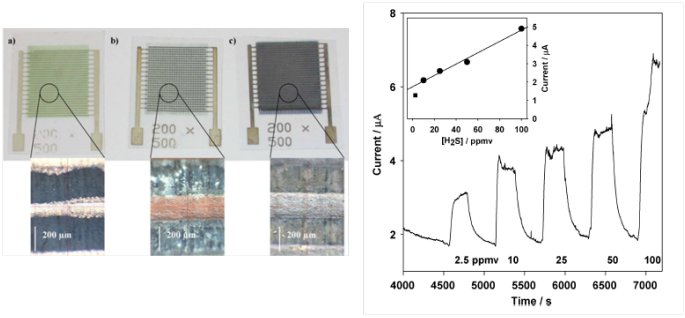

Figure 1.28: (left) interdigitated electrodes with inkjet printed films of (a) PANI, (b) PANI-$CuCl_2$ pre H_2S exposure, and (c) PANI-$CuCl_2$ post H_2S exposure; (right) current-time transient obtained for a PANI-$CuCl_2$ sensor on exposure to increasing concentrations of H_2S gas. Inset shows the calibration plot obtained. [47]

todetectors have been reported in literature. Börbel et al.[44] published a work about the realization of a highly sensitive photodetector made up of inkjet printed HgTe nanoparticles-based ink (composed of HgTe crystals dispersed in chlorobenzene with concentration of 2 wt %) onto a glass substrate. They found an increase of the detector sensitivity with the number of printed layers reaching 65 mAW^{-1} at 10 V for six layer devices (Figure 1.29) [13]. Furthermore very recently Lilliu et al.[48] demonstrated the realization of an organic photodiode where both the transparent hole conductor (PEDOT:PSS) and the photoconductive layer (poly(3-hexylthiophene)(P3HT) and phenyl C61 butyric acid methyl ester (PCBM) dissolved in a mixture of ortho-dichlorobenzene and 1,3,5-trimethylbenzene) have been deposited by means of inkjet printing. An example of commercially available printed sensor is OnVu^{TM}, a novel time-temperature indicator (TTI) that has been jointly developed by Ciba and FreshPoint [49]. Such sensor, based on organic pigments that change colour over time and if temperatures rises and which can be printed (by means of flexographic process) in labels or directly on the packages, allows producers, retailers and consumers to monitor the cold chain from the point of packaging to consumption, thereby ensuring the freshness of the food products it is applied on (see Figure 1.30).

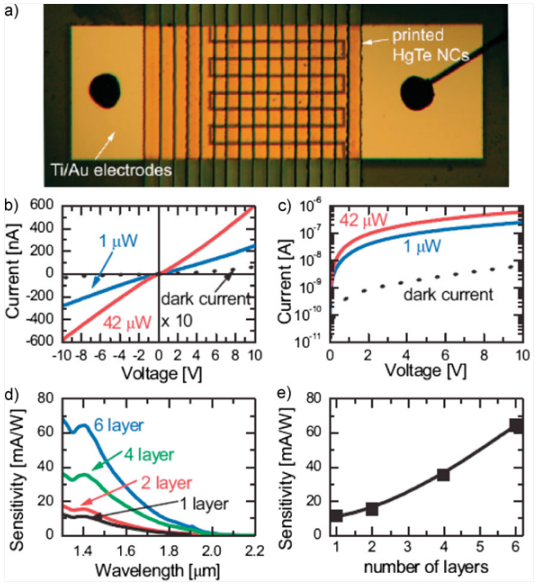

Figure 1.29: (a) Optical image of inkjet printed HgTe nanocristals based photodetector. (b) Linear and (c) logarithmic IV characteristic six printed layer device. (d,e) Sensitivity of the detector increases with the number of printed layers. [13]

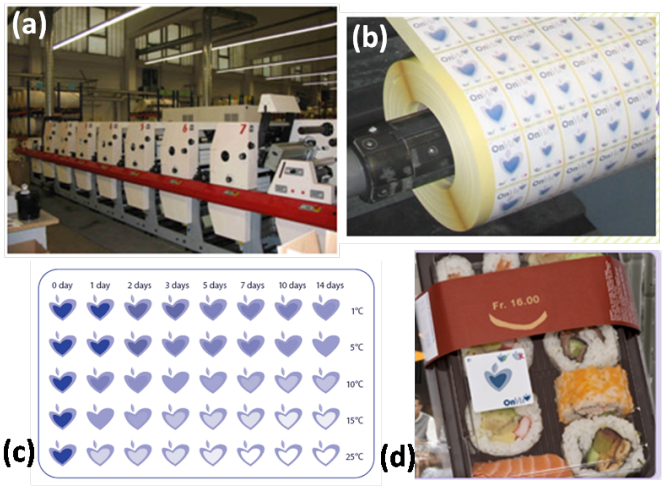

Figure 1.30: (a) Flexographic printers, (b) printed OnVu labels, (c) time and temperature dependent response of the sensor, (d) OnVu label on food packaging. [49]

1.3.5 Optics

The controlled deposition of materials allowed by non-contact printing techniques, above all laser direct writing and inkjet, makes these technologies suitable for micro-optics applications. In Figure 1.31 an array of micro-lenses (a) and an optical waveguide system fabricated by means of DOD inkjet printing are shown [15]. Figure 1.32 instead, shows photograph of a photonic crystals with flower-leaf pattern realized by means of inkjet printing (a), UV-vis spectra of the flower and leaf (b), SEM images of the red flower (280 nm) and green leaf (220 nm) patterned regions (c, d), reported by Cui et al.[50].

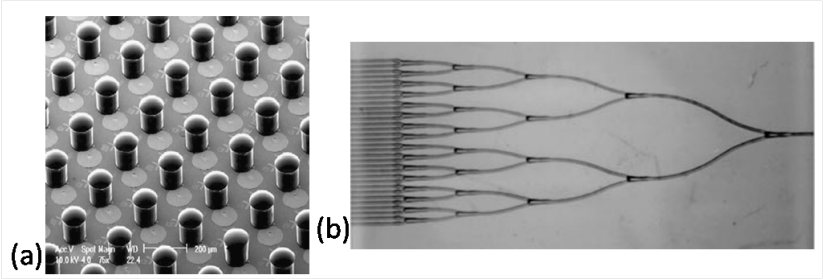

Figure 1.31: Inkjet printed array of micro-lenses (a) and optical waveguides (b). [15]

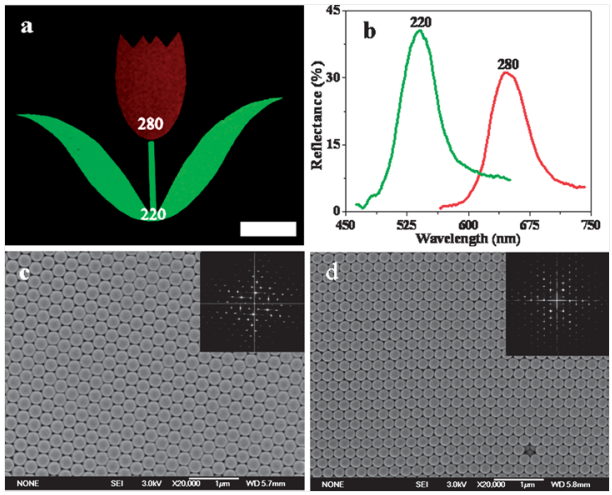

Figure 1.32: (a) Photonic crystals with flower-leaf pattern realized by means of inkjet printing; (b) UV-vis spectra of the flower and leaf; (c, d) SEM images of the red flower (280 nm) and green leaf (220 nm) patterned regions. [50]

1.3.6 Other applications: biomedical

Another widely investigated application of printed technologies, and above all of inkjet printing, involves the biomedical and pharmaceutical field. Event if these should not properly belong to the class of PE applications, it is interesting to pay attention to them in order to fully comprehend the potential employment and to have a wider scenario of printing technologies. One of the most studied field concerns the employment of printing techniques for tissue engineering. Cellular patterns construction developed printing methods include soft lithography, laser-directed cell-writing and inkjet printing. Roth et al.[51] demonstrated a method of applying high-throughput inkjet printing to control cellular attachment and proliferation by precise, automated deposition of collagen. In particular, their experiments involved the growth of both smooth muscle cells derived from rat aorta and dorsal root ganglia neurons onto collagene printed patterns. A similar approach has been used by Sanjana and Fuller[52], who reported about the use of inkjet printing to fabricate neuron-adhesive patterns using poly(ethylene) glycol as the cell-repulsive material and a collagen/poly-d-lysine (PDL) mixture as the cell-adhesive material. Figure 1.33 shows cells, after 8-10 days in culture adhered to printed patterns, in this case the text MIT, the acronym for Massachusetts Institute of Technology, where the experiment took place. Another widespread application regards the realization of

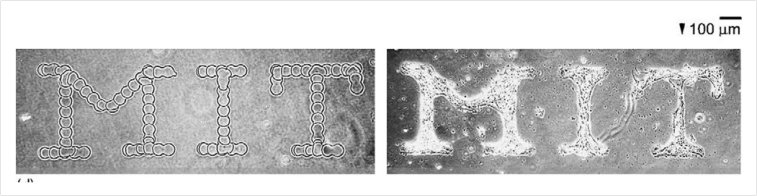

Figure 1.33: (Left) Collagen/PDL mixture printed onto a uniform PEG inhibitory background; (right) cells adhered to patterns after 8-10 days in culture. [52]

DNA synthesis and the fabrication of DNA [53] and bacterial colony arrays and complex patterns (e.g. directly ejecting Escherichia coli onto agar-coated substrates [54]) by means of inkjet printing techniques. Several companies, as PerkinElmer [55], have developed commercial inkjet/micro-dispensing systems for such applications. Moreover inkjet technology is used for controlled drugs/polymers/cells release in coating of biomedical implantation equipments as stents and bioabsorbable polymer nerve guidance

conduits [43].

Bibliography

[1] E. Coatanéa, V. Kantola, J. Kulovesi, L. Lahti, R. Lin, M. Zavodchikova, *Printed Electronics, Now and Future*, Bit Bang - Rays to the Future, ed. Y. In Neuvo & S. Ylönen, **2009**, Helsinki University of Technology (TKK), MIDE, Helsinki University Print, Helsinki, Finland, 63-102. ISBN 978-952-248-078-1. 2, 3, 5, 7, 23, 25

[2] H. Kempa, Institute of Print and Media Technology, Chemnitz University of Technology, Chemnitz, Germany. Online. URL: http://en.wikipedia.org/wiki/File:ComplementaryTechnologies.png 3

[3] U. Caglar, *Studies of Inkjet Printing Technologies with Focus on Electronic Materials*, PhD Thesis, Tampere University of Technology, **2009**. ISBN 978-952-15-2317-5. 2, 5, 6, 16

[4] H. Al-Chami, *Inkjet Printing of Transducers*, Master thesis, University of British Columbia, **2010**. 4, 7, 22

[5] A. Karwa, *Printing Studies with Conductive Inks and Exploration of New Conducting Polymer Compositions*, Master Thesis, Center for Materials Science and Engineering, Rochester Institute of Technology, New York, **2006**. 5, 6

[6] P. Calvert, *Chem. Mater.*, **2001**, 13, 3299-3305. 22

[7] D. Gamota, P. Brazis, K. Kalyanasundaram, J. Zhang, *Printed Organics and Molecular Electronics*, Kluwer Academic Publishers, **2004**. ISBN: 1402077076. 6

[8] Y. Xia, G. M. Whitesides, *Angew. Chem. Int. Ed.*, **1998**, 37, 550-575. 6

[9] Y. Xia, G. M. Whitesides, *Annu. Rev. Mater. Sci.*, **1998**, 28, 153-84. 6

[10] B. Michel, A. Bernard, A. Bietsch, E. Delamarche, M. Geissler, D. Juncker, H. Kind, J.-P. Renault, H. Rothuizen, H. Schmid, P. Schmidt-Winkel, R. Stutz, H. Wolf, *IBM J. RES. & DEV.*, **2001**, 45, 697. 6

[11] P. Cosseddu, *Correlation between interface-dependent properties and electrical performances in OFETs*, PhD Thesis, University of Cagliari, **2006**. 7

[12] T. Kawase, T. Shimoda, C. Newsome, H. Sirringhaus, R.H. Friend, *Thin Solid Films*, **2003**, 438-439, 279-287. 7, 21

BIBLIOGRAPHY

[13] M. Singh, H. M. Haverinen, P. Dhagat, G. E. Jabbour, *Adv. Mater.*, **2010**, 22, 673-685. 10, 22, 24, 26, 29, 30

[14] T. Sekitani, Y. Noguchi, U. Zschieschang, H. Klauk, T. Someya, *Proceedings of the National Academy of Sciences*, **2008**, 105, 4976-4980. 16, 21

[15] K. K. B. Hon, L. Li, I. M. Hutchings, *CIRP Annals - Manufacturing Technology*, **2008**, 57, 601-620. 7, 9, 10, 11, 20, 21, 27, 28, 31

[16] M. Colina, P. Serra, J. M. Fernandez-Pradas, L. Sevilla, J. L. Morenza, *Biosensors and Bioelectronics*, **2005**, 20, 8, 16381642.

[17] http://www.optomec.com 9

[18] http://www.sirris.be/homePage.aspx 10

[19] Lord Rayleigh, *Proc. London Math. Soc.*, **1878**, 10, 4. 11

[20] Lord Rayleigh, *Proc. Roy. Soc.*, **1879**, 29, 71. 11

[21] B-J. de Gans, P. C. Duineveld, U. S. Schubert, *Adv. Mater.*, **2004**, 16, 3, 203-213. 11, 12, 16, 17, 18, 26

[22] *Background on Ink-Jet Technology*, MicroFab Technote 99-01, **1999**. 11, 12, 13

[23] Hansell, U.S. Patent, **1950**, 2, 512, 743. 12

[24] B. Ballarin, A. Fraleoni-Morgera, D. Frascaro, S. Mazzarita, C. Piana, L. Setti, *Shyntetic Met.*, **2004**, 146, 201-205. 12

[25] *Dimatix Materials Printer DMP-2800 Series User Manual*, FUJIFILM Dimatix, **2008**. 14

[26] J-U. Park, M. Hardy, S. J. Kang, K. Barton, K. Adair, D. K. Mukhopadhyay, C. Y. Lee, M. S. Strano, A. G. Alleyne, J. G. Georgiadis, P. M. Ferreira, J. A. Rogers, *Nat. Mat.*, **2007**, 6, 782-789. 16

[27] W. Ohnesorge, *J. Appl. Math. Mech.*, **1936**, 16, 355-358. 16

[28] J. E. Fromm, *IBM J. Res. Dev.*, **1984** 28, 322-333. 16

[29] N. Reis and B. Derby, *Mater. Res. Soc. Symp. Proc.*, **2000** 625, 117. 16

[30] N. Reis, C. Ainsley, B. Derby, *J. Appl. Phys.*, **2005** 97, 094903. 16

[31] T. Kawase, T. Shimoda, C. Newsome, H. Sirringhaus, R. H. Friend, *Thin Solid Films*, **2003**, 438-439, 279-287. 16, 17

[32] B. Derby, N. Reis, *MRS Bull.*, **2003**, 28, 815-818. 16

[33] B-J. de Gans, L. Xue, U. S. Agarwal, U. S. Schubert, *Macromol. Rapid Commun.*, **2005**, 26, 310-314. 17, 19

[34] A. L. Yarin, *Annu. Rev. Fluid Mech.*, **2006**, 38, 159-192. 18, 19, 21

[35] R. Rioobo, M. Marengo, C. Tropea, *Exp. Fluids*, **2002**, 33, 112-124. 18, 20

[36] G. E. Cossali, A. Coghe, M. Marengo, *Exp. Fluids*, **1997** 22, 463-72. 21

[37] D. Kim, S. Jeong, B. K. Park, J. Moon, *Appl. Phys. Lett.*, **2006**, 89, 264101. 22

[38] H. Yan, Z. Chen, Y. Zheng, C. Newman, J. R. Quinn, F. Dötz, M. Kastler, A. Facchetti, *Nature*, **2009**, 457, 679-687.

[39] C. W. Sele, T. Werne, R. H. Friend, H. Sirringhaus, *Adv. Mater.*, **2005**, 17, 997.

[40] K. X. Steirer, J. J. Berry, M. O. Reese, M. F. A. M. van Hest, A. Miedaner, M. W. Liberatore, R. T. Collins, D. S. Ginley, *Thin Solid Films*, **2009**, 517, 2781-2786. 23, 24

[41] P. Kopola, M. Tuomikoski, R. Suhonen, A. Maaninen, *Thin Solid Films*, **2009**, 517, 5757-5762. 25

[42] A. Maaninen, *Research and development activities in printed intelligence*, **2008**, VTT Technical Research Centre Of Finland. Available on-line: *www.vtt.fi* 25

[43] http://www.microfab.com 26, 27, 28, 33

[44] M. Börberl, M. V. Kovalenko, S. Gamerith, E. J. W. List, W. Heiss, *Adv. Mater.*, **2007**, 19, 3574. 29

[45] O. Azucena, J. Kubby, D. Scarbrough, C. Goldsmith, *IEEE MTT-S Int. Microwave Symp. Dig.*, **2008**, 075-1078. 26

[46] T. H. J. van Osch, J. Perelaer, A. W. M. de Laat, U. S. Schubert, *Adv. Mater.*, **2008**, 20, 343-345. 26, 28

[47] K. Crowley, A. Morrin, R. L. Sheperd, M. in het Panhuis, M. R. Smyth, G. G. Wallace, A. J. Killard, *IEEE Sensors Journal*, **2010**, 10, 9, 1419-1426. 27, 29

[48] S. Lilliu, M. Böberl, M. Sramek, S. F. Tedde, J. E. Macdonald, O. Hayden, *Thin Solid Films*, **2011**, doi:10.1016/j.tsf.2011.08.004 29

[49] http://www.onvu.com/en/index.asp 29, 30

[50] L. Cui, Y. Li, J.a Wang, E. Tian, X. Zhang, Y. Zhang, Y. Song, L. Jianga, *J. Mater. Chem.*, **2009**, 19, 5499-5502. 31

[51] E. A. Roth, T. Xu, M. Das, C. Gregory, J. J. Hickman, T. Boland, *Biomaterials*, **2004**, 25, 3707-3715. 32

[52] N. E. Sanjana, S. B. Fuller, *Journal of Neuroscience Methods*, **2004**, 136, 151-163. 32

[53] L. R. Allain, M. Askari, D. L. Stokes, T. Vo-Dinh, *Fresenius J. Anal. Chem.*, **2001**, 371, 146-150. 32

BIBLIOGRAPHY

[54] T. Xu, S. Petridou, E. H. Lee, E. A. Roth, N. R. Vyavahare, J. J. Hickman, T. Boland, *Biotechnol. Bioeng.*, **2004**, 85, 29-33. 32

[55] http://www.perkinelmer.com 32

2

Experimental

In this chapter several details of my research activity will be presented. Mainly, two different kinds of Organic Thin Film Transistors (OTFTs) were fabricated and characterized:

- Organic ElectroChemical Transistors (OECTs);
- Organic Field Effect Transistors (OFETs).

The working principle and the performances of such devices will be discussed in chapter 3 for OECTs and in chapter 4 for OFETs, while hereafter informations regarding the fabrication/characterization procedure followed will be given: the first section provides some technical skills and informations about the printer employed for the realization of the devices, the *FUJIFILM Dimatix Materials Printer 2800*; in the second section the main physical and chemical properties of the materials employed as substrates for the devices are reported; the third and the fourth sections comprise the description of chemical and physical properties and printing process details (as the printing parameters optimization and the approach for the resolution of some technical issues) about respectively the conductive and the semi-conductive inks used. Noticeably, dielectric-based inks were not be employed for the realization of the transistors' insulating layer, therefore they will not be treated. The physical and chemical properties of thermally evaporated Parylene C layer used as transistors gate dielectric are reported in the second section. Finally, the fifth section reports a brief description of the experimental techniques employed in order to characterize the devices.

2.1 Technology - Dimatix Materials Printer 2800

The inkjet printer used for the fabrication of all devices reported in this thesis is the *Dimatix Materials Printer 2800* (DMP2800), a piezoelectric DOD printer provided by FUJIFILM Dimatix [1]. In Figure 2.1 a digital photo of DMP2800 is showed, while

Figure 2.1: Digital photo of Dimatix Materials Printer 2800. [2]

in Figure 2.2 a diagram of the main printer's components is reported. The printer

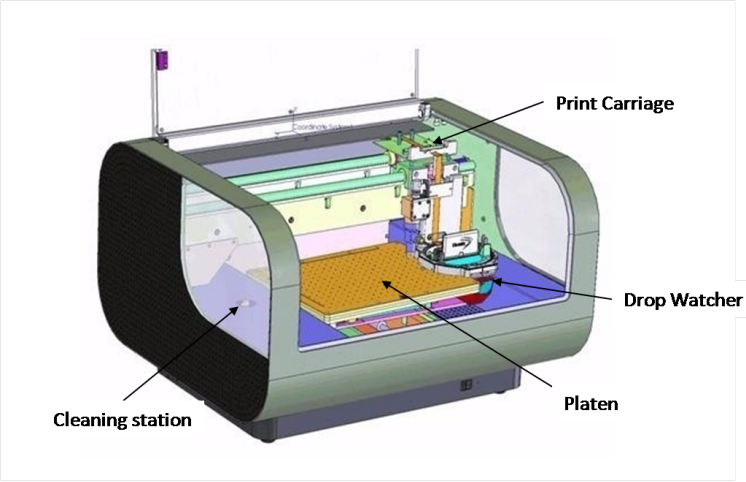

Figure 2.2: Schematics of the main components of DMP 2800.

includes four main parts:

- *Print Carriage*: it is the physical support of the cartridge and it represents the core of the printer itself.
- *Platen*: it's the substrates' holder. It can be heated until 60 °C and it is provided with a vacuum system. The platen temperature is an important printing parameter. It affects, indeed, the drying time of the ink-jetted droplets on the substrate, and can be one of the major causes of the undesired nozzle clogging. The vacuum system has the function of holding the substrate on the platen during the printing process but unfortunately if the substrate is not very flat, stiff or smaller than the platen, holding the substrate by means of adhesive tape is more effective.
- *Cleaning Station - Blotting pad*: it is the cartridge maintenance station, where the cleaning cycles are performed.
- *Drop Watcher Station*: this is the system which allows direct viewing of the jetting nozzles, the faceplate surrounding the nozzles, and the actual jetting of the fluid.

The entire system is controlled by an application software also provided by FUJIFILM Dimatix. In the following subsections the main functionalities and potentialities of the system are briefly described. The explanation of such technical skills is necessary to fully comprehend and appreciate the results achieved in the present work. Some of the informations given in these subsections can be easily found in the printer manual [2] but the most part of them arose from direct experiences.

2.1.1 Print Carriage

The *Print Carriage* (Figure 2.3) is the core of the printing system. It is the support for the cartridge and includes the *Fiducial camera*, a very useful tool for alignment procedures and for evaluation of the printed pattern quality. During printing the carriage moves horizontally (X direction) above the substrate, while the vertical shift (Y direction) is achieved by means of the platen motion. In other words, the printing action proceeds through subsequent horizontal scans of the print carriage, and subsequent vertical shifts of the substrate. This peculiar printing procedure strongly affects the deposition of the droplets of ink on the substrate and, consequently, the choice of the optimal printing parameters in order to achieve the best print quality. The

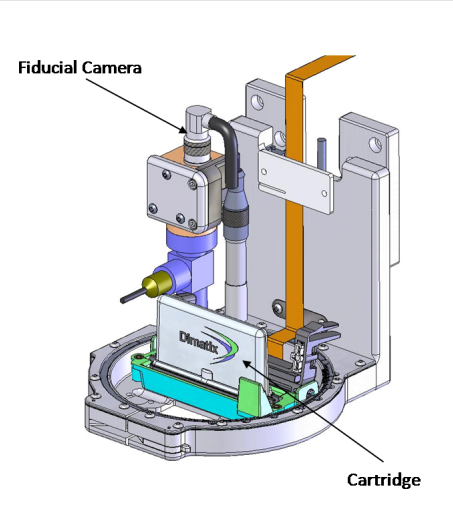

Figure 2.3: Print Carriage.

maximum Z-axis adjustment (distance between the platen and the nozzle plate) is 25 mm. The possibility to calibrate the cartridge altitude is very useful in printing on a thick substrate. The *Cartridge* is composed of two main parts shown in Figure 2.4: a *Fluid Module*, which contains a plastic bag which acts as ink reservoir, and a *Jetting Module*, where 16 jetting nozzles, at a distance of 254 μm, are located in a single row; each orifice size is about 21.5 μm. Even if Dimatix indicates a maximum volume of 1.5

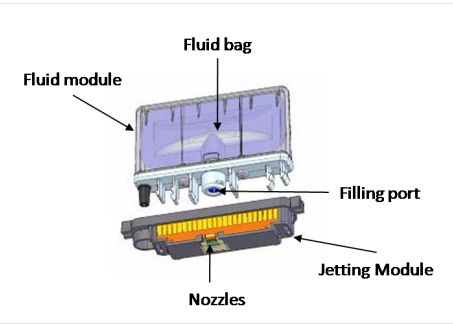

Figure 2.4: Cartridge and its two main parts: the Fluid Module and the Jetting module.

mL for the fluid module, the ink reservoir can easily support up to 3 mL of ink. The cartridge is compatible with most solvents:

a) Aliphatic alcohols (high boiling point better than low in all cases)

b) Aromatic hydrocarbons such as anisole, trimethylbenzene

c) Aliphatic hydrocarbons such as hexane, dodecane

d) Cellusolves

e) Glycols

f) Lactate esters

g) Aliphatic and aromatic ketones

h) Polyethylene glycols, polypropylene glycols

The cartridge has a built-in heater which is capable of heating the fluid to a maximum temperature of 70 °C in the jetting structure. It should be noted that heating of ink can cause faster nozzle clogging, especially when a high volatility solvent-based ink is used. For this reason, in most of cases, keeping the cartridge at RT is the best choice. The reservoir of fluid is not heated and there is not a built-in cooling mechanism. The fluid physical characteristics (given by the producer [2]) required to reach the optimum printing performances are the follows:

- *Viscosity*: 10 - 12 cps at jetting temperature
- *Surface Tension*: 28 - 33 dyne/cm at jetting temperature
- *Low Volatility*: Boiling points higher than 100 °C
- *Degassing*: Degassing can be done with a vacuum system, by ultrasonic baths or by spinning
- *Filtering*: it is recommended to filter the fluids with a 0.2 μm nylon filter
- *Acidity*: pH between 4 and 9 is suggested

2.1.2 Drop Spacing and Resolution

Spot size and line width are dependent on the interaction between the ink-jetted droplets and the specific substrate used. Dimatix supplies two models of piezo-driven jetting cartridges which differ for the nominal drop volume they can eject: DMC-11601

and DMC-11610 models are able to jet 1 pL and 10 pL droplets respectively. It's important to underline that such volume values are nominal, the effective volume of a jetted drop depends on the firing voltage and the jetting frequency used. It's quite problematic using cartridges with drop volume of 1 pL due to easier nozzle clogging, especially for ink made of dispersion of nanoparticles in a liquid vehicle. Generally, a 40 μm spot can be produced on a polymeric substrate with a 10 pL drop. Determining the spot size of the ink on the substrate is a fundamental operation to set an appropriate *Drop Spacing* in order to achieve the desired resolution of the printed pattern. The *Drop Spacing* is the distance between the center of two subsequent drops, both in X and in Y direction, that the printer deposits on the substrate to create the pattern. As shown in Figure 2.5 in the X direction the printer manages the ejection of a drop from the correct nozzle according to an encoder signal and to the image resolution corresponding to the drop spacing setted, while in the Y direction the distance between two subsequent spots is determined by the *Cartridge Mounting Angle* (angle between the scan direction of the cartridge and the nozzle plate), but also by the intrinsic resolution of the printer, i.e. the distance between two subsequent nozzles in the nozzle plate (254 μm). The

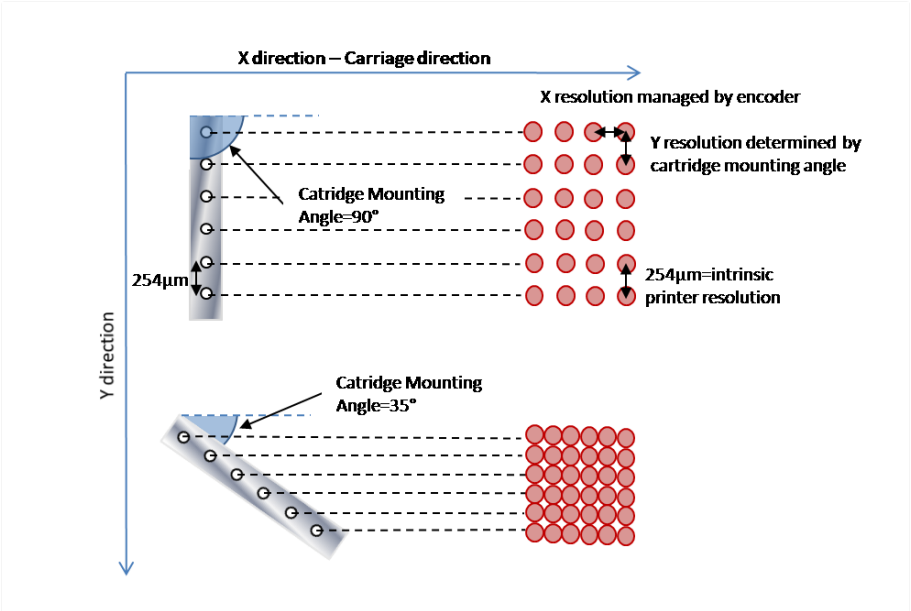

Figure 2.5: Determination of pattern resolution in X and Y direction. The resolution in X direction is managed by an encoder and depends on the drop spacing setted. The resolution in Y direction depends on the cartridge mounting angle.

Cartridge Mounting Angle is set manually through a rotating system which allows the operator to rotate the cartridge at the desired angle by means of two graduated scales (Figure 2.6). The drop spacing thus is adjustable between 5 and 254 μm and it is useful

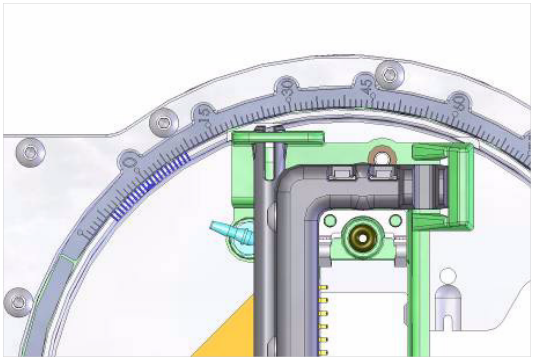

Figure 2.6: Cartridge alignment scales. It is used to modify the drop spacing in the Y axis.

for altering the fill density of patterns, which could be a critical feature, above all in printing semiconductor-based inks. Also, the drop spacing is strictly correlated to the specific pattern printed. For the optimization of the quality of the final printed device it is thus necessary to change drop spacing for different patterns. The mathematical relation that links drop spacing and resolution is reported in equation 2.1. So, as the mounting angle decreases, the print resolution increases.

$$DropSpacing\,[\mu m] = \frac{25400}{resolution\,[dpi]} \tag{2.1}$$

As a rule of thumb the optimal drop spacing to set in order to obtain a continuous, uniform and smooth printed film is the half size of the droplets deposited [3]. Since the size of the printed drops depends on the interaction forces between the particular fluid and the substrate used, before printing the desired pattern, it is desirable to measure the size of a single droplet deposited. This procedure can be carried out using the *Fiducial Camera*.

2.1.3 Jets control

Controlling the quality of jets ejected is crucial in order to achieve the best print quality. It can be done in two different and complementary ways: caring for the cartridge

maintenance and monitoring the ink droplets ejection. The maintenance operations are supported both by software and hardware of the printer, and are designed in order to initialize and maintain the optimal jetting performances. In the cleaning station there is a replaceable adsorbing pad, which has the function of soaking up the ink from the nozzle plate. Four main functions can be combined forming *Cleaning Cycles*:

- *Purging*: The fluid is pushed out of the nozzles by an application (the DMP contains also a pump) of air pressure to outside of fluid bag. Purging is required for the initial use of the cartridge to push air out of the fluid path (air bubble may cause nozzle clogging). Despite this procedure leads to a huge ink spreading it is the most efficient solution in clearing clogged nozzles.

- *Spitting*: A predetermined number of drops are jetted at a predetermined frequency in order to clear the nozzles and to keep fluid path surfaces wet.

- *Blotting*: The nozzle plate is kept in contact with the cleaning pad (no wiping) to remove the excess of fluids that may be present in proximity of the nozzles. This operation prevent and, in some cases, resolve the puddling of ink around nozzles, that may cause misdirected firing and, consequently, the presence of satellite-drops around the printed pattern. When cartridges filled with different fluids are switched, the cleaning pad has to be changed before performing blotting operation, otherwise a contamination between different fluids occurs.

- *Meniscus Control*: In order to prevent ink from flowing out of the cartridge nozzles a low vacuum is applied to the ink reservoir. The level of vacuum should be decreased if some of nozzles don't fire, i.e. if the pumping force applied to the ink reservoir is not high enough to overcome meniscus vacuum, while it should be increased in fluid falls down from nozzles due to gravity force.

The desired cleaning cycle can be performed before (almost mandatory to achieve satisfactory printing performances), during and after printing and also during resting time. Monitoring and adjusting the ink jets is possible by using the *Drop Watcher Camera System*, that includes a replaceable *Drop Watcher Pad* which collects the fluids ejected, and a digital camera with a magnification of 150× (image displayed resolution of 2.25 μm per pixel). Once the nozzles are positioned over the system, it allows direct observation of the jetting of the ink, the image area represents an actual

area of about 1.4 mm x 1.1 mm on the cartridge, covering 5 nozzles, but the framing can be shifted and all the 16 nozzles present in the cartridge can be visualized. Jets are considered good-performing if, first of all, they are made of single, spherical drops, their direction is perpendicular to the nozzle plate and parallel one another, drops have matched velocities. These features permit a high precision in droplets deposition and allow to obtain minimal spreading on the substrate. Some of non ideal effects are showed in Figure 2.7.

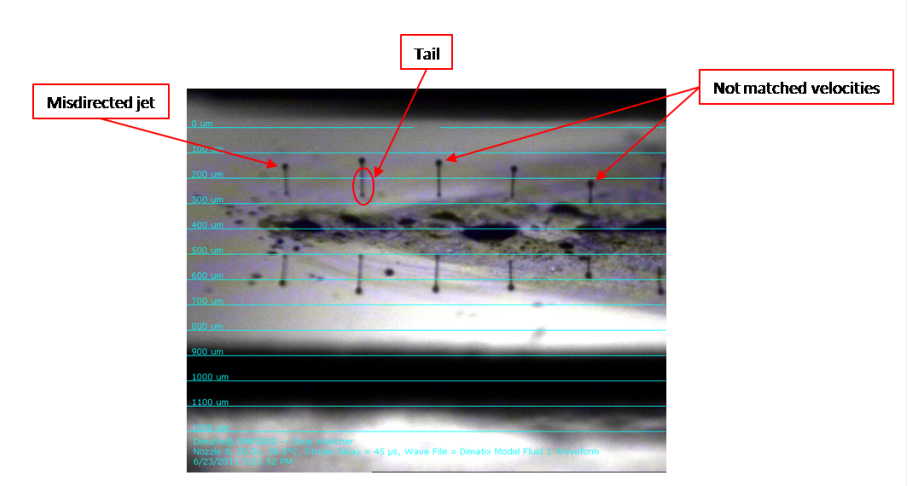

Figure 2.7: Drop watcher image and some not ideal effects: misdirected jets, not matched velocities and tails.

During jetting observation several parameters can be setted and/or modified:

- *Firing Voltage*: It corresponds to the bias applied to deform the piezoelectric crystal for the droplet's ejection. It can be adjusted for each nozzle independently. Obviously, different inks requires different firing voltages in order to reach the optimal jetting performances. Generally a high firing voltage produces quite compact drops but with a long tail, conversely a low firing voltage permits to reduce tails length, to reduce drop velocity and to avoid droplets scattering at the impact with the substrate (and, subsequently, to obtain a better print quality). On the other hand, a low firing voltage may bring to misdirected jets and increases the probability of clogging nozzles during printing.

- *Jetting Frequency*: It's the frequency with which nozzles eject droplets. It affects

the print velocity, the print precision and it is strictly dependent on the particular pattern as described afterwards.

- *Number of Jetting Nozzles*: As the jetting frequency, also the choice of the number of nozzles used is strictly dependent on the specific pattern and precision required. If high precision and definition of the printed pattern (for example in printing interdigitated structures) are required, using a few jets is suitable. On the contrary, when rough layers of material have to be printed, the use of many nozzles leads to a faster print process together with a good uniformity of the material deposited. It should be noticed that printing with more than one nozzle implies to use adjacent nozzles: choosing the group of nozzles with the overall best jetting performances is really critical and sometimes it could be quite difficult.

Checking the good jetting performance of the chosen nozzles just before printing is absolutely advisable.

2.1.4 Alignment procedure and check of the printed pattern quality

The *Fiducial Camera* is a tool consisting of a camera, mounted on the print carriage, able to frame all parts of the substrate. Its field of view has a width of 1.62 mm and a height of 1.22 mm with a resolution of 2.54 μm per pixel. The operator can select three different light operation modes: bright field, dark field and both (there are two light sources); the bright field requires high light intensity (adjustable by the operator) while the dark field requires only very low light intensity and permits to easily view fluids on highly refractive substrates. The camera is used before printing to set the print origin on the substrate or to align a pattern on a pre-patterned substrate and, after printing, to check the print quality. The fiducial camera, also, allows to measure the size of single drops or lines printed, as displayed in Figure 2.8 for the measure of drop size of silver-based conductive ink on polyethylene terephthalate substrate.

2.2 Materials - Substrates

Different kinds of materials have been employed as substrate for the printed devices reported in the present work. Their main peculiarities are reported in the following subsections.

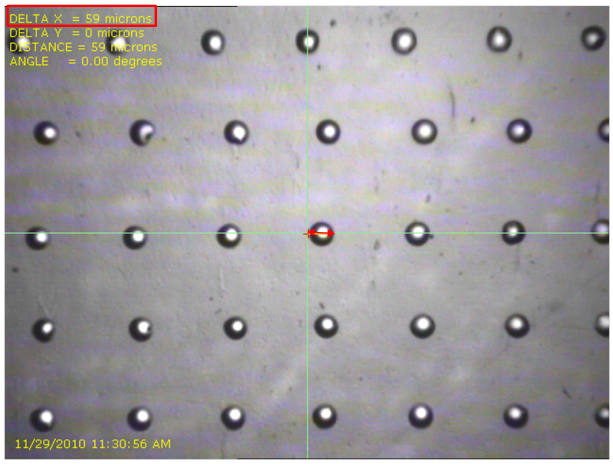

Figure 2.8: Measurement of drop size (silver-based conductive ink on polyethylene terephthalate substrate) by means of the fiducial camera.

2.2.1 Polyethylene terephthalate

Polyethylene terephthalate, usually called PET or simply *polyester*, is the most commonly used thermoplastic polyester. PET consists of polymerized units of the monomer ethylene terephthalate, with repeating $C_{10}H_8O_4$ units. In Figure 2.9 the chemical structure of PET is reported. In particular we used *biaxially oriented PET* (boPET) films,

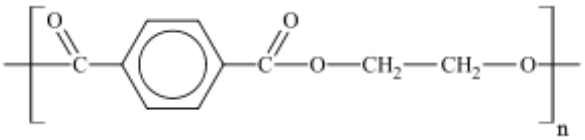

Figure 2.9: Chemical structure of polyethylene terephthalate.

provided by Goodfellow [4], as carriers for devices. BoPET is a polyester film made from scratched PET. Substrates of three different thicknesses were tested: 175 μm, 50 μm and 13 μm. BoPET films are characterized by the following properties:

- dimensionally stable;
- good chemical resistance except to alkalis, which hydrolyse it;
- highly transparent when in thin films;

- upper working temperature nominally in the range $115 - 150\,^{\circ}\mathrm{C}$, but, when it is employed in form of thin films, we observed deformation of substrates for temperatures above $60\,^{\circ}\mathrm{C}$;
- good flexibility - tensile strength in the range 190-260 MPa.

Thinner films are obviously more flexible than the thicker ones. This feature can be an advantage in some applications, e.g. in realization of transistors as bending sensors, pressure, and in general mechanical deformation, but it may constitute a cause of increasing difficulty in handling and cleaning procedures. The 175 μm substrates were cleaned by subsequent 15 min ultrasonic baths in acetone and isopropyl alcohol, then washed with deionized water and finally dried under nitrogen flow before their location on the printer platen (fixed by means of adhesive tape) and the assembly of the devices. Washing thinner substrates (13 μm and 50 μm) resulted much more complicated in order to avoid scratches and pleats on the surface caused by the use of tweezers or gloves. The best solution found to clean such kind of substrates is to spray with a nitrogen flow on their surface once located on the platen just before printing. This procedure leads to less cleaned substrates than the thicker ones but, since they are also lighter, the vacuum system of the platen alone is able to anchor them and no adhesive tape is required during printing. Not using the adhesive tape prevents the substrate contamination with glue.

2.2.2 Polyethylene naphthalate

Polyethylene naphthalate (PEN) is a polyester chemically quite similar to PET but which is more temperature resistant. The chemical structure of PEN is reported in Figure 2.10. It has been provided from Goodfellow [4] in form of biaxially-oriented 125

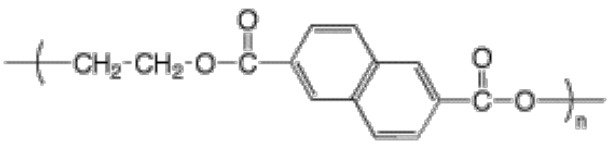

Figure 2.10: Chemical structure of polyethylene naphtalate

μm thick films. The main differences between PET and PEN are:

- upper working temperature around $190\,^{\circ}\mathrm{C}$ rather than $150\,^{\circ}\mathrm{C}$;

- Young's modulus several times higher than that of PET in the $100-150\,^{\circ}\mathrm{C}$ region;

Even if the higher temperature resistance of PEN makes it more suitable in printing inks which require post-processing at high temperatures, we noticed that this material is more easily subject to scratches and damages on the surface than PET leading to worst performances as devices carrier.

2.2.3 Kapton

Kapton is the brand name of a *polyimide* film, first developed by DuPont [5], widely used in flexible electronics as substrate for flexible printed circuits and in aerospace. It is well known for its excellent high temperature properties and radiation resistance, inherently low flammability and smoke emission, low creep and high wear resistance [4]. The complete chemical name for Kapton is *poly(4,4'-oxydiphenylene-pyromellitimide)* and its chemical structure is shown in Figure 2.11. Kapton films, usually transparent amber

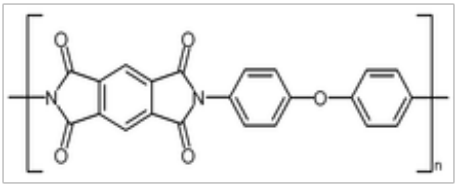

Figure 2.11: Chemical structure of poly(4,4'-oxydiphenylene-pyromellitimide).

coloured if thinner than 125 μm, can remain stable in a wide range of temperatures, from $-270\,^{\circ}\mathrm{C}$ to $320\,^{\circ}\mathrm{C}$. For this reason 13 μm thick films provided by Goodfellow were employed as substrates for OTFTs in which source, drain and gate electrodes were inkjet printed using the already mentioned CCI-300 silver-based ink, which requires curing temperature above $100\,^{\circ}\mathrm{C}$ for sintering. On the other hand, unfortunately, the poor chemical resistance of Kapton to alcohols makes it not particularly compatible with such an ethanol-based ink as CCI-300. Furthermore, as for thin PET film, it is not easy to handle avoiding scratches and pleats on the surface.

2.2.4 Polyvinylidene fluoride

The chemical structure of *polyvinylidene fluoride* (PVDF) is shown in Figure 2.12. It is a thermoplastic fluoropolymer with low reactivity and high purity level. The most

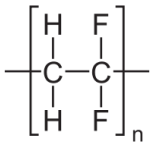

Figure 2.12: Chemical structure of polyvinylidene fluoride.

interesting property of PVDF is its piezoelectricity, i.e. its ability to convert mechanical stimulus in electricity and vice versa. In other words, when a mechanical stimulus is applied to a piezoelectric material, an electric potential will arise at its boundaries, and vice versa, when an electric potential is applied at its boundaries a mechanical deformation of material will occur. The piezoelectricity of PVDF derives from the structure of polymer chain in its β *form* reported in Figure 2.13: electrical dipoles formed by the bond between Fluorine and Carbon atoms are aligned throughout the polymer chain forming a polarization in the whole material. Mechanical compression or decompression of PVDF induces, thus, compression or decompression of dipoles chain leading to a variation of polarization across the polymer chains. In this thesis PVDF 50

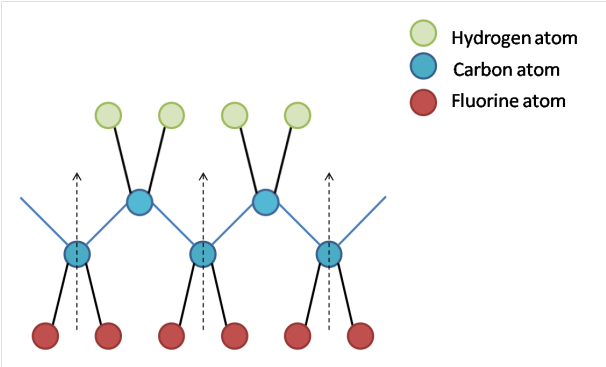

Figure 2.13: β form structure of PVDF.

μm thick films were used to fabricate pressure sensors depositing on both faces of the piezoelectric film some conductive electrodes by means of inkjet printing. In particular we employed CCI-300 silver-based ink (see subsection 2.3.2). Cabot suggests a curing temperature in the range $100 - 350\,^{\circ}\mathrm{C}$ but heating the PVDF films at temperatures $T \geq 60\,^{\circ}\mathrm{C}$ leads to a huge deformation of the substrate as shown in Figure 2.14. Thus, during printing and for the following annealing the substrate was kept at a constant

temperature of 60 °C. This drawback leads to a very slow complete drying of printed patterns and, consequently, to an increase of manufacturing time.

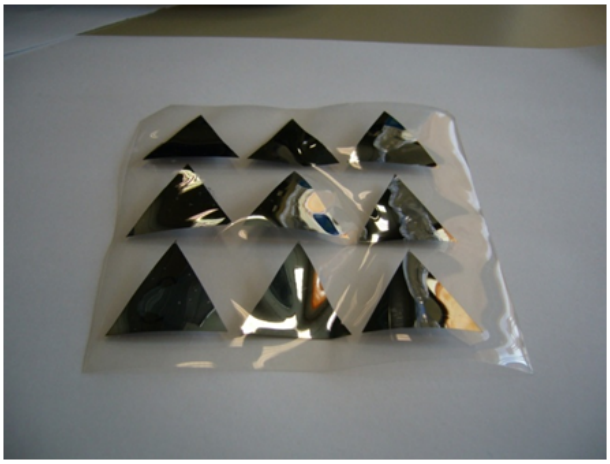

Figure 2.14: Deformation of PVDF substrate after thermal annealing at $T \geq 60\,°C$.

2.2.5 Parylene C

Parylene C belongs to the family of *poly(p-xylylene)* polymers, widely used in organic electronics as barrier for moisture and as gate dielectric of devices. Such polymers are usually deposited starting from dimer form through Chemical Vapour Deposition (CVD) process (for details see Appendix A). The monomer of parylene C is composed of a benzenic ring to which two -CH_2- groups are connected in para position, while a chlorine atom (hence the name parylene C) is connected in ortho position (see Figure 2.15). The main properties of parylene C are listed below [6][7]:

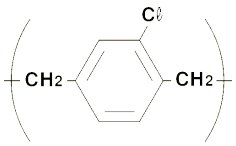

Figure 2.15: Chemical structure of parylene C.

- high molecular weight;
- high cristallinity;

- low permeability to gases and moisture;
- highly transparent;
- biocompatibility;
- uniform thickness and good dielectric properties (almost pore-free when deposited in enough thick films) - relative dielectric constant value of 3.15 (value acquired at 60 Hz), and electrical resistivity (at 20 °C) of 6×10^{16} Ω/cm [8];
- high elongation to break;
- compatibility with most of the solvents used in the cleaning and processing of electronic circuits and systems;
- capability to form layers perfectly conformal to the substrate.

These properties make parylene C a suitable material to employ both as gate dielectric of organic transistor and as protective layer for packaging of devices. Furthermore, thanks to its high resistance to chemical attacks, it is particularly adequate for inkjet printing of multi-layered structures. Thus it has been employed in this work as gate dielectric in the realization of inkjet printed OFETs in *bottom gate-bottom contact* configuration: once a layer of parylene was deposited on the gate electrode, the source and drain electrodes were printed on it and then an organic semiconductor, both in liquid phase (by means of inkjet printing, drop casting or spin coating) and through thermal sublimation of solid crystals, was deposited above the entire structure without any dissolution or damaging risk for the dielectric layer.

2.3 Materials - Conductive inks

For the fabrication of the conductive electrodes of the devices reported in this thesis two inks were used: a polymeric aqueous dispersion (waterborne dispersion of PEDOT:PSS particles) and a silver-based ink. The first was used to realize electrodes of both OFETs and OECTs, while the second was employed for OFETs electrodes and PVDF-based pressure sensors metallizations. Hereafter their main properties and the experimental skills in the inkjet printing of such materials will be discussed.

2.3.1 PEDOT:PSS-based ink

Poly(3,4-ethylenedioxythiophene) or PEDOT (and sometimes PEDT) is a polythiophene derivative based on 3,4-ethylenedioxythiophene or EDOT monomer, which is composed by an aromatic thiophene ring with the carbon atoms in position 3 and 4 connected by means of a double ethereal bridge (Figure 2.16). It has been developed during the second half of 1980's by scientists at the Bayer AG research laboratories in Germany [9]. This polymer showed some very interesting properties: high conductivity

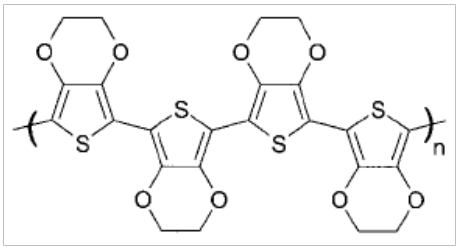

Figure 2.16: Chemical structure of PEDOT chain. [11]

(ca. 300 S/cm); almost complete transparency when deposited in thin, oxidized films; very high chemical stability in the oxidized state. Unfortunately, even if initially it has been studied and developed in order to give a soluble conducting polymer, PEDOT was found to be an insoluble polymer [11]. Such insolubility represented a huge limitation for the employment of PEDOT in organic electronic applications and above all for its usage as ink in printed electronics techniques. This crucial issue has been overcome by doping the polymer chain with other chemicals. One of the dopants used for this scope is *poly(styrene sulfonic acid)* (PSS) and hereafter only this kind of doping is discussed, since it leads to the PEDOT derivative used in the experimental activity of this thesis. PSS is a water-soluble polyelectrolyte which acts as an oxidant removing electrons from the thiophenic rings of PEDOT chain (Figure 2.17). PEDOT thus results positively charged while, consequently, PSS acquires a negative charge leading to a polar blend ($PEDOT^+$:PSS^-) soluble in organic polar solvents as H_2O, called *poly(3,4-ethylenedioxythiophene):poly(styrene sulfonate)* (PEDOT:PSS). The solubility of PEDOT is not the only effect of the PSS doping. A lowering in conductivity of PEDOT:PSS compared to PEDOT until values under 1 S/m in solid state thin films was observed [13]. The explanation of such effect concerns the formation of large insulating

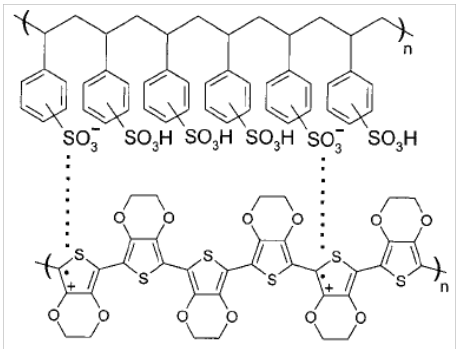

Figure 2.17: Chemical structure of PEDOT:PSS blend. [11]

PSS regions surrounding conductive spots of PEDOT when PEDOT:PSS is deposited in thin films [14]. The electrical conduction in a PEDOT:PSS thin film is thus opposed by the PSS walls between PEDOT grains.

PEDOT:PSS treatment with ethylene glycol

It was discovered that the conductivity of a PEDOT:PSS film can be enhanced by over 100-times adding some organic compounds, e.g. methyl sulfoxide (DMSO), N,N-dimethyl formamide (DMF) [15], glycerol, sorbitol [16], to the PEDOT:PSS aqueous solution. Some studies also proposed a treatment of PEDOT:PSS with *ethylene glycol* (EG), which not only has the effect of enhancing the electrical conductivity of the film over 200-folds, but also it renders the PEDOT:PSS treated film insoluble in water. The mechanism responsible for this conductivity enhancement is quite controversial. Crispin et al.[12] suggested that EG induces a reduction of PEDOT:PSS particles size leading to thinner insulating PSS layer around conductive PEDOT grains. Conversely Ouyang et al.[13] proposed that the addiction of EG causes a conformational change in PEDOT chains, which changes from coil to linear structure (Figure 2.18 left). This change is induced by the transformation of the PEDOT chain resonant structure from a benzoid to a quinoid structure (Figure 2.18 right), the benzoid structure is the favourite for a coil conformation of PEDOT chain, while the quinoid one is the favourite for a linear or expanded-coil conformation. Since the interaction forces among PEDOT chain in linear structure are stronger than those in coil structure, such transformation leads to an increase of the interchain interaction, resulting in both conductivity enhancement and

insolubility of EG-treated PEDOT:PSS. It is noteworthy that these effects have been observed both by adding EG into PEDOT:PSS aqueous solution and by immersing dried PEDOT:PSS film in EG for a few minutes [13]. The insolubility of EG-PEDOT:PSS

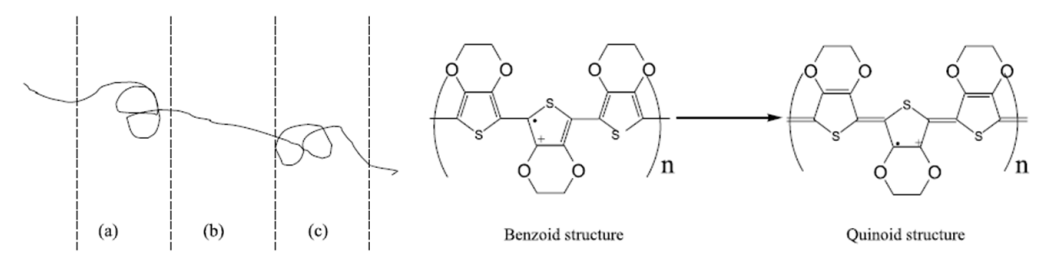

Figure 2.18: (Left) Schematic of untreated PEDOT chain coil conformation((a) and (c)) and EG-treated PEDOT chain linear conformation. (Right) Scheme of transformation of the PEDOT chain from the benzoid to the quinoid structure. [13]

films becomes a huge advantage in fabricating PEDOT:PSS based devices which have to get in direct contact with aqueous solutions as will be discussed in chapter 3 for the realization of the organic electrochemical transistors reported in this thesis. The high conductivity and the aqueous processability in liquid phase together with the high chemical stability and the optical transparency of PEDOT:PSS, allowed it to become the most used conductive polymer employed in organic electronic applications e.g. in OLEDs, OPVs, and conductive electrodes/contacts in organic transistors.

Inkjet printing of Clevios^{TM} P Jet HC

Clevios^{TM} P Jet HC is the trade name of the PEDOT:PSS-based ink used for the experimental activity presented in this thesis. It was provided by H. C. Starck [17] and actually it is supplied by Heraeus [18]. It is a formulation optimized for inkjet printing applications of *Clevios^{TM} P*, which is a waterborne dispersion of PEDOT:PSS sub-micrometer sized gel particles, which after solvent drying and thermal annealing, form a continuous and transparent conductive film. The physical properties of the ink are reported in Table 2.1. Before filling the cartridge, the Clevios^{TM} P Jet HC formulation, as supplied, was subjected to 15 min ultrasonic bath to assure the re-dispersion of possible particles agglomerates. With the same purpose it was then filtered with a syringe nylon filter. Both these procedures were made in order to avoid nozzles clogging

Physical property	*Range*
Solids content	0.6 - 1.2 %
Conductivity	30 - 90 S/cm
Viscosity	5 - 20 mPa s

Table 2.1: Clevios^{TM} P Jet HC physical properties.

Action	*Time*	*Frequency*	*Post Delay*
Spit	500 ms	1.5 kHz	2 s
Purge	1 s	–	–
Spit	500 ms	1.5 kHz	2 s

Table 2.2: Cleaning cycle procedure used before each printing and during printing when needed.

during printing process. It should be noted that both 0.45 μm and 0.2 μm filters were used and a longer nozzles lifetime was observed employing the 0.2 μm filtered ink. Often keeping the cartridge in rest for about 30 min after the cartridge filling operation may permit the complete dissolution of the foam eventually present in the ink after the sonication procedure. If the air bubbles of the foam reach the nozzle meniscus they may, in fact, occlude it. In order to maintain the nozzles in optimal conditions, cleaning cycles were performed before and, in case of long lasting print processes, also during printing (approximately each 100 scans). The details of the cleaning cycle operations performed before each printing and during printing when needed are reported in Table 2.2. Also during the time the cartridge was idle a Spit operation, during 200 ms at frequency of 1.5 kHz, was performed every 300 s. Despite all these cares are really useful to achieve satisfactory performances, printing of Clevios^{TM} P Jet HC ink is quite problematic in terms of reproducibility of jetting performances and cartridge lifetime because misdirected jetting and nozzle clogging occur frequently and rarely can be adjusted. The observed average life time of a cartridge filled with Clevios^{TM} P Jet HC ink is 2 days, however if very long resting time is planned (e.g. all night long), it is advisable to keep the nozzle plate in contact with deionized water while the cartridge is idle. However, this procedure could cause the complete empting of the fluid module. Table 2.3 reports the optimized cartridge and printer main settings used in

Main settings	
Firing Voltages range	15 - 18 V
Cartridge Print Heigh	500 μm
Platen Temperature	40 - 60 °C
Cartridge Temperature	RT - 30 °C
Maximum Jetting Frequency range	5 - 25 kHz

Table 2.3: Main cartridge and printer settings used in printing Clevios^{TM} P Jet HC ink.

printing Clevios^{TM} P Jet HC ink. During printing, the platen was heated until 60 °C in order to promote fast solvent drying, and to reduce ink spreading on the substrate. If printing is planned to be long lasting (e.g. if many devices have to be printed, if pattern is large or if the process is quite slow due to few nozzles or low jetting frequency used) it was observed that keeping the platen at lower temperature (40 °C) may avoid solvent evaporation at the nozzles meniscus which can cause misdirected jets and in the worst case clogging of some nozzles. For the same reason in this case it is advisable to set the cartridge temperature at values equal or lower than 30 °C. The choice of some settings as the number of printing nozzles, the maximum jetting frequency and the drop spacing are strictly correlated to the specific pattern printed and to the substrate used, as discussed in the following subsection.

Optimization of printing parameters for different pattern's geometries

Three kinds of pattern were realized by means of inkjet printing of PEDOT:PSS-based ink:

- *Gate electrodes of Organic Field Effect Transistors*: such structures, printed on 175 μm thick PET substrate using a DMC-11610 cartridge, consist in rectangular patterns of various sizes, depending on the particular OFETs array which has to be realized: typical used sizes are 1 cm × 5 cm for linear-channel OFETs and 5 mm × 5 cm (or less) for intedigitated-channel OFETs. Since high resolution is not essential while film continuity and high conductivity are required for the gate electrode pattern, it was printed using all the available 16 nozzles and the highest achievable jetting frequency (25 kHz) in order to get highest possible throughput and overlapping from 2 to 4 ink-jetted PEDOT layers with a drop spacing of 20

μm to achieve a highly conductive contact. Between two subsequent printing 3 minutes were waited to allow partial drying of the previously printed layer. Since the printing process may be long-lasting (because usually several patterns were printed and their size was quite large), generally cleaning cycles were performed during printing and the cartridge was kept at a constant temperature of 30 °C in order to avoid nozzle clogging. Figure 2.19 shows two details of the first and the second printed layers of a PEDOT:PSS gate electrode realized. After printing,

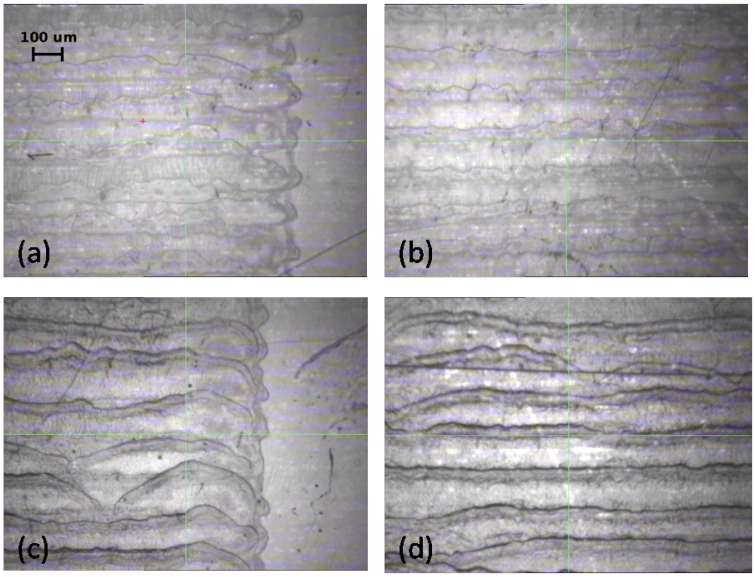

Figure 2.19: Optical images, taken by means of the Fiducial Camera, of the printed PEDOT:PSS gate electrode of OFETs realized: first layer of deposited material at the edge with PET substrate (a) and inwards of the printed pattern; subsequent second printed layer (c and d).

samples were annealed at 60 °C on a hot plate or in a oven for at least 8 h to allow complete evaporation of the solvent.

- *Source and Drain electrodes of Organic Field Effect Transistors*: printing OFETs source and drain electrodes is much more problematic. The pattern usually consists in two (for the realization of linear channel OFETs) or more (for interdigitated channel OFETs) thin conductive stripes. The separation space between the stripes determines the channel length of the final transistor realized (see Figure 2.20). The source and drain single layer electrodes were patterned on Parylene

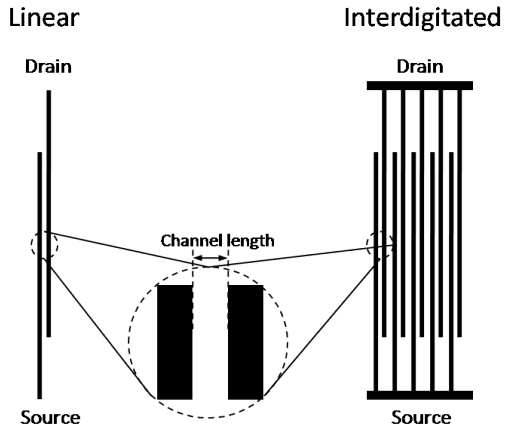

Figure 2.20: Schematic of the pattern used to print source and drain OFET electrodes both for linear and interdigitated devices. The inset shows a zoom view of the channel region.

coated PET substrate using 2 adjacent nozzles of a DMC-11610 cartridge. Printing with only 1 nozzle proved to be hazardous because the clogging of the jetting nozzle used during printing led to an incomplete final printed pattern. It was found that printing in vertical direction permits to achieve more accurate drop deposition and, consequently, higher resolution of printed patterns. In order to guarantee continuity and good conductivity of each single stripe a drop spacing of 5 μm was used. A cleaning cycle was performed only just before printing; it is absolutely not suitable to perform cleaning cycles also during printing because in the cleaning procedures the nozzle plate can be slightly moved resulting in misaligned printed stripes. During printing the cartridge was kept at RT and the platen at 60 °C to promote fast solvent drying and, subsequently, to reduce ink spreading on the substrate. The maximum jetting frequency was setted at 25 kHz avoiding long lasting of the process. An excessive time spent by the nozzle plate over the heated platen, in fact, could damage the used nozzles due to solvent evaporation at the nozzle meniscus. With such settings channel lengths in the range of 120 - 160 μm were achieved. In Figure 2.21 an optical image of source and drain electrodes printed in linear configuration are shown, while Figure 2.22 reports two different details of interdigitated structures realized. The attempts made with the aim to obtain shorter channels failed, mainly because

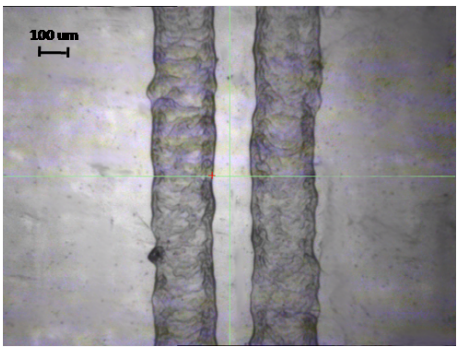

Figure 2.21: Optical image of source and drain PEDOT:PSS electrodes of linear channel OFET. Channel length: 135 μm.

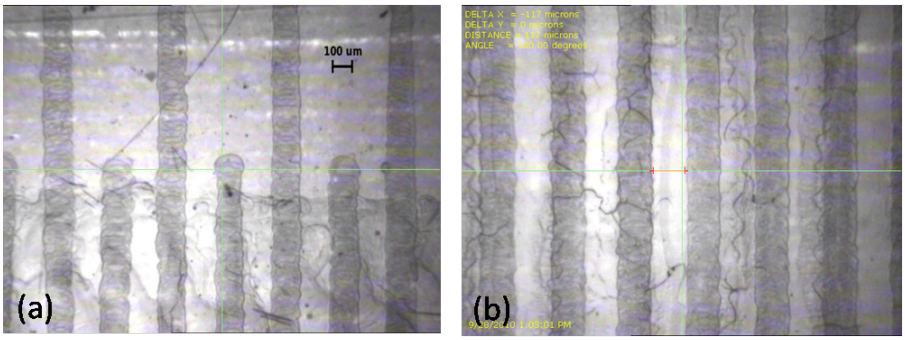

Figure 2.22: (a, b) Two optical images of interdigitated source and drain PEDOT:PSS printed electrodes. The channel length achieved is 120 μm.

fluctuations in droplets jetted direction flight, caused by changing of wetting condition around the nozzles, induce irregularity in printed patterns leading to the formation of short circuits between source and drain electrodes. This effect has also been observed by Kawase et al.[19]. With the same purpose it was tried to print patterns employing the DMC-11601 cartridge, dispensing lower volume droplets (1 pL). In this case the formulation of the ink had to be modified since it was observed that employment of Clevios^{TM} P Jet HC ink as supplied caused sudden clogging of the nozzles. The recipe used consisted in Clevios^{TM} P Jet HC, with adding of 25%v/v ethylene glycol and 0.6%v/v dodecylbenzene sulfonic acid (DBSA). The mixture was stirred for 15 min at room temperature, then it was subjected to 2 h ultrasonic bath and finally it was filtrated through a 0.2 μm nylon filter before filling the DMC-11601 cartridge. The pattern printed in a interdigitate configuration and showed in Figure 2.23, was achieved employing 3 jetting nozzles with a firing voltage of 8 V, a maximum jetting frequency of 25 kHz and a drop spacing of 5 μm. An average channel length of 50 μm was achieved. Unfortunately, devices realized with such a structure exhibited a current of the order of tens of microAmpere when tens of volts was applied between source and drain electrodes, even if no short circuit between the electrodes was visible by means of an optical microscopy.

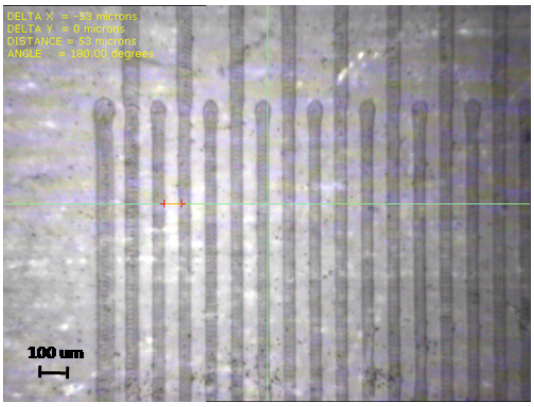

Figure 2.23: Interdigitated source and drain PEDOT:PSS electrodes, printed with a cartridge ejecting 1 pL drops, with a channel length of 50 μm.

- *Electrodes and active layer of Organic ElectroChemical Transistors*: also this kind

of devices were assembled on transparent and flexible PET sheets and again before filling the cartridge, the PEDOT:PSS aqueous dispersion was treated in ultrasonic bath for 15 min and filtered with a 0.2 μm nylon filter. The device structure is much simpler in this case. Device planar layout, in three different geometries, is depicted in Figure 2.24: source, drain and gate electrodes are all made of an inkjet printed highly conductive PEDOT:PSS film. In this kind of structure source and drain are interconnected forming a unique electrode (further details can be found in chapter 3). The three geometries realized differs from the ratio between the gate and the channel areas (Ag/Ach) as displayed in Figure 2.24. The planar pattern was printed with a drop spacing in the range 15 - 20 μm in order to minimize ink spreading on the substrate and was realized overlapping 2, 3 or 4 PEDOT:PSS printed layers, waiting for 60 s between two subsequent printed layers. Usually 8 nozzles and a maximum jetting frequency of 25 kHz were used.

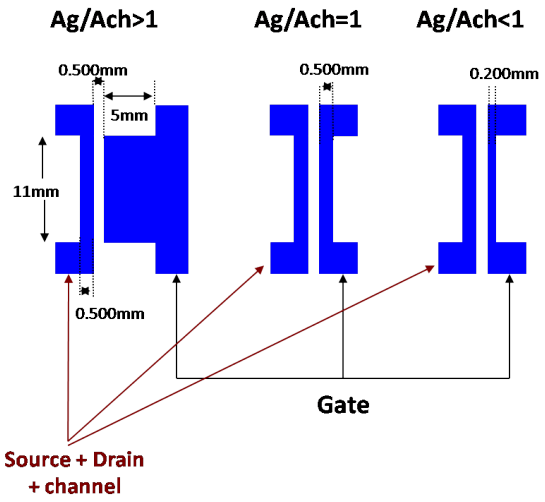

Figure 2.24: Schematic of the three geometries patterns with different gate to channel areas ratio.

Sometimes a lower jetting frequency (until 5 kHz) should be required in order to improve a higher level of accuracy in droplets deposition. During printing, the substrate was kept at a constant temperature of 60 °C and the cartridge at 30 °C. With such settings a cleaning cycle was performed at the beginning of the printing process and generally no cleaning procedure was needed during printing.

Chemical name	*Weight %*
Ethanol	10 - 70
Ethylene Glycol	10 - 40
Silver	2 - 30

Table 2.4: Chemical composition of Cabot Conductive Ink CCI-300.

After printing, solvent was let dry on a hot plate for 8 h always at 60 °C. In Figure 2.25 a photo, taken by means of an optical microscopy with magnification of 5×, of the channel region of a 2 layer inkjet printed OECT device (Ag/Ach < 1) is reported.

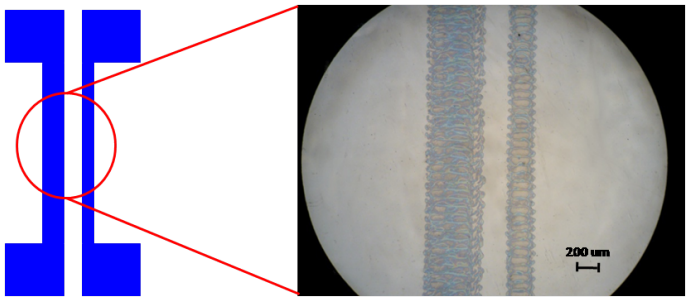

Figure 2.25: Detail of the channel region (taken by means of an optical microscopy with magnification of 5×) of a 2 layer inkjet printed OECT device with Ag/Ach < 1.

2.3.2 Silver ink

The silver-based ink used in the experimental activity presented in this thesis, supplied by Cabot Corporation [20] with the trade name of *Cabot Conductive Ink CCI-300*, is designed for piezoelectric inkjet printing of conductive features on several substrates. It contains surface modified ultra-fine silver nanoparticles in a liquid vehicle composed of ethanol and ethylene glycol in proportion reported in Table 2.4. In Table 2.5 instead the physical properties of CCI-300 ink as provided by the supplier are reported. As PEDOT:PSS-based ink, also CCI-300 was subjected to 15 min ultrasonic bath and 0.2 μm filtering before filling the cartridge. Generally a cleaning cycle as that reported in Table 2.2 was performed just before printing and never during printing process. In fact printing performances employing CCI-300 ink are surely much more effective

Physical property	*Range*
Silver solid loading	19 - 21 wt%
Density	1.23 - 1.24 g/mL
Surface Tension at 25 °C	30 - 33 mN/m
Viscosity at 22 °C	11 - 15 cP
Bulk resistivity	4 - 80 $\mu\Omega$ cm

Table 2.5: Physical properties of Cabot Conductive Ink CCI-300.

Main Settings	DMP-11610	DMP-11601
Firing Voltages range	20 - 30 V	12 - 15 V
Cartridge Print Heigh	1 mm	1 mm
Platen Temperature	60 °C	60 °C
Cartridge Temperature	RT	RT
Maximum Jetting Frequency range	2 - 25 kHz	10 kHz

Table 2.6: Main cartridge and printer settings used in printing Cabot Conductive Ink CCI-300 using both DMP-11610 and DMP-11601 cartridge.

than those achieved employing PEDOT:PSS based ink. First of all clogging of nozzles is less frequent, jetting performances are more reproducible and one single cartridge can be easily used until the complete emptying of the fluid module. Nevertheless, if structures which require high precision in droplets position have to be printed, it is highly recommendable to a new or at least previously not intensively used cartridge. The main settings optimized for inkjet printing of CCI-300 using both DMC-11610 and DMC-11601 cartridges are summarized in Table 2.6. The firing voltage range used is wide in this case since the optimal value strongly depends on the age of the cartridge and on the particular pattern to print. Figure 2.26 shows a comparison of the stroboscopic view of a droplet formation, employing a DMP-11610 cartridge, at 5 kHz with a firing voltage of 17 V and with a firing voltage of 22 V. It should be noted that a higher voltage leads to a higher drop velocity and to the formation of a long tail. These features are not suitable if high precision is required, but they prevent clogging of jetting nozzles. Conversely, lower voltage provides a slower spherical droplet. With this condition the ink spreading at the impact with the substrate is reduced, leading

to a better resolution of the printed pattern, but the clogging of the jetting nozzles can occur easier, especially if high jetting frequency is used.

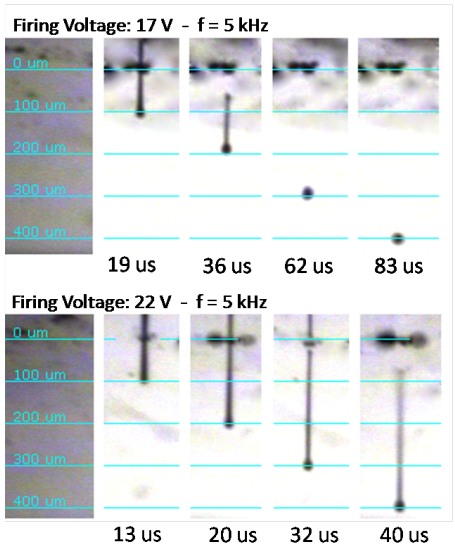

Figure 2.26: Stroboscopic images, taken by means of the Drop Watcher tool, of the emission of a CCI-300 ink droplet at a jetting frequency of 5 kHz with a firing voltage of 17 V (top) and 22 V (bottom). A higher voltage leads to the formation of a fast droplet with a visible tail, while applying a lower voltage, a slow spherical drop is ejected.

Optimization of printing parameters for different pattern's geometries

- *Gate electrodes of Organic Field Effect Transistors*: as for PEDOT:PSS gate electrodes described in the previous subsection, also the realization of silver gate electrodes does not require high resolution. They were printed, using a DMP-11610 cartridge, on different substrates: 175 μm, 50 μm, 13 μm thick PET films, 125 μm thick PEN film and 13 μm thick Kapton film. Fortunately, the main difference in printing CCI-300 ink onto these different substrates doesn't concern the cartridge and printer settings but the time and temperature of post printing annealing procedure. In fact, all PET substrates have to be annealed at temperature below or equal to 60 °C in order to avoid substrate deformation, PEN can be annealed at 80 °C without deformation while Kapton films sustains 100 °C annealing. Obviously a higher annealing temperature leads to faster drying of the solvent and consequently to shorter time of manufacturing: gate electrodes

on PET dried in an averaging time of 12 h, on PEN roughly in 9 h and on Kapton in less than a hour. The printed patterns consist in rectangular stripes of different dimensions, depending on the geometry of the final device. Satisfactory quality of the printed patterns was achieved using 2 nozzles, a drop spacing of 15 μm and a maximum jetting frequency of 25 kHz. Gate structures were always realized printing one single layer. After the annealing step a 1.5 μm thick layer of parylene C was deposited on the whole structure by means of the chemical vapour deposition procedure described in Appendix A.

- *Source and drain electrodes of Organic Field Effect Transistors*: the patterns used in printing source and drain electrodes employing CCI-300 ink are of the same type of that depicted in Figure 2.20. Electrodes, also in this case, were printed onto the surface of the parylene layer which coats the gate electrode and the substrate in order to achieve a bottom-gate/bottom-contact structure of the device. A distinction has to be made between printing source and drain electrodes in linear and in interdigitated configuration. Interdigitated structures were always printed in vertical direction, i.e. perpendicularly to the movement of the print carriage, using 1 single firing nozzle, with a drop spacing of 20 μm. In Figure 2.27 a detail of the structure realized using a firing frequency of 2 kHz is showed. An average channel length of 50 μm was achieved using these settings. Usually more than one interdigitated structure was printed during the

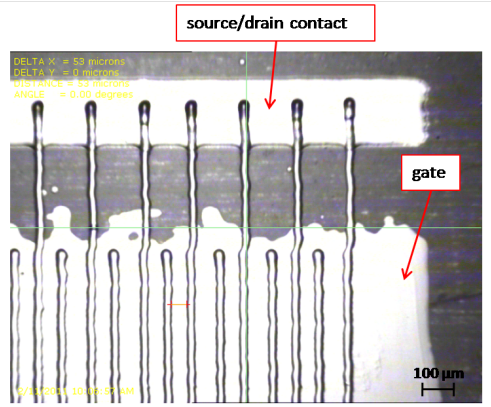

Figure 2.27: Interdigitated source and drain electrodes printed onto the parylene layer which coats the previously printed gate electrode and the substrate.

same printing process, typically arrays of 8 devices placed in a horizontal row were realized. The maximum jetting frequency of the nozzle is the most crucial parameter to set to achieve the best printed pattern quality. If this parameter is set to too high values, when the printer doubled the jetting frequency in a single scan, the piezoelectric crystal could show a delayed response: this effect normally builds up leading to ejection of droplets in the incorrect instant and becoming critical from the printing of the fourth device in a single row. This technical problem hitched the final printed patterns in two ways: short-circuits in the source and drain electrodes and discontinuities in printed silver lines that made up the interdigitated structures (Figure 2.28). By lowering the jetting frequency from 20 kHz to 3 kHz, this effect was suppressed. Unfortunately lowering the frequency involved two main drawbacks i.e. the rise of the duration of the printing process and the increase of inertia in first droplets emission leading to a not optimal pattern quality in the first line of each device. This last problem could be overcome printing dummy lines before each inderdigitated structure. The most

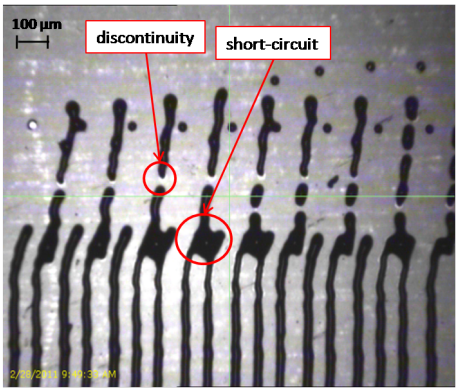

Figure 2.28: Photograph showing problems risen in inkjet printing of interdigitated source and drain electrodes with high jetting frequency: short-circuits between source and drain electrodes and discontinuities in printed silver lines.

important advantage in printing interdigitated structures employing silver-based ink instead of PEDOT:PSS-based ink is surely the higher resolution achieved resulting in the halving of the channel length. On the other hand the water-solubility allows to clean the parylene coated substrate with deionized water to remove PEDOT:PSS bad-printed structures and reuse it (even if this have to

be considered an extreme and not a standard procedure). Washing parylene substrates from silver ink through ethanol baths is instead unfeasible since the parylene changes its surface energy after the treatment becoming much more hydrophobic (this effect is shown in Figure 2.29). As already mentioned also

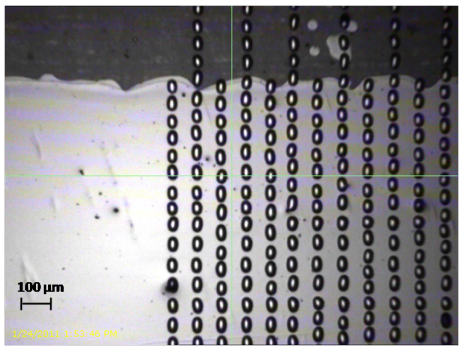

Figure 2.29: Hydrophobicity of parylene surface after washing in ethanol.

linear channel devices were realized. Two different approaches were used for the printing procedure of such structures. The first one was analogous to that used in printing intedigitated structures: one single nozzle of a DMP-11610 cartridge, with a maximum jetting frequency of 5 kHz and a drop spacing of 20 μm was employed to print in vertical direction a linear channel device (shown in Figure 2.30 in a horizontally oriented photograph) with channel length in the range 50 - 60 μm. The second approach was developed with the scope of shortening the

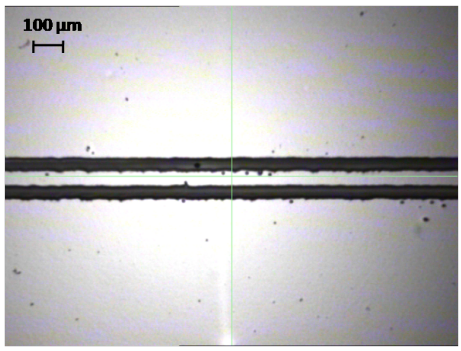

Figure 2.30: Optical image of source and drain silver electrodes of linear channel OTFT. Channel length: 60 μm.

channel length. It comprised two printing steps, as showed in Figure 2.31: the

former consisted in printing a series of narrow (width of 10 μm) parallel stripes using one single nozzle of a DMP-11601 cartridge in horizontal direction i.e. in the direction of the print carriage movement. Drop spacing of 8 μm, firing voltage of 13 V and maximum jetting frequency of 10 kHz were the printing parameters used. After printing, sample annealed for half an hour at 60 °C to permit solidification of the narrow printed stripes; the result of this first step is showed in Figure 2.31 (left). These thin stripes exhibited a resistance of the order of 10^9 Ω, so, they cannot be employed as conductive electrodes. Next two bigger rectangular stripes (width of about 250 μm) were printed above the pre-patterned structure. The dried narrow stripes previously printed constituted a wall for the ink, avoiding spreading effect and thus allowing to achieve a channel length in the range of 30 - 40 μm. In this second printing step one single nozzle of a DMP-11610 cartridge, with a maximum jetting frequency of 10 kHz and a drop spacing of 17 μm, was used. After another thermal annealing at 60 °C for one hour, the final device configuration shown in Figure 2.31 (right) was realized.

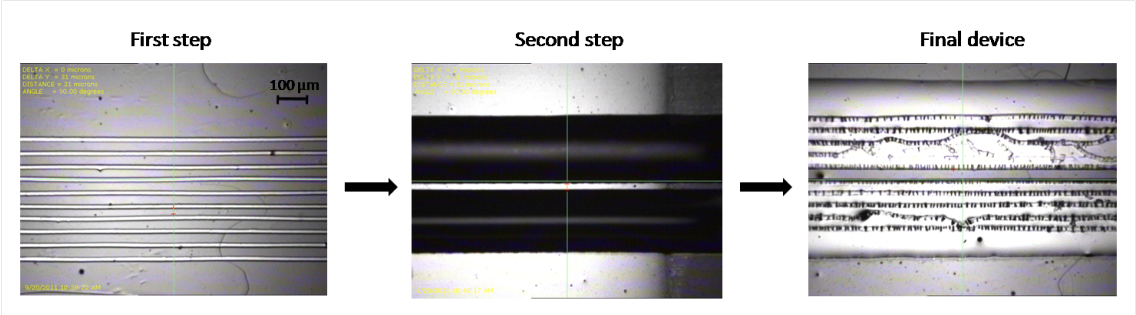

Figure 2.31: Printing steps for the realization of silver source and drain electrodes of linear short channel (L=30 μm) OTFTs.

- *Metal electrodes on PVDF film*: three kinds of pattern were printed, employing the CCI-300 ink, on PVDF 50 μm thick film. The first (Figure 2.32 (a)) consists in 12 circles with a diameter of 3 mm arranged in a triangular shape. The second and the third patterns, shown in Figure 2.32 (b) and (c), were printed on the other side of the substrate, once the pattern (a) was dried. For both patterns 2 jetting nozzles with a firing voltage of 20 V, a drop spacing of 20 μm and a maximum jetting frequency of 5 kHz were used. As already mentioned, the samples were

annealed at 60 °C for several hours in order to avoid substrate deformation. In Figure 2.33 the photos of the three different patterns realized on PVDF are shown.

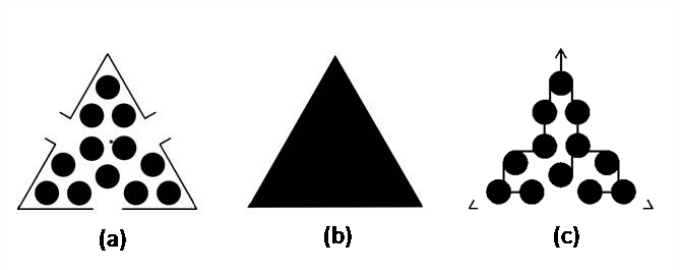

Figure 2.32: Schematics of the three patterns printed on the two sides of PVDF substrate.

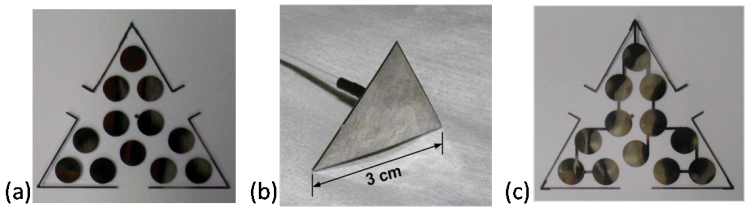

Figure 2.33: Photos of the three different patterns realized on PVDF film employing CCI300 ink.

2.4 Materials: Semiconductor-based inks

As already mentioned, the deposition of organic semiconductors constitutes the final step for the bottom gate-bottom contact OFETs realized. Two p-type soluble organic semiconductors were tested in form of ink: 6,13-bis(triisopropylsilylethynyl)pentacene and poly(3-hexylthiophene). Their properties are described in the following subsections. The description of the printing parameters optimized for the deposition of TIPS-pentacene based inks will be reported in the last section of chapter 4, where the results achieved, which are strictly correlated to the deposition method, will be discussed.

2.4.1 TIPS-pentacene based inks

Pentacene and TIPS-pentacene

Pentacene is the organic semiconductor which exhibits the highest performances in terms of stability and of the measured mobilities (up to 1 cm^2/Vs for polycrystalline pentacene films [21] and up to 30 cm^2/Vs for pentacene single crystals [22]). It is an organic molecule with chemical formula $C_{22}H_{14}$ and with a planar structure composed of five linearly fused benzene rings, depicted in Figure 2.34. It appears, at ambient conditions, as a purple powder and it is typically deposited by means of thermal evaporation, since it shows insolubility in most common organic solvents. It was employed as active layer in some of OTFTs reported in this work and it was deposited through the thermal sublimation equipment described in Appendix A. Pentacene unprocessability in liquid phase represents a huge limitation in terms of its deposition by means of low cost techniques as inkjet printing. Also, pentacene has a crystalline order, often referred to as *herringbone* packing (depicted in Figure 2.36(a)), with only minimal π-stacking which results in a poor dispersion of the electronic bands in the solid, implying that pentacene transport properties may be limited by its crystal packing [23]. In order to overcome

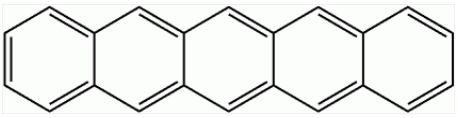

Figure 2.34: Chemical structure of pentacene.

the insolubility issue, several pentacene derivatives have been developed by substitution with different functional groups. By means of such functionalizations, also the tuning of electronic properties, such as charge injection barriers, HOMO-LUMO gaps, charge transfer rates, and molecular ordering of pentacene can be accomplished. Among the pentacene derivatives developed *triisopropylsilylethynyl-substituted (TIPS)* pentacene is the most popular and appropriate for its use in thin-film transistors [25]. Its complete name, *6,13-bis(triisopropylsilylethynyl)pentacene* suggests its chemical structure, depicted in Figure 2.35: the carbon atoms of the triisopropylsilylethynyl chains are chemical bond with the carbon atoms in position 6 and 13 of the pentacene molecule. It has sufficient solubility in common organic solvents (e.g. toluene, chlorobenzene, tetrahydrofuran and chloroform [24]) and, in addition, the bulky functionalized groups

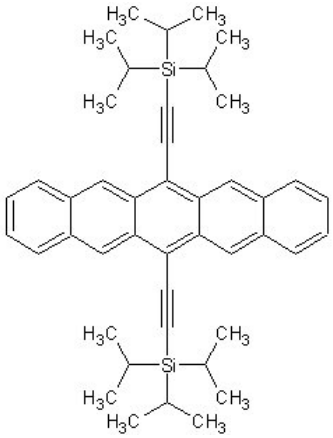

Figure 2.35: Chemical structure of TIPS pentacene.

in TIPS-pentacene efficiently maximize π-orbital overlap [23]. In fact, the bulky group substitution on the central aromatic ring disrupts aromatic edge-to-face interactions, preventing the adoption of the herringbone packing motif, typical of the unsubstituted pentacene crystals: the triple bond between the carbon atoms (see Figure 2.35) allows adjacent molecules to interact in a face-to-face π-stacking orientation, since the substituents are hold away from the aromatic surface. This inter-molecular interaction improves π-orbital coupling and potentially increases the carrier mobility [23][26]. In Figure 2.36 the molecular packing arrangements with average distances between the π-faces in the solid state pentacene (a) and TIPS-pentacene (b) are shown. Thanks to its

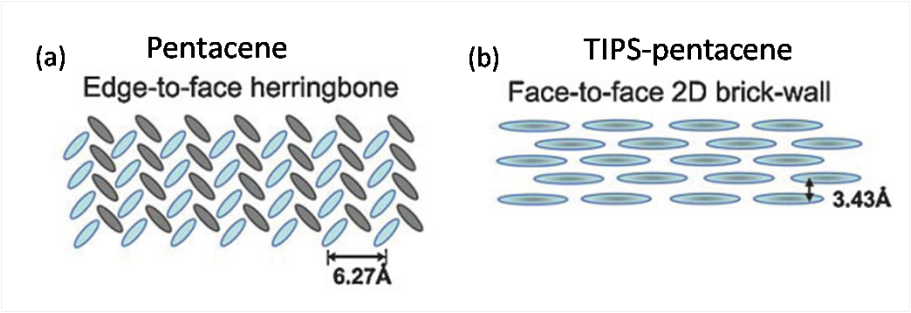

Figure 2.36: Molecular packing arrangements with average distances between the π-faces in the solid state (a) pentacene and (b) TIPS-pentacene. [29]

solubility in a wide range of organic solvents, TIPS-pentacene is commonly spin coated

[26], drop cast [24][27] and inkjet printed [28] in order to constitute the active layer in OTFTs. The electrical characteristics of such devices were found to be highly dependent on processing conditions i.e. the solvent used, the post processing treatment and the deposition method, since they determine the morphology of the deposited semiconductor film [26][29]. The highest electrical performances have been found in transistor with single crystal TIPS-pentacene semiconductor because they are free of grain boundaries and molecular disorder which limit the charge transport through the material. Generally using high boiling point solvent and drop casting allow slower solvent evaporation leading to highly ordered films. Mobilities up to 1.8 cm^2/Vs in drop cast TIPS-pentacene OTFTs are reported in literature [26].

2.4.2 P3HT-based inks

Poly(3-hexylthiophene)

Poly(3-hexylthiophene) (P3HT) is a π-conjugated polymer emerged in last years as a reference semiconducting material for the active layer of polymer field-effect transistors (PFETs) [30]. The 3-hexyl substituents can be placed in the polythiophenic chain with two different regioregularities: head to tail (HT) and head to head (HH) (see Figure 2.37(top)). Regio-random P3HT has both the HH and HT regioregularities randomly distributed, while regioregular P3HT has only one kind of 3-hexylthiophene, either HH or HT (its chemical structure is shown in Figure 2.37(bottom)). The latter showed better ordering and crystallinity in its solid states, and substantially improved electroconductivities; regioregular P3HT (rr-P3HT) is therefore much more utilized as active layer for field-effect transistors [28]. Also it is easily processable in solution with a wide range of organic solvents (e.g. tetrahydrofuran, xylene, toluene, chloroform, chlorobenzene [28]) and can be thus deposited from liquid phase by means of spin coating [32], drop casting, aerosol [33] and either inkjet printing [34]. The charge carrier mobility in P3HT OTFTs is strictly related to the film morphology and the degree of crystallinity. These depend not only on the material intrinsic properties such as regioregularity, molecular weight (MW) and molecular ordering but also on the processing conditions such as surface treatments, thermal treatments, solvents and deposition techniques [35]. Different groups found that charge carrier mobility tends to increase with increasing of molecular weights of P3HT [36][37]; also, generally the

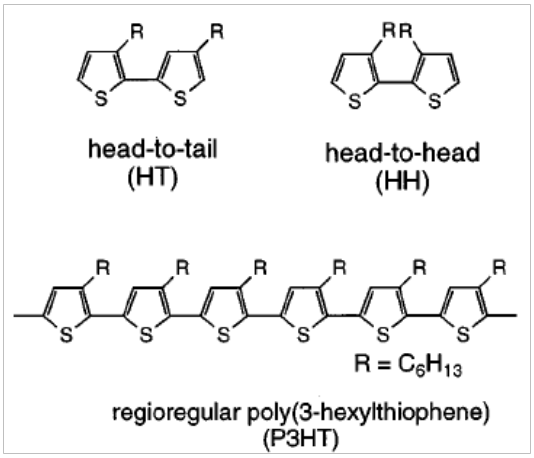

Figure 2.37: Chemical structure of P3HT: (top) schematics of head to tail (HT) and head to head (HH) regioregularity; (bottom) HT regioregular P3HT chain. [28]

mobilities obtained from cast films are higher, because slow evaporation of the solvent enables slower growth of films and, consequently, allows ordering [28]. The highest mobility values reported in literature for P3HT OTFTs is 0.1 cm^2/Vs [30][37].

Inkjet printing of P3HT-based inks

Inkjet printing of a P3HT-based ink resulted a very problematic issue above all for the jetting performances: misdirected jets, clogging of nozzles and not matched velocities of jets occurred very frequently. Several attempts were made changing the concentration of the polymer in different solvents. The best results were achieved using a blend of P3HT (Plexcore® OS 2100; HT-rr>98%, supplied by Rieke Metal) and polystyrene (supplied by Sigma-Aldrich) (20:80 w/w ratio) in a mixed solvent composed of chlorobenzene (CB) and cyclohexanone (CHN) (80:20 v/v ratio) with a solute concentration of 0.5 wt.%. The same solution was used also by Lim et al.[38] in inkjet printing single-drop approach. They suggested that optimization of the solubility of semiconducting component in the blend solution using solvent mixture leads to the formation of semiconductor nanowires with ordered molecular stacking embedded in an insulating polymer matrix in the inkjet-printed single-droplet blend film; the injected holes, thus, can be transported through P3HT nanowires and he insulating matrix protectively encapsulates the nanowires. Our solution stirred for about 3 hours on a hot

Main settings	
Firing Voltages range	12 - 17 V
Cartridge Print Heigh	1 mm
Platen Temperature	RT
Cartridge Temperature	40 °C
Maximum Jetting Frequency	25 kHz
Drop spacing	15 μm
Number of jetting nozzles	16

Table 2.7: Main cartridge and printer settings used in printing P3HT-based ink.

plate at 90 °C, then P3HT-based ink was filtered with a 0.2 μm filter before filling the cartridge and kept at 40 °C while the substrate at room temperature during printing process. A uniform and continuous layer of material covering the whole channel region was deposited employing all the 16 available nozzles of a DMP-11610 cartridge with a jetting frequency of 25 kHz, an average firing voltage of 14.5 V and a drop spacing of 15 μm. The printing parameters are summarized in table 2.7 while an image, taken by means of an optical microscope with magnification of 5×, of the printed P3HT active layer is reported in Figure 2.38. Because of the not optimal jetting performances

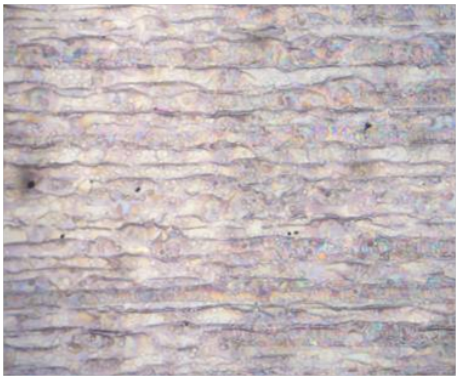

Figure 2.38: Optical image (magnification 5×) of the P3HT/PS (20:80 w/w ratio) blend solution in CB/CHN (80:20 v/v ratio) inkjet printed active layer.

observed with such a ink, often it is advisable to execute cleaning cycles not only at the beginning but also during the printing process. After deposition samples with P3HT as semiconductor were annealed at 130 °C for 1 h in a hot plate.

2.4.3 ActivInk^{TM} 1400 based ink

The *ActivInk^{TM} 1400* is an organic semiconductor provided by Polyera Corporation [39] in form of a dark red powder with purity above 99.5%. It is known that it has a n-type behaviour but its chemical structure is confidential. In this work it was employed only as n-type semiconductor for the realization of an inverter logic gate, as it will be discussed in Chapter 4. It was dissolved in 1,2 dichlorobenzene with concentration of 1% wt.; the solution was then stirred for 1 h at 90 °C and deposited on the device by spin coating at 1500 rpm for 60 s. After semiconductor deposition devices were annealed at 90 °C on a hot plate for at least 2 h.

2.5 Characterization Techniques

In this last section of the second chapter, the experimental techniques used to characterize the morphology and the electrical performances of the fabricated devices are briefly described.

2.5.1 Atomic Force Microscopy

Atomic Force Microscopy (AFM) is an high-resolution type of *Scanning Probe Microscopy* (SPM), a group of surface characterization techniques used to image and measure properties of material surfaces, which includes also the precursor of AFM, the *Scanning Tunnelling Microscopy* (STM). STM was first developed in 1982, at IBM Zurich Research Laboratory, by Binning and Rohrer [40], an invention that earned them the Nobel Prize for Physics in 1986. The basic principle of SPM technology is that of investigate the properties of materials surfaces monitoring the interactions forces between a sharp tip positioned very close (few nanometers) to the studied surface and the surface itself. Binning, Quate and Gerber invented the AFM in 1985 [41] overcoming the main limit of STM, i.e. the possibility to investigate only conductive surfaces. Figure 2.39 shows the schematic of an Atomic Force Microscope. Once the tip placed at the end of a cantilever approaches the surface of interest, the interaction forces rising between the tip and the sample bend the cantilever according to the Hook's law. The amount bending of the cantilever, measured by a laser spot reflected on to a photo detector, can be used to calculate the interaction force. Since the probe moves across the sample surface by means of a piezoelectric ceramics the forces measured are used

to build the morphology of the surface. AFM can be used in three different operation

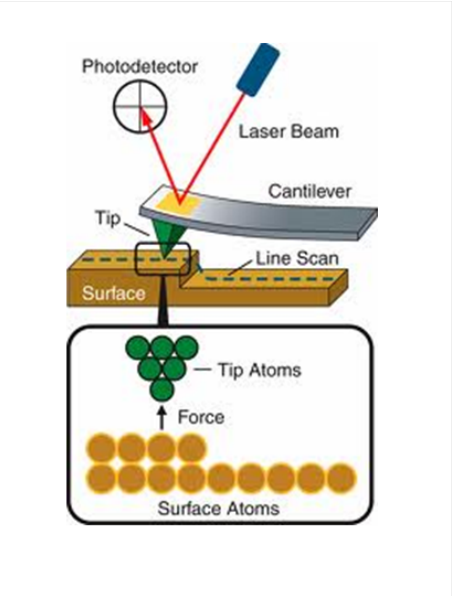

Figure 2.39: Schematic of Atomic Force Microscope.

modes: *contact*, *non-contact* and *semi-contact* or *tapping* modes, only briefly described below, further details can be founded in the reported bibliography [40][41][42][43].

Contact mode

In the Contact mode AFM the deflection of the cantilever is driven by the repulsive forces which arise at a distance of a few angstroms between the atoms of the tip and the atoms of the sample. This operation mode comprises two different working configurations:

- in *constant heigh mode* configuration the tip is kept in physical contact with the sample surface and the piezo-tube is left in the same z position during the scan, therefore the cantilever is deflected as it moves over the surface corrugation: the repulsive forces arising between the electronic clouds of the atoms when they are in contact and the attractive forces at distances longer than a couple of angstroms lead to the deflection of the cantilever which thus accommodates changes in topography. The image is formed analysing the deflections of the cantilever detected by the photodiode.

- in *constant force mode* configuration the interaction force between the tip and the sample is kept constant by means of a feedback circuitry which detects the cantilever deflection and gives the required commands to the piezo-tube (which is free to move vertically) that brings the cantilever deflection back to the imposed initial value. The image is formed monitoring the changes of the piezo-tube along the z-axis.

Non Contact mode

In the Non Contact mode AFM the system vibrates a stiff cantilever near its resonant frequency (typically from 100 to 400 kHz) above the sample with none or little contact between the tip and the sample. The typical distance between the tip and the surface of the sample is in the order of tens to hundreds of angstroms and the amplitude of vibrations is around a few tens of angstroms. The detection mechanism is based on the monitoring of the changes in the resonant frequency or vibration amplitude (dependent on the spring constant of the cantilever and subsequently by the tip-sample interaction forces) as the tip approaches the sample surface: the system keeps it constant thanks to a feedback circuitry which moves the scanner vertically keeping also the distance between the tip and sample constant. As in the previously described contact constant-force mode AFM, the motion of the scanner is used to form the image. Non contact AFM is suitable in investigating soft samples because it reduces degradation and damage risks for the sample. At the same time it provides sub-angstrom vertical resolution of the image, as contact AFM.

Semi-contact mode

Semi-contact mode AFM, also called *tapping* mode, is similar to Non Contact AFM, as also in this operation mode the cantilever vibrates near the surface sample but with the difference that at the bottom of the vibration path the tip hits or *taps* the sample. For some samples this operation mode is more suitable than the contact mode because it limits lateral friction or drag of the tips over the sample surface preventing damage and at the same time it is more effective than the non contact mode for imaging larger scan sizes. [44]
The van der Waals curve in Figure 2.40 shows the operating region for Contact, Non Contact and Semi-contact mode AFM.

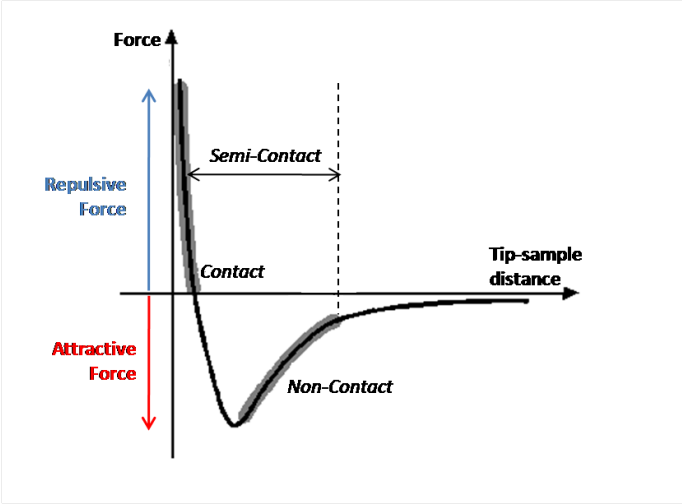

Figure 2.40: Interatomic force vs. distance curve.

2.5.2 X-Ray Diffraction

X-Ray Diffraction (XRD) is a non-destructive technique widely used to investigate the crystallographic structure and chemical composition of materials and thin films. The samples can be both crystalline materials (SC-XRD, *Single Crystal X-Ray Diffraction*) and polycrystalline or powdered solid samples (XRPD, *X-Ray Powder Diffraction*). Since XRPD is the most commonly used, usually it is called simply XRD. The analysis is based on the observation of the scattered intensity pattern produced by the diffraction of an incident X-ray hitting the sample. The diffraction spectra depends on the wavelength of the incident radiation and on the crystallographic structure of the investigated sample. In 1913 Sir W. H. Bragg and his son Sir W. L. Bragg explained the formation of the diffraction pattern from the scattering of a X-ray hitting on a crystalline material developing the notorious relationship, known as the *Bragg's Law*:

$$n\lambda = 2d \sin\theta \tag{2.2}$$

where: θ is the angle of incidence, λ is the wavelength of the incident X-Ray radiation, d is the distance between atomic layers in a crystal and n is an integer. For the determination of the crystal structure of NaCl, ZnS and diamond in 1915 the Braggs was awarded with the Nobel Prize in physics. In Figure 2.41 a schematic visualization of the Bragg's law is reported. When a monochromatic radiation (or subatomic particle

wave) with a wavelength λ comparable to atomic spacings d is incident on a crystalline sample at an angle θ, the Bragg diffraction occurs only when the path length of the rays reflected from successive planes differs by an integer number n of wavelengths [45][46]. This condition of constructive interference (maximum scattered intensity) is satisfied,

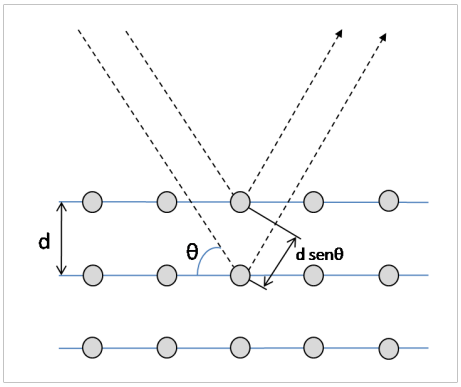

Figure 2.41: Schematic visualization of Bragg's diffraction. The condition for constructive interference i.e. for maximum scattered intensity is satisfied only when the distance travelled by the rays reflected from successive planes differs by an integer number n of λ.

varying the incidence angle θ, by different d-spacing in polycrystalline materials, thus allowing to understand the crystallographic structure of the investigated material. The intensity of the diffraction peaks plotted in function of θ constitutes the *diffractogram*, a graph which characterizes the sample. A typical diffractometer consists of a source of radiation, a monochromator to choose the wavelength, slits to adjust the shape of the beam, the sample and a detector. Also a goniometer is used for fine adjustment of the sample and the detector positions [47]. The most used kind of diffractometer for thin film and powdered sample investigation is the $\theta/2\theta$ *diffractometer*. In such system the sample is located in the centre of the instrument, the x-ray beam is directed on the sample surface with an incidence angle θ and at the same angle the detector monitors the scattered radiation [48]. Such a kind of diffractometer operates in two different scan configurations, which differs in the mutual position and angular velocity of the source/sample and the detector: in the $\theta/2\theta$ *scan configuration* the sample and the detector move with an angular velocity of $\dot{\theta}$ and $2\dot{\theta}$ respectively, while in the θ/θ *scan configuration* the source and the detector move with the same angular velocity $\dot{\theta}$ [49]. The rotations are performed by the goniometer, which is the central part

of a diffractometer. Typically the sample is mounted on the rotational axis, while the detector and/or x-ray source move along the periphery, but both axes of rotation coincide. [50][51]

2.5.3 Photocurrent Spectroscopy

The experimental technique named *photocurrent spectroscopy* is based on the opto-electronic phenomenon of photoconductivity, i.e. the increase of the electrical conductivity of a material when it is exposed to electromagnetic radiation (visible light, ultra-violet light, infrared light, or gamma radiation). Essentially the physical phenomenon of photoconduction in a semiconductor is based on the absorption of a photon by an electron (*internal photoelectric effect*). If the photon energy is high enough, the photon absorption causes the excitation of the electron across the forbidden bandgap i.e. from the valence band to the conduction band in inorganic semiconductors, and from HOMO to LUMO in organic semiconductors. Also transition from impurity levels eventually present in the bandgap can occur and they correspond to absorption of radiation with energy lower than the bandgap. It should be noted that, since in an organic molecule several anti-bonding orbitals are present (LUMO representing the lowest one), the absorption of radiation with energy higher than the bandgap corresponds to transitions between higher energy levels for an organic semiconductor. Thus, when electromagnetic radiation is absorbed by a material such as a semiconductor, the number of free electrons and holes changes and raises its electrical conductivity. In fact, when a load resistor is used in series with the semiconductor and a bias voltage is applied to the circuit, a voltage drop across the load resistors can be measured as the change in electrical conductivity of the semiconductor varies the current flowing through the circuit. This current is named *photocurrent*. The conductivity of a semiconductor in darkness condition can be expressed as function of electron end holes concentration, indicated with n_0 and p_0 respectively, as follows:

$$\sigma = e(n\mu_n + p\mu_p) \tag{2.3}$$

where e is the electronic charge and $\mu_{n/p}$ is the electrons/holes mobility. When the material is exposed to an electromagnetic radiation with an appropriate energy, the absorption of a photon results in the generation of an electron-hole pair and thus in an

increase of the conductivity:

$$\sigma + \Delta\sigma = e[(n + \Delta n)\mu_n + (p + \Delta p)\mu_p)] \tag{2.4}$$

Consequently, the current density $J = \sigma E$, where E is the electrical field applied, increases to the value:

$$J = (\sigma + \Delta\sigma)E = J_{bulk} + J_{ph} \tag{2.5}$$

Through the measurement of the variation of J in the sample is therefore possible to detect the light absorption by the material. Indeed, when a photon is absorbed by an organic semiconductor the formation of an electron-hole pair is not so easy as for inorganic materials. In fact the absorbed photon can be emitted immediately by the material or an exciton can be created. An exciton is a bound state of an electron and a hole, which in inorganic semiconductors has a weak binding force (1 meV to 20 meV), and so it can easily dissociate forming an electron-hole pair, while in organic semiconductors the excitonic bond is stronger (between 100 eV and 300 eV). Typically, the presence of two different polaronic states on distinct molecules is required in order to generate the photocurrent signal. Also, once generated, the electron-hole pair has an average life time τ, at the end of which the charge carriers are not more available for conduction. τ is affected above all by recombination processes due to the presence of trap levels in the forbidden gap. The recombination processes can decrease τ until a critical value, under which no photocurrent signal can be detected. Also, traps can bond charge carrier only for a certain time (which depends on the energy associated to the trap in the band gap) but also in this case the macroscopic effect will be a decrease in the detectable photocurrent due to charge trapping. [48] [52]

Experimental set-up

In Figure 2.42 the block diagram of the experimental set-up used for PC measurements performed at the University of Bologna is reported. As radiation source a *QTH (Quartz Tungsten Halogen) lamp* (22 V, 150 W) is employed. The white light produced by the lamp is collected by a *Cornerstone 260 monochromator* (spectral resolution $\Delta\lambda$=1 nm), which selects the output wavelength radiation by means of a rotating diffraction grid and projects it on the sample through a system of optical mirrors. Two slits are located at the entry and at the exit of the monochromator in order to collimate the light beam, in particular we used 500 μm window slits. Between the lamp and the monochromator

a *chopper* (a dark disk with periodic holes rating in order to chop the incident light beam) is placed. A photodiode mounted on the chopper thus gives a reference square wave signal, corresponding to the dark/light alternative periods (frequency=16 Hz), to a *Stanford Research 530 lock-in amplifier*, which basically makes the sampling of the alternate signal from the photodiode, in order to separate the signal from the noise generated by the measuring system. The circuit employed is reported in Figure 2.43: it

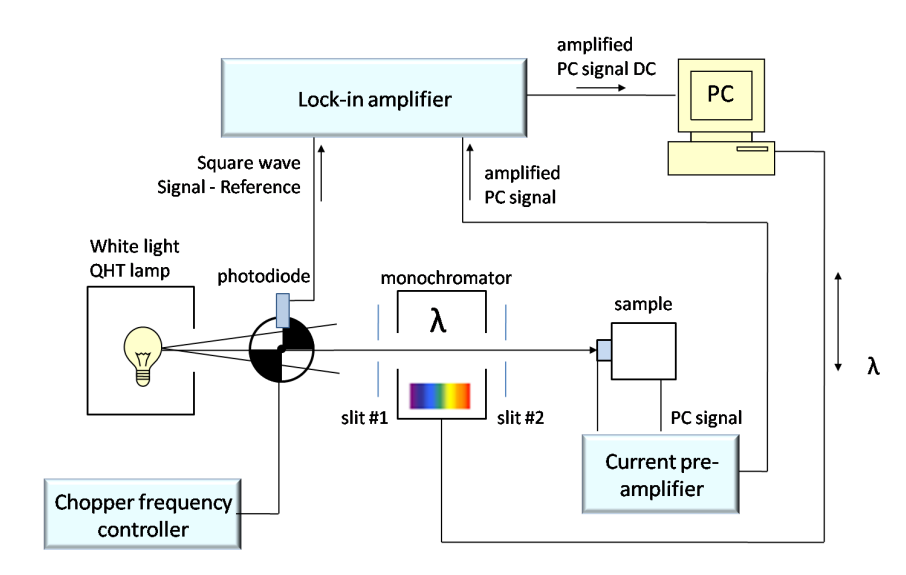

Figure 2.42: Block diagram of photocurrent experimental set-up.

is biased with a 1.5 V chemical battery, a load resistance of 100 kΩ and a capacitance of 4 nF are employed. The capacitance in parallel with the resistance constitutes a low pass filter in order to cut the high frequencies and do not let them enter the lock-in amplifier. The PC signal, i.e. the voltage drop in the load resistance, is collected by a *Keithley 428 current pre-amplifier* and sent to the lock-in in input. The amplified DC signal is then sent by the lock-in to a personal computer, which records it. The collected photocurrent spectra have to be normalized to the intensity of light incident on the sample, since it varies with the wavelength. For the measure of light intensity spectrum we used a thermopile, a thermal detector which consists in a series connection of a certain number of thermocouple junction. A thermocouple junction consists of two different metals connected in series. To detect the radiation, one junction is blackened to absorb the radiation. The temperature rise of the junction generates a voltage. An increase

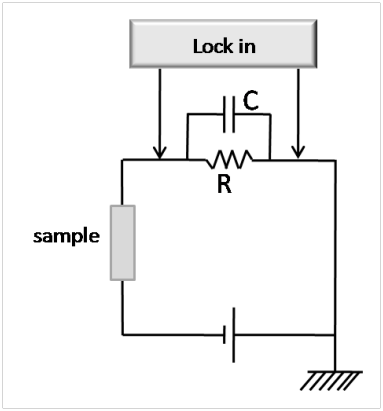

Figure 2.43: Electrical circuit employed in PC measurements.

in the output voltage is obtained by increasing the number of thermocouple junctions. The thermopile thus senses the light intensity converting the incident radiation into a temperature variation. In Figure 2.44 the voltage spectrum of the light intensity as a function of the incident wavelength is reported. Using the thermopile voltage spectrum,

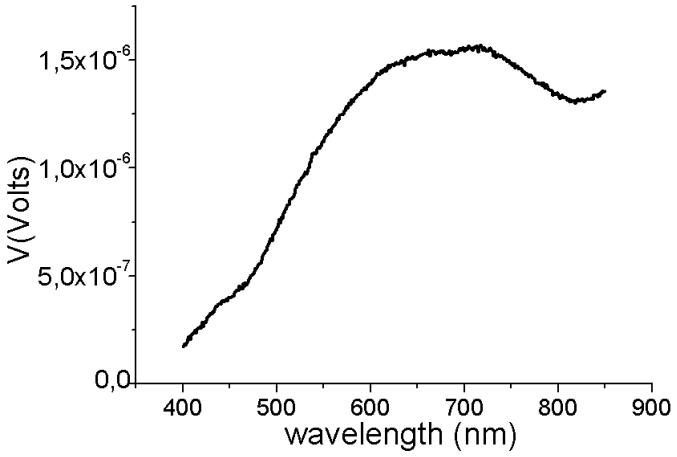

Figure 2.44: Voltage spectrum of incident light intensity with input and output slits width of 500 μm.

also the flux of photons incident on the sample is achievable through the relation:

$$\Phi = \frac{signal}{rA_{tp}h\nu} \tag{2.6}$$

where r=7.8 μV/μW is the thermopile responsivity, A_{tp}=0.0078 cm^2 is the thermopile area and $h\nu$ is the energy of the incident photon. In Figure 2.45 the photon flux incident on the sample is reported.

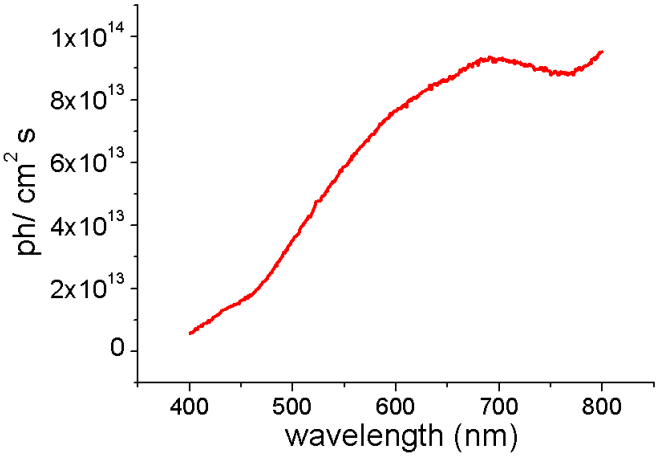

Figure 2.45: Photon flux spectrum of incident light intensity with input and output slits width of 500 μm.

2.5.4 Optical Absorption Measures

The *optical absorption measurement* is another indirect method of investigation of the internal photoelectric effect described in the previous subsection. It consists in the measure of the intensity of the radiation transmitted by the sample I_t when a monochromatic light beam with intensity I_0 strikes on it. Two different parameters can be thus defined: the transmittance $T_\lambda = I_t/I_0$ and the absorptance $A_\lambda = (I_t - I_0)/I_0$, which give information about the photo-induced electronic transitions in the organic molecules.

Experimental set-up

The experimental equipment used for the absorption measurements is quite similar to that employed for the photocurrent ones and it is reported in Figure 2.46. Also these measures have been performed in the PHOS laboratories at the University of Bologna. The white light emitted by a QTH lamp (23 V, 100 W) used as light source, passes

through a chopper rotating with a frequency of 13 Hz, which gives the reference square wave to a *Stanford Research 830 lock-in amplifier*. The choppered light is collected by a *500M SPEX monochromator* (spectral resolution $\Delta\lambda = 0.02$ nm) and then the monochromatic radiation selected is focussed on the sample. Two slits (width = 2000 μm) located at the entry and at the exit o in the monochromator have been used to collimate the light beam. In back of the sample a *pyroelectric sensor* (powered with a 9 V battery) collects the radiation transmitted by the sample and transmits the produced voltage signal to the lock-in. The amplified DC signal is finally recorded by a personal computer. In particular we used a lithium tantalate ($LiTaO_3$) based

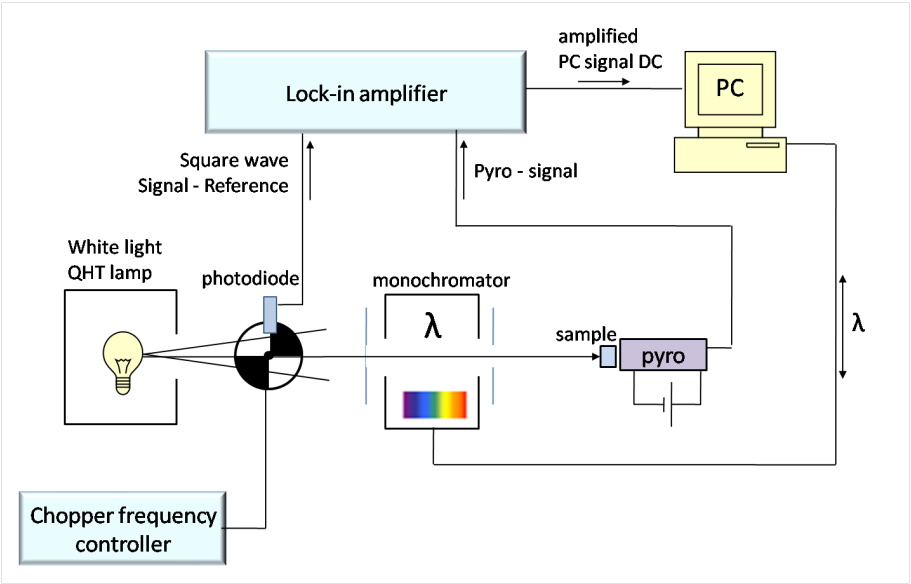

Figure 2.46: Block diagram of optical absorption experimental setup.

pyroelectric detector. In pyroelectric materials, as $LiTaO_3$, the change in temperature modifies the positions of the atoms slightly within the crystal structure, such that the internal polarization of the material changes. This polarization change gives rise to a voltage across the crystal [47]. Pyroelectric sensors are typically constituted by some pyroelectric crystals placed between two electrodes forming a planar capacitor. When light radiation is applied, the temperature of pyroelectric crystals increases by fractions of a degree centigrade, the consequent rise of voltage propagates to the capacitor plates reflecting the intensity of the incident radiation. The responsivity of the employed sensor is r= 300 V/W.

2.5.5 Electrical Characterization

Two kinds of electrical characterization of the devices realized were executed:

Temperature-dependent resistance measurements

The temperature-dependent resistance measurements were performed on PEDOT:PSS printed sample using the two probes method. The sample was kept in a vacuum chamber and brought to the desired temperature in the $25 \div -100\,^{\circ}\mathrm{C}$ range using a *ASCON 1/16 DIN - 48×48 mm Temperature Controller*. Both a *Keithley 2400 source meter* and a *Keithley 6517 electrometer* were employed in the measurements. From a comparison of two- and four-terminal measurements, the latter carried out only at room temperature, the contact resistance was found to be the 10% of the value measured with the two probes method.

OTFTs current-voltage characteristics

The electrical measurements on OTFTs were carried out in air, at room temperature, using two *Keithley 2600 source meters* controlled by Labview software. In order to power an OTFT, two voltages have to be applied to the device: the drain voltage V_{ds} and the gate voltage V_{gs} (both referred to the usually grounded source electrode). The complete electrical characterization of the transistor includes the acquisition of two different curves:

1. the I_{ds} vs V_{ds} curve, named *output characteristic*, where the gate voltage is kept constant while the drain voltage is swept in a proper range. Usually I_{ds} vs V_{ds} characteristics for different values of V_{gs} are recorded.

2. the I_{ds} vs V_{gs} curve, named *transfer characteristic*, where the drain voltage is kept constant while the gate voltage is swept in a proper range. During such a measure also the current flowing between the gate and the source electrodes (I_{gs}) is collected in order to monitor possible leakage phenomena.

Bibliography

[1] www.dimatix.com 40

[2] *Dimatix Materials Printer DMP-2800 Series User Manual*, FUJIFILM Dimatix, **2008**. 40, 41, 43

[3] S. Lilliu, *private communication.* 45

[4] Website of Goodfellow company: *http://www.goodfellow.com.* 49, 50, 51

[5] Website of DuPont company: *http://www2.dupont.com.* 51

[6] C. A. Harper, E. M. Petrie, *Plastics materials and processes: a concise encyclopaedia*, John Wiley & Sons, **2003**. ISBN: 0471456039. 53

[7] C. Kärnfelt, C. Tegnander, J. Rudnicki, J. P. Starski, A. Emrich, *IEEE T. Microw. Theory*, **2006**, 54, 3417-3425. 53

[8] J. J. Licari, *Coating materials for electronic applications: polymers, processes, reliability, testing*, William Andrew, **2003**. ISBN: 0815514921. 54

[9] Bayer AG, Eur. Patent 339 340, **1988**. 55

[10] F. Jonas, L. Schrader, *Synth. Met.*, **1991**, 821, 41-43.

[11] L. Groenendaal, F. Jonas, D. Freitag, H. Pielartzik, J. R. Reynolds, *Adv. Mater.*, **2000**, 12, 7, 481-494. 55, 56

[12] X. Crispin, S. Marciniak, W. Osikowicz, G. Zotti, A. W. Denier van der Gon, F. Louwet, M. Fahlman, L. Groenendaal, F. de Schryver, W. R. Salaneck, *J. Polym. Sci., Polym. Phys.*, **2003**, 41, 2561. 56

[13] J. Ouyang, Q. Xu, C-W Chu, Y. Yang, G. Li, J. Shinar, *Polymer*, **2004**, 45, 8443-8450. 55, 56, 57

[14] H. J. Lee, J. Lee, S. Park, *J. Phys. Chem. B*, **2010**, 114, 2660-2666. 56

[15] J. Y. Kim, J. H. Jung, D. E. Lee, J. Joo, *Synt. Met.*, **2002**, 126, 311-316. 56

[16] S. K. M. Jönsson, J. Birgerson, X. Crispin, G. Greczynski, W. Osikowicz, A. W. Denier van der Gon, W. R. Salaneck , M. Fahlman, *Synt. Met.*, **2003**, 139, 1-10. 56

BIBLIOGRAPHY

[17] http://www.hcstarck.com/en/home.html 57

[18] http://www.heraeus.com/en/home/default.html 57

[19] T. Kawase, T. Shimoda, C. Newsome, H. Sirringhaus, R.H. Friend, *Thin Solid Films*, **2003**, 438-439, 279-287. 63

[20] http://www.cabot-corp.com/ 65

[21] H. Klauk, D. Gundlach, J. A. Nichols, T. N. Jackson, *IEEE Transaction on Electron Devices*, **1999**, 46, 6. 73

[22] R. G. Endres, C. Y. Fong, L. H. Yang, G. Witte, Ch. Wlle, *Comput. Mater. Science*, **2004**, 29, 362. 73

[23] J.E. Anthony, D. L. Eaton, S. R. Parkin, *Org. Lett.*, **2002** 4, 1, 15-18. 73, 74

[24] C. S. Kim, S. Lee, E. D. Gomez, J. E. Anthony, Y-L. Loo,*Appl. Phys. Lett.*, **2008**, 93, 103302. 73, 75

[25] O. L. Griffith, J. E. Anthony, A. G. Jones, D. L. Lichtenberger, *J. Am. Chem. Soc.*, **2010**, 132, 580-586. 73

[26] S. K. Park, T. N. Jackson, J. E. Anthony, D. A. Mourey, *Appl. Phys. Lett.*, **2007**, 91, 063514. 74, 75

[27] J. P. Hong, A. Y. Park, S. Lee, J. Kang, N. Shin, D. Y. Yoon, *Appl. Phys. Lett.*, **2008**, 92, 143311. 75

[28] J. A. Lim, W. H. Lee, H. S. Lee, J. H. Lee, Y. D. Park, K. Cho, *Adv. Funct. Mater.*, **2008**, 18, 229. 75

[29] J. A. Lim, H. S. Lee, W. H. Lee, K. Cho, *Adv. Funct. Mater.*, **2009**, 19, 1515-1525. 74, 75

[30] H. Sirringhaus, P. J. Brown, R. H. Friend, M. M. Nielsen, K. Bechgaard, B. M. W. Langeveld-Voss, A. J. H. Spiering, R. A. J. Janssen, E. W. Meijer, P. Herwig, D. M. de Leeuw, *Nature*, **1999**, 401, 685. 75, 76

[31] Z. Bao, A. Dodabalapur, A. J. Lovinger, *Appl. Phys. Lett.*, **1996**, 69, 26, 4108-4110. 75, 76, 131

[32] S. K. Park, Y. H. Kim, J. I. Han, D. G. Moon, W. K. Kim, M. G. Kwak, *Synth. Met.*, **2003**, 139, 377-384. 75

[33] C. K. Chan, L. J. Richter, B. Dinardo, C. Jaye, B. R. Conrad, H. W. Ro, D. S. Germack, D. A. Fischer, D. M. DeLongchamp, D. J. Gundlach, *Appl. Phys. Lett.*, **2010**, 96, 133304. 75

[34] S. P. Speakman, G. G. Rozenberg, K. J. Clay, W. I. Milne, A. Ille, I. A. Gardner, E. Bresler, J. H. G. Steinke, *Org. El.*, **2001**, 2, 65-73. 75

[35] M. Arif, J. Liu, L. Zhai, S. I. Khondaker, *Appl. Phys. Lett.*, **2010**, 96, 243304. 75

[36] J. Liu, M. Arif, J. Zou, S. I. Khondaker, L. Zhai, *Macromolecules*, **2009**, 42, 9390-9393. 75

[37] J-F. Chang, J. Clark, N. Zhao, H. Sirringhaus, D. W. Breiby, J.W. Andreasen, M. M. Nielsen, M. Giles, M. Heeney, I. McCulloch, *Phys. Rev. B*, **2006**, 74, 115318. 75, 76

[38] J. A. Lim, J-H. Kim, L. Qiu, W. H. Lee, H. S. Lee, D. Kwak, K. Cho, *Adv. Funct. Mater.*, **2010**, 20, 3292-3297. 76

[39] www.polyera.com 78

[40] G. Binning, H. Rohrer, Ch. Gerber, E. Weibel, *Phys. Rev. Lett.*, **1982**, 49, 57-60. 78, 79

[41] G. Binning, C. F. Quate, Ch. Gerber, *Phys. Rev. Lett.*, **1986**, 56, 930-933. 78, 79

[42] G. Meyer and N. M. Amer, *Appl. Phys. Lett.*, **1988**, 53, 2400. 79

[43] Y. Martin, C. C. Williams, H. K. Wickramasinghe, *J. Appl. Phys.*, **1987**, 61, 4723. 79

[44] http://www.mechmat.caltech.edu/∼kaushik/park/1-2-0.htm 80

[45] http://epswww.unmn.edu/xrd/xrdbasics.pdf 82

[46] http://web.pdx.edu/*sim*pmoeck/phy381/Topic5a-XRD.pdf 82

[47] http://en.wikipedia.org 82, 88

[48] P. Cosseddu, *Correlation between interface-dependent properties and electrical performances in OFETs*, PhD Thesis, University of Cagliari, **2006**. 82, 84

[49] http://dcssi.istm.cnr/Galli/XRPD/ 82

[50] B. E. Warren, *X-ray diffraction*, Addison-Wesley Pub. Co., **1969**. 83

[51] B. D. Cullity, *Elements of x ray diffraction*, Addison-Wesley Pub. Co., **1956**. 83

[52] R. H. Bube, *Photoconductivity of Solids*, John Wiley & Sons, New York, **1960**. 84

3

Application: inkjet printed Organic Electrochemical Transistors

The third chapter is fully dedicated to the results concerning the *Organic ElectroChemical Transistors (OECTs)*, belonging to the family of Organic Thin Film Transistors (OTFTs) and widely studied as chemical and biological sensors. They constituted one of the typologies of devices realized by means of inkjet printing and reported in this thesis. First, a theoretical background about the working principle of an OECT will be given. Then the main results achieved will be discussed. These can be roughly summarized in two points:

- inkjet printing exhibited to be a simple and reliable printing procedure for obtaining robust working devices;
- it was demonstrated that the working range of the OECTs realized (i.e. the gate voltage range in which they can operate) may be predictably varied by changing the ratio between the gate and the channel areas.

3.1 Organic ElectroChemical Transistors

In the past 20 years Organic ElectroChemical Transistors (OECTs), as a subset of Organic Thin Film Transistors (OTFTs), have attracted particular interest for their simple

fabrication and low operating voltages. Also, the capability of working in aqueous environments make OECTs suitable for biological and chemical sensing application [1] [2]. The first OECT was reported in 1984 by White and co-workers [3]. In their device the conductivity of a poly(pyrrole) film was modulated by the application of a gate voltage through an electrolyte. Indeed an OECT is made up of two electrodes, source and drain, connected with an active layer (channel) realized with an organic semiconductor, and a third electrode, the gate, separated from the active layer by an electrolyte. In Figure 3.1 a schematic view of an OECT is showed. The source-drain current is modulated

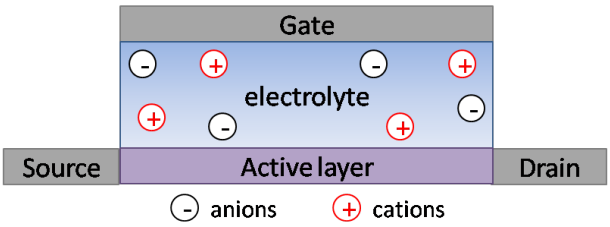

Figure 3.1: Schematic view of an OECT.

by electrochemical doping or de-doping of the active layer, mediated by the ionic motion between the electrolyte and the semiconductor film when a gate voltage is applied through the electrolyte. In order to explain in more details the operation principle of such a device, the case in which the active layer of the electrochemical transistor is constituted of PEDOT:PSS (see chapter 2 for further informations), first reported in 2002 by Nilsson[5], will be considered hereafter. PEDOT:PSS is the most commonly used organic polymers for this application and, furthermore, it is the material employed for the realization of the inkjet printed OECTs reported in this work.

3.1.1 PEDOT:PSS based electrochemical transistors

PEDOT:PSS can be employed as active layer material of a OECT because, as many conjugated polymer systems, it has the ability to conduct not only electrons but also ions. Thus, if in the PEDOT:PSS/electrolyte system there is a surplus of counter ions in the polymeric film, the ions from an aqueous solution enter the polymer film and their conduction in the material increases; in particular, this primarily occurs in the PSS phase and is thus effectively independent on the oxidation state of PEDOT [4]. However, when employed as active layer in OECTs, PEDOT is generally pristinely

doped and is therefore in its high conducting, partially oxidized state. From this state the material can either be further oxidized to a more conducting state or reduced to the semi-conducting neutral polymer [4]. The reduction (left to right) and oxidation (right to left) reactions of PEDOT:PSS occur according with the following equation [4]:

$$PEDOT^+ : PSS^- + M^+ + e^- \Longleftrightarrow PEDOT^0 + M^+ : PSS^- \tag{3.1}$$

where M^+ represents a cation and e^- is an electron. Despite OECTs can operate in accumulation or depletion mode, most published works refer to the second one. D. A. Bernards and G. G. Malliaras [2] in 2007 proposed a model that describes the behaviour of depletion mode OECTs. In this analysis they supposed that the source electrode is grounded and a voltage V_d is applied to the drain electrode; a current I_{ds} thus flows through the polymeric channel between source and drain contacts (Figure 3.2(a)). As the gate electrode is positively biased ($V_g > 0$), cations M^+ of the electrolyte enter into PEDOT:PSS film and reduce PEDOT to its neutral state according with the equation 3.1 from left to right, resulting in the de-doping of the channel and, consequently, in the decrease of the I_{ds} current (see Figure 3.2(b)). The model involves two different circuits: an electronic circuit consisting in the holes/electrons transport between source and drain through the active layer, described by the Ohm's Low, and a ionic circuit which accounts for transport of cations and anions through the electrolyte. According with this interpretation, the typical behaviour of a depletion mode OECT ($V_g > 0$), shown in Figure 3.3, can be explained. In the first quadrant, i.e. when $V_d > 0$ two regimes of behaviour can be distinguished: when $V_d < V_g$ the channel is uniformly de-doped leading to a quadratic dependency of I_{ds} from V_d; when instead $V_d \geqslant V_g$, de-doping occurs only in the channel region where $V(x) < V_g$ leading to a linear I_{ds} vs. V_d behaviour. In the third quadrant ($V_d < 0$) portions of the channel can be completely de-doped when the intrinsic (negative) dopant density is equal to the density of the injected cations; thus, when the drain voltage further decreases towards more negative values, I_{ds} starts to saturate and a channel pinch-off arises leading to the current saturation. If the gate electrode is grounded or negatively biassed, the PEDOT:PSS channel gets reoxidized (the reaction 3.1 goes to the reverse direction from right to left) and a high current flows again between source and drain electrodes [7]. It should be noted that, even if the reduction/oxidation reactions of PEDOT:PSS are reversible, for gate voltages above ca. 2 V an irreversible loss of channel conductivity occurs. At

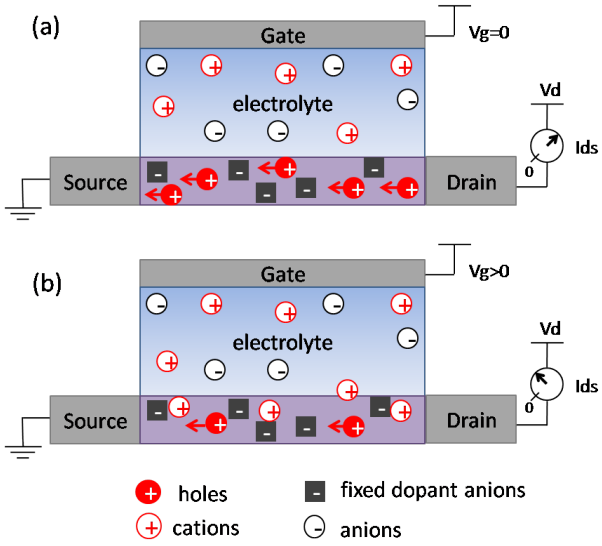

Figure 3.2: (a) OECT without gate voltage applied (V_g=0). PEDOT is in its high conducting state: source-drain current (I_{ds}) is determined by the intrinsic conductance of the PEDOT:PSS layer. (b) OECT with positive gate voltage (V_g >0) applied. PEDOT is reduced in its neutral state: I_{ds} is reduced as a consequence of the de-doping of PEDOT:PSS active layer.

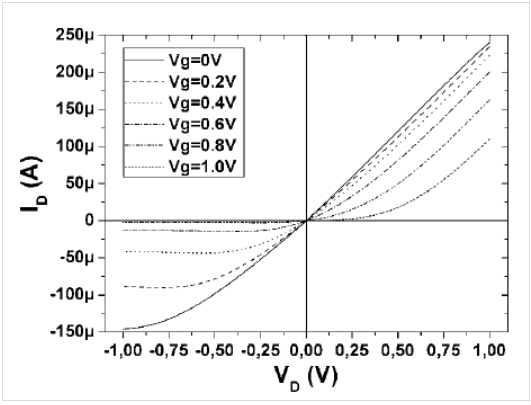

Figure 3.3: Typical output characteristic of PEDOT:PSS OECT. [7][8]

elevated oxidation potentials, in fact, PEDOT can be oxidized to a non-reversible non-conducting state; such a state is called *over-oxidized state* and the phenomenon is called *overoxidation* [9][10]. Barsh et al.[11] suggested that the overoxidation phenomenon in polythiophene films involves a mechanism that breaks the conjugation of the polymer chain. Even if works about the overoxidation mechanism in PEDOT:PSS films has not been published yet, it is highly probable it is similar to that proposed for polythiophene [12].

3.2 Results

In this section the main results achieved in the fabrication and characterization of all-organic, semitransparent OECTs realized by means of inkjet printing of PEDOT:PSS electrodes on plastic substrates will be discussed. Recently, Kaihovirta et al.[13] presented all-polymer electrochemical transistors fabricated by means of flexography. This is an extremely interesting example of OECT realized with a high throughput manufacturing technique. However, inkjet printing offers a greater flexibility in the choice of the substrates to print. A first example of an inkjet printed OECT was presented by Mannerbro et al.[14], who adapted a conventional desktop thermal inkjet printer to the deposition of an aqueous dispersion of PEDOT:PSS onto photo-paper. Conversely, as already mentioned, the present work deals with the realization of OECTs made with a piezoelectric, drop-on-demand, inkjet printing technique that, in principle, has looser constraints than thermal printing in terms of ink composition and properties as fully explained in chapter 1. It should be noted that this technological feature represents the first important aspect of novelty of the present work with respect to the state of the art. Also, a post-processing treatment with Ethylene Glycol on the printed devices is proposed in order to improve the mechanical robustness of the device; such a treatment, in fact, ensured a perfect reproducibility of device electrical curves with time, even after many electrical cycles. Last but not least, the results hereafter reported demonstrate that the OECTs working range (i.e. the gate voltage range in which they can operate) may be predictably varied by changing the ratio between the gate and the channel areas.

3.2.1 Experimental summary

The experimental details about the realization of the OECTs reported in this work are described in the subsection 2.3.1 (in particular printing settings are reported in the paragraph named *Optimization of printing parameters for different pattern's geometries*). Summarizing, all-PEDOT:PSS OECTs were fabricated on transparent and flexible 175 μm thick PET sheets by means of inkjet printing. Substrates were cleaned by subsequent 15 min ultrasonic baths both in acetone and in isopropyl alcohol, then washed in deionized water and finally dried under nitrogen flow. The devices were entirely inkjet printed in air by means of Fujifilm Dimatix Material Printer (DMP) 2800 using a DMC-11610 cartridge. This cartridge contains 16 nozzles with a diameter of 21.5 μm and each nozzle generates 10 pL drops of ink. For all electrodes, an aqueous dispersion of PEDOT:PSS was employed (Clevios^{TM} P Jet HC provided by H. C. Starck). This is made of sub-micrometer sized gel particles, which after solvent drying and thermal annealing, form a continuous and transparent conducting film. Before filling the cartridge, PEDOT:PSS-based ink was sonicated for 15 minutes and then filtered with a 0.2 μm nylon filter to avoid the presence of agglomeration which could cause nozzles clogging. During printing, substrates have been kept at a constant temperature of 60 °C to help fast solvent evaporation. Electrodes were fabricated superimposing 2, 3 or 4 printed layers, waiting for 60 s in printing two subsequent layers with a drop spacing in the range $15 \div 20$ μm . After printing, samples were annealed on a hot plate at 60 °C for 8 h. After annealing, Ethylene Glycol was deposited on the structure by means of spin coating, then the devices were dried in an oven at 60 °C for 12 h. Between gate and source-drain electrodes, a 6 μL drop of aqueous PBS (Phosphate Buffered Saline) 0.01 M electrolytic solution (NaCl 0.138 M; KCl 0.0027 M provided by Sigma-Aldrich) was deposited only a few seconds before the electrical characterization was performed; the channel device consists of the electrolyte-covered PEDOT:PSS film area between source and drain. Samples were characterized by AFM investigation, optical absorption spectroscopy, and electrical measurements.

3.2.2 Inkjet printed PEDOT:PSS film preliminary characterization

First, a complete characterization of printed PEDOT:PSS lines was performed, in order to establish printing quality, electrical conductivity properties and optical transparency.

By printing PEDOT:PSS ink with a suitable choice of drop spacing, it is possible to obtain uniform layers formed by the superposition of several single drops. In Figure 3.4 the height profile (top) and the AFM image (bottom) of a PEDOT:PSS single droplet deposited by means of inkjet printing on a PET substrate are shown. The droplet height and diameter resulted of about 90 nm and 15 μm respectively. Further AFM

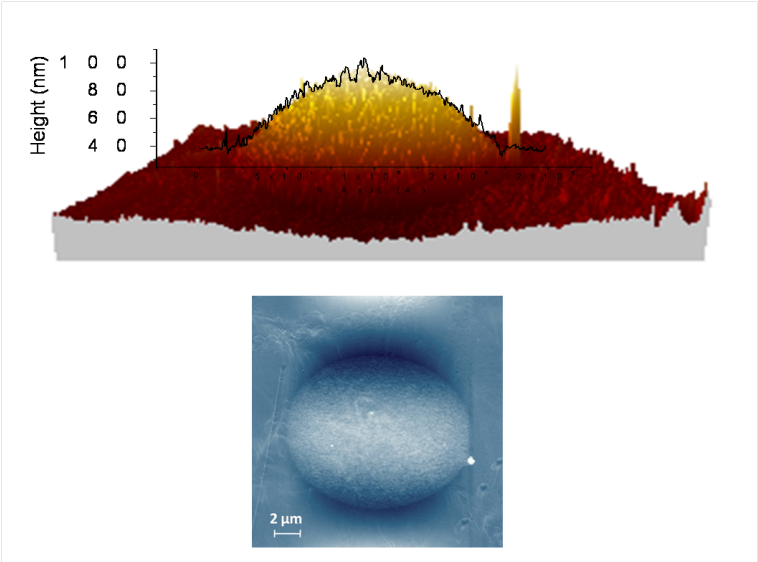

Figure 3.4: Height profile (top) and AFM image (bottom) of a PEDOT:PSS single drop inkjet printed on PET substrate.

characterization was performed on thin (width 100 μm) PEDOT:PSS stripes (optical image reported in Figure 3.5(c)) deposited on PET substrate, composed with one and two layers of printed material. The AFM image of the double layer sample and the height profile of the single layer stripe are shown in Figure 3.5(a) and (b) respectively. From these measurements the total thickness on one layer resulted of about 200 nm. Also, optical absorption measurements were executed on a sample of 3 superimposed printed layers employing the experimental set-up described in subsection 2.5.4. More than 80% (the values are normalized with respect to PET) of radiation is transmitted through the PEDOT:PSS layers (Figure 3.6) in the range between 400 and 800 nm, thus ensuring a high level of transparency of the final devices. This value is comparable with that of a spin-coated layer with a similar thickness according to the datasheet of the PEDOT:PSS compound. Transparency is useful for bio-sensing applications

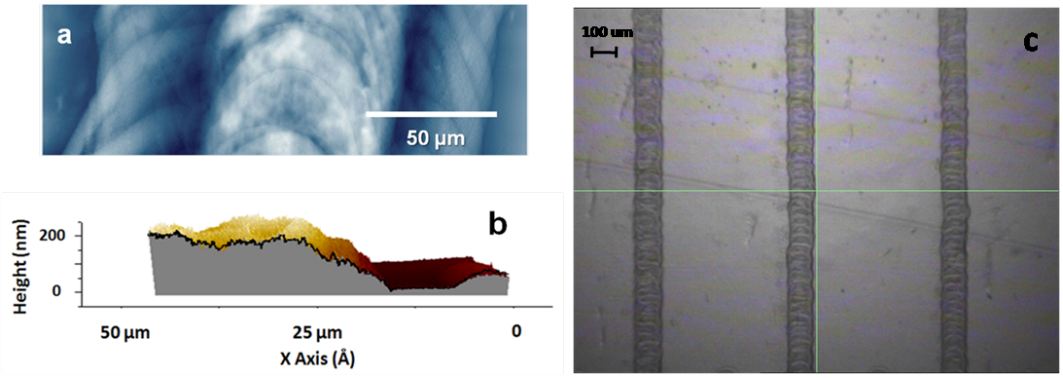

Figure 3.5: (a) AFM image of a double layer of PEDOT:PSS printed on top of a PET substrate. (b) The profile of a single layer of PEDOT:PSS stripe. (c) Optical image of PEDOT:PSS lines inkjet printed on top of a PET substrate.

as it could allow to optically inspect devices with conventional optical transmission microscopy. Finally, in order to establish the conductivity properties, temperature-dependent resistance measurements were performed on three inkjet printed structures consisting in 2, 3 and 4 superimposed PEDOT:PSS printed layers and with the same geometry. Our results show that 3 layers are enough for ensuring a complete electrical connection in the PEDOT:PSS network: in fact we observed that the resistance of a 2 layers-structure is more than double than that of a 3 layer-structure that is in turn only slightly higher than that of a 4-layers structure, as can be observed in Figure 3.7. All the samples measured showed the typical resistive behaviour [15] displayed by a conducting polymer.

3.2.3 Inkjet printed OECTs electrical characterization

After the first characterization step just described, we proceeded with the fabrication of all-PEDOT:PSS OECTs. The devices were realized with a planar layout in three geometries differing from the ratio between the gate and the channel areas (Ag/Ach) as already explained in chapter 2 (see Figure 2.24). Figure 3.8(a) shows the schematic used to record the output characteristics, i.e. the current (I_{ds}) vs. voltage (V_d) plot (shown instead in Figure 3.8(b)) of one of the printed PEDOT:PSS-based OECT with a Ag/Ach>0 geometry. The electrochemical gating of the PEDOT:PSS channel in contact with the gate electrode via the electrolyte is clearly visible: when a zero gate

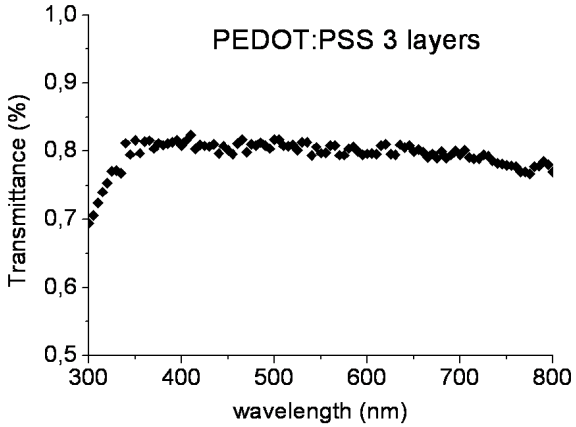

Figure 3.6: Transmittance of a triple layer of PEDOT:PSS printed on a PET substrate. The values are normalized with respect to PET. More or less 80% of the radiation is transmitted for all wavelengths in the visible range.

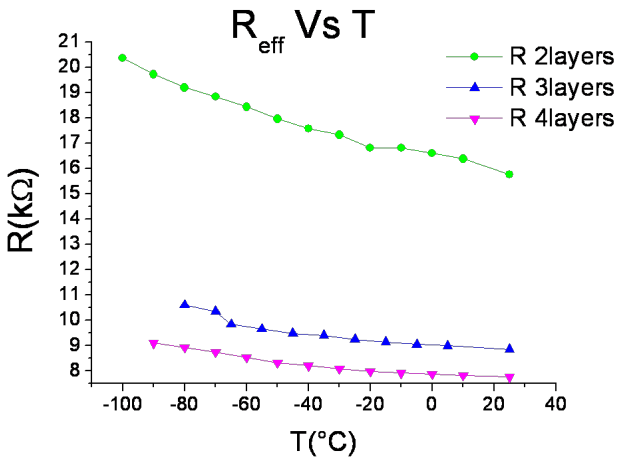

Figure 3.7: Resistance vs. Temperature plot of a printed line with 2, 3 and 4 layers.

voltage is applied to the gate electrode (V_g=0 V), the transistor is in the ON state, reaching a maximum saturation current; as the gate electrode is positively biased, the current decreases and at V_g=1 V the current is suppressed (OFF state). As drain voltage increases in absolute value (towards more negative values), the drain current begins to saturate, leading to the typical depletion mode p-type field effect transistor output characteristic behaviour, as expected. The electrical response of the device can

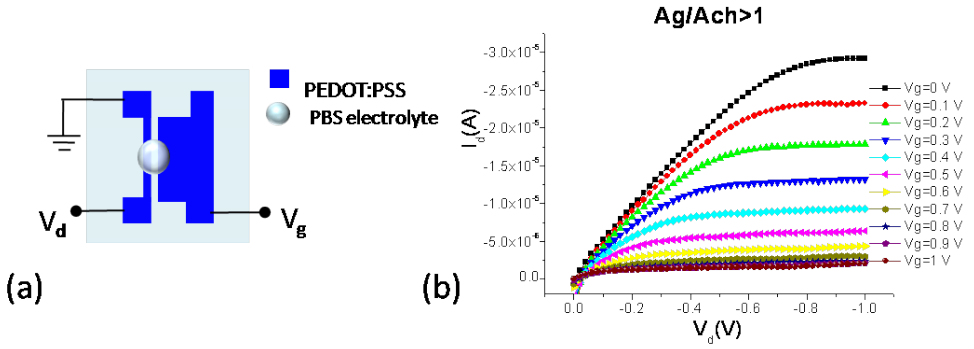

Figure 3.8: (a) Schematic (top view) used to record the OECT output characteristic; (b) current (I_d) vs. voltage (V_d) plot of one of the printed PEDOT:PSS-based OECT with a Ag/Ach>0 geometry.

be evaluated calculating the current modulation $\Delta I/I_0 = |I - I_0|/I_0$ where I is the drain-source current for $V_g \neq 0$ while I_0 is the ON current (V_g= 0 V) in the saturation regime. The plot of such a response, for a OECT realized with Ag/Ach>0 geometry (at V_d=-0.8 V) is reported in Figure 3.9.

Ethylene Glycol treatment

Although their good electrical performances, printed devices tended to delaminate from plastic substrates (as PET) or at least to severely degrade even after one operation because of the PEDOT:PSS thin film solubility in water. In order to overcome this issue the printed structures were treated with Ethylene Glycol (EG); the treatment consists on spin coating of EG over the whole structure after printing and thermal annealing and thus it can be done as a final fabrication step. A direct mixing of EG into the PEDOT:PSS ink was also attempted but it had a detrimental effect to the quality of the printed layers. The treatment with EG is known to increase the conductivity

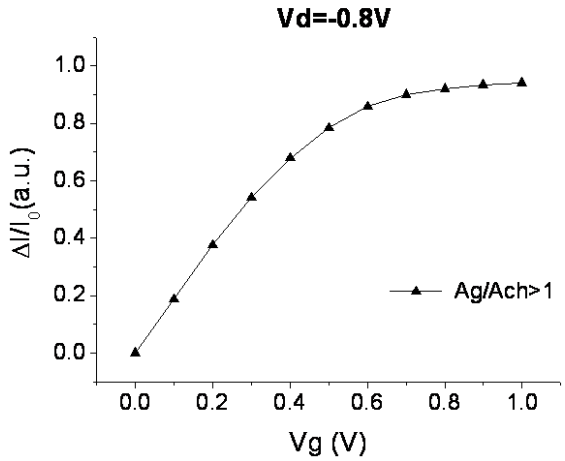

Figure 3.9: Response of inkjet printed OECT with Ag/Ach>0 geometry.

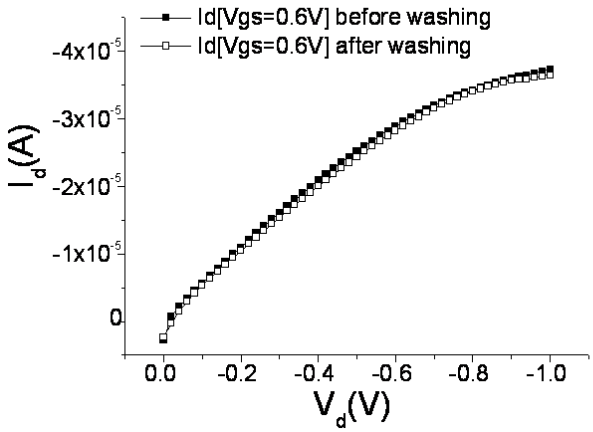

Figure 3.10: The effect of washing on the behaviour of a device printed with PEDOT:PSS and then treated with Ethylene Glycol. It is clear that the current of the device is perfectly stable and no difference is appreciable between measurements before and after washing.

of PEDOT:PSS and also contributes to increasing the mechanical robustness of the printed devices (see chapter 2, section 2.3.1). As a matter of fact, after the treatment, several runs of measurements can be performed on the same device without problems of degradation or delamination, as shown in Figure 3.10, where it is evident that the current vs. drain voltage curve does not change at all before and after washing with deionized water, and drying under nitrogen flow.

3.2.4 Effect of the device geometry on the device response

The first influence of the device geometry noticed regards the different device electrical response. Figure 3.11 reports the $\Delta I/I_0$ vs. V_g curve for three devices with different ratio between the gate area (Ag) and the channel area (Ach). In agreement with results of Cicoira et al.[6] for PEDOT:PSS based OECTs (but with Pt gate electrode) photolytographically patterned and employing PBS as electrolyte, also for our devices the current modulation $\Delta I/I_0$ increases with Ag/Ach. Such a behaviour could become crucial in the application of OECTs as enzymatic sensors of analytes added in a buffer solution (e. g. H_2O_2). In such applications, in fact, the $\Delta I/I_0$ signal employing only PBS as electrolyte represents the *background* signal of the sensor and, typically, as it increases, the sensitivity decreases. In order to further analyse the effect of the device

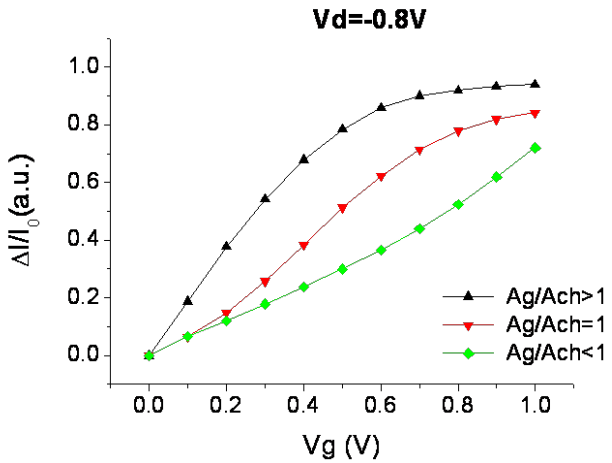

Figure 3.11: Current modulation for three OECTs with different ratio between the gate area (Ag) and the channel area (Ach).

geometry on the device response two different kinds of measurements were executed.

Figure 3.12 reports the first: two measurements of I_{ds} vs. V_g spanning from positive to negative voltages, taken on the same asymmetric (i.e. with different values of gate and channel areas) structure, by exchanging channel and gate. Currents are normalized with respect to the channel width. Basically, in the type 1 device (left), the smallest structure is taken as the channel and the largest as the gate (therefore Ag/Ach>1) while in the type 2 device (right), the largest structure is taken as the channel and the smallest as the gate (therefore Ag/Ach<1). It is clear that the transconductance (fitting lines in the bottom portion of Figure 3.12) is different in the two devices, showing that one can tune the transistor characteristics (i.e. not only current but also the operative voltage range) by tuning the device geometry. In other words, the maximum (on) current is reached in both cases for negative values rather than for zero voltage, and in type 1 measurements, the on-voltages (Von) is more negative than in type 2. This behaviour is further confirmed by the second kind of measurements performed, shown in Figure 3.13, where the I_{ds} vs. V_g curves of three different devices with the same channel dimensions (width of 500 μm) and different gate dimensions are reported: also in this case the transconductance varies with the device geometry. This feature is very useful in the design of biosensors, where the transconductance relates to sensitivity, as well as in the design of electronic circuitry. It should be noticed that this observation not only confirms again the dependence from the geometry of the device behaviour, which was previously observed also for metal-gated devices (only for Voff) [6], but also enlightens a novel feature, i.e. the possibility of extending the operational range of such devices as a peculiarity of all-polymer structures. Thus, we observed two novel phenomena in all-PEDOT devices: the dependence of Von on the geometry of device and the fact that they may have a negative Von.

Role of the gate electrode material

According to Lin and Lonergan [16], an OECT can operate in two different regimes, depending on the interface between the electrolyte and the gate electrode. The first is the *capacitive* or *non-Faradaic* regime, where the channel polymer reduction or oxidation is coupled to the charging of an ionic double layer at the gate electrode, and, consequently, the application of a bias to the gate induces a transient current in the electrolyte. In the second, the *Faradaic* regime, the oxidative doping of the channel polymer is coupled to a reduction process at the gate electrode; in this regime the

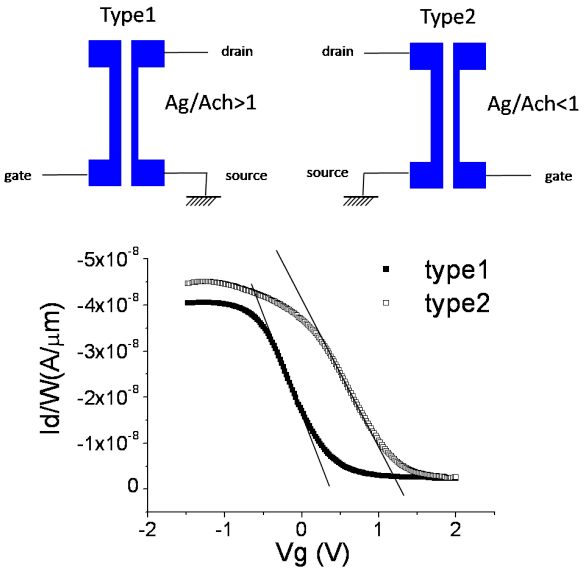

Figure 3.12: (Top) Schematic representation of the employed asymmetric geometry in which by exchanging the channel and the gate it is possible to modify the Ag/Ach ratio; (bottom) I_{ds} vs. V_g curves taken on the same device by exchanging the channel and the gate. The solid lines define the different transconductances exhibited in the two cases. The dimensions of gate width are 500 and 200 μm for type 1 and type 2 devices, respectively.

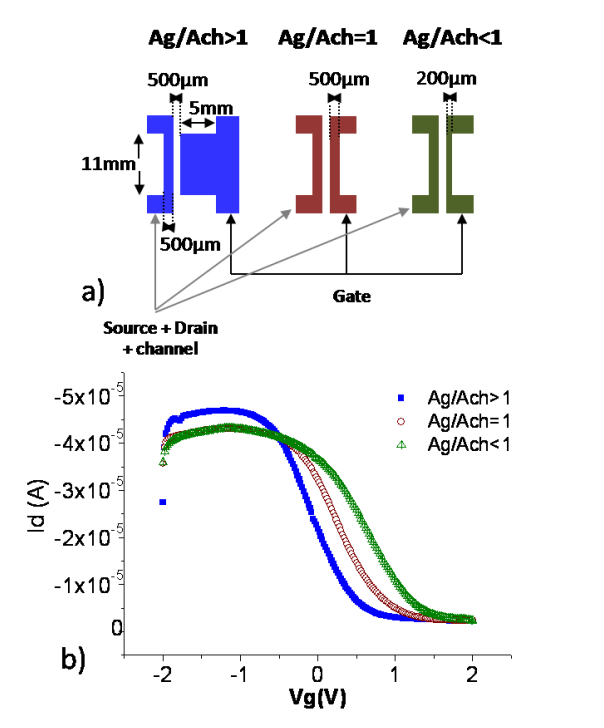

Figure 3.13: The effect of three different geometries on the transfer characteristics of the device. The channel dimension is always the same (500 μm), while the gate dimension is changing.

reduction/oxidation reactions induces a steady-state current in the electrolyte. The working regime of an OECT is capacitive or Faradaic in dependence of the behaviour of the gate electrode, i.e. if it is polarizable or not, respectively. Tarabella et al.[17] recently reported about the different behaviour of Ag-gated and Pt-gated OECTs with an halide-based aqueous solution. They observed that in devices with Ag gate, a large steady-state gate-source current was recorded, indicating that Faradaic processes occurred at the gate electrode. On the other hand, only a small source-drain current was recorded for Pt-gated devices. In Figure 3.14 such currents are plotted vs. the gate voltage; noticeably, I_{gs} of Ag-gated OECT is much higher than that of Pt-gated OECT. This different behaviour can be explained in terms of the potential distribution between gate electrode and the channel, shown in Figure 3.15 for both devices. In Pt

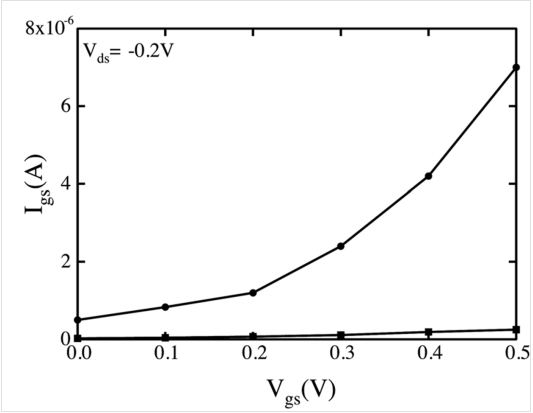

Figure 3.14: Gate-source current vs. the gate voltage for Pt-gated (squares) and Ag-gated (circles) OECTs. [17]

OECTs, the ionic double layer formed causes a potential drop at the interface between gate electrode and the electrolyte (non-Faradaic regime), while in Ag devices the potential applied at the gate always drops at the electrolyte/channel interface, allowing a steady-state current to flow from the gate to the electrolyte solution and no double layer formed (Faradaic regime). According to such an interpretation they observed that the response of the devices varied with the area of the gate electrode for OECTs employing Pt electrode, consistently with its polarizable nature, while Ag OECTs did not change their response varying the area of the gate electrode.
Apparently, in our all-PEDOT devices, Voff (but also Von) depends on the gate to

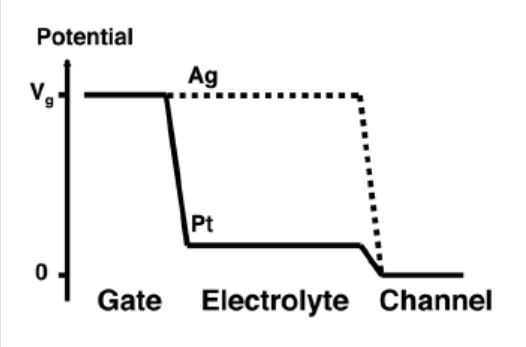

Figure 3.15: Potential distribution between the gate electrode and the channel in Ag-gated and Pt-gated OECTs. [17]

channel area ratio. This should support the idea of a polarizable gate where a non-Faradaic process occurs. On the other hand, being the gate made with PEDOT:PSS, it is able to be oxidized or reduced exchanging charges with the solution, as well as the channel. Therefore, we tentatively attribute this characteristic of devices whit both the channel and the gate electrode made with PEDOT:PSS, to a possible competitive behaviour in the doping-dedoping mechanism for both channel and gate. Indeed, when a positive gate voltage is applied, the channel is reduced, i.e. de-doped, while, at the same time, the gate is oxidized, i.e. doped. On the opposite, by applying a negative gate voltage, the channel is doped and the gate is de-doped. This implies that, only when the gate is enabled to adsorb all cations in the solution (i.e. for negative voltage, thus de-doping), the maximum (on) current flows in the channel (i.e. the channel is fully doped). It is also noteworthy that the gate-source currents recorded had values lower of one order of magnitude than the corresponding drain-source currents along the whole working range of the device. In Figure 3.16 both the I_{ds} vs. V_g plot and the corresponding I_{gs} vs. V_g plot are reported for Ag/Ach>1 geometry (Type 1, Figure 3.16(a)) and for Ag/Ach<1 geometry (Type 2, Figure 3.16(b)). Comparing such values with those reported in literature [16][17], the all-PEDOT devices seems to have a more capacitive-like instead of Faradaic-like behaviour. Finally, table 3.1 shows the results obtained on different devices, differing also for the number of printed layers (for both channel and gate). These results show that the dependence on the areas ratio is clearly visible whatever is the number of layers that compose the structure.

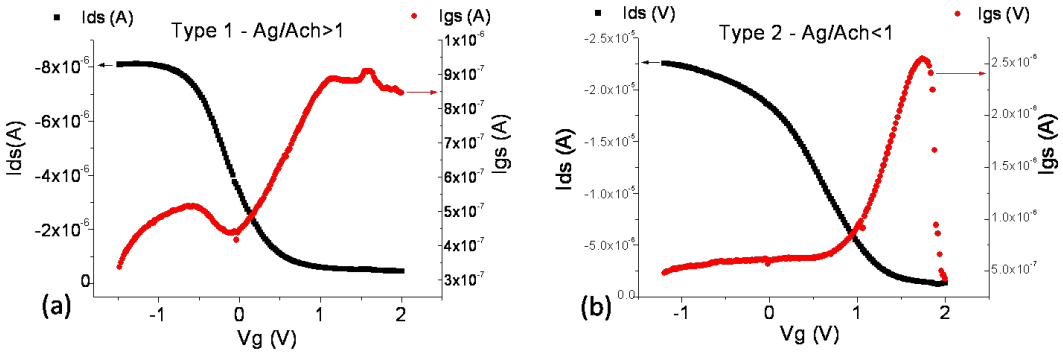

Figure 3.16: I_{ds} vs. V_g plot and the corresponding I_{gs} vs. V_g plot for Ag/Ach>1 geometry (Type 1)(a) and for Ag/Ach<1 geometry (Type 2)(b).

Layers	*Ag/Ach*	*Von (V)*	*Voff (V)*	*Working range (V)*
2	>1	−0.60	0.45	1.05
	=1	−0.40	0.97	1.37
	<1	−0.17	1.34	1.51
3	>1	−0.60	0.53	1.13
	=1	−0.31	0.91	1.22
	<1	−0.11	1.38	1.49
4	>1	−0.54	0.63	1.17
	=1	−0.25	1.17	1.42
	<1	−0.32	1.40	1.72

Table 3.1: Results obtained on different devices, differing also for the number of printed layers (for both channel and gate).

Bibliography

[1] D. A. Bernards, D. J. Macaya, M. Nikolou, J. A. DeFranco, S. Takamatsu and G. G. Malliaras, *J. Mater. Chem.* , **2008**, 18, 116-120. 96

[2] D. A. Bernards and G. G. Malliaras, *Adv. Funct. Mater.*, **2007**, 17, 3538-3544. 96, 97

[3] H. S. White, G. P. Kittlesen, M. S. Wrighton, *J. Am. Chem. Soc.* **1984**, 106, 5375. 96

[4] J. Isaksson, *Oraganic Bioelectronics - Electrochemical Devices based on Conjugated Polymers*, Linköping Studies in Science and Technology, **2007**. ISBN 978-91-85831-03-6. 96, 97

[5] P. Andersson, D. Nilsson, P.-O. Svensson, M. Chen, A.Malmstrom, T. Remonen, T. Kugler, M. Berggren, *Adv. Mater.*, **2002**, 14, 1460. 96

[6] F.Cicoira, M. Sessolo, O. Yaghmazadeh, J. A. DeFranco, S. Y. Yang, G. G. Malliaras, *Adv. Mater.*, **2010**, 22, 1012. 106, 107

[7] M. Berggren, R. Forchheimer, J. Bobacka, P.-O. Svensson, D. Nilsson, O. Larsson, and A. Ivaska, *Organic Semiconductors in Sensor Applications*, *Chapter 9: PEDOT:PSS-Based Electrochemical Transistors for Ion-to-Electron Transduction and Sensor Signal Amplification*, Springer Berlin Heidelberg New York. ISBN 978-3-540-76313-0. 97, 98

[8] D. Nilsson, *An Organic Electrochemical Transistor for Printed Sensors and Logic*, Dept. of Science and Technology Linkping University, **2005**. ISBN 91-85297-26-7. 98

[9] D. Nilsson, M. Chen, T. Kugler, T: Remonen, M. Armgarth, M. Berggren, *Adv. Mater.*, **2002**, 14, 1, 51-54. 99

[10] D. Nilsson, N. Robinson, M. Berggren, R. Forchheimer, *Adv. Mater.*, **2005**, 17, 3, 353-358. 99

[11] U. Barsch, F. Beck,*Electrochimica Acta*, **1996**, 41(11-12), 1761-1771. 99

[12] P. Tehrani, *Electrochemical switching in conducting polymers printing paper electronics*, **2008**. ISBN 978-91-7393-801-3, 99

[13] N. Kaihovirta, T. Makela, X. He, C.-J. Wikman, C.-E. Wilen, R. Osterbacka, *Org. El.*, **2010**, 11, 1207-1211. 99

[14] R. Mannerbro, M. Ranlof, N. Robinson, R. Forchheimer, *Synth. Met.*, **2008**, 158, 556-560. 99

BIBLIOGRAPHY

[15] A. Mantovani Nardes, M. Kemerink, R. A. J. Janssen, J. A. M. Bastiaansen, N. N. M. Kiggen, B. M. W. Langeveld, A. J. J. M. Van Bremen, M. M. de Kok, *Adv. Mater.*, **2007**, 19, 1196-1200. 102

[16] F. Lin, M.C. Lonergan, *Appl. Phys. Lett.*, **2006**, 88, 133507-1. 107, 111

[17] G. Tarabella, C. Santato, S.Y. Yang, S. Iannotta, G.G. Malliaras, F. Cicoira, *Appl. Phys. Lett.*, **2010**, 97, 123304-1123304-3. 110, 111

4

Application: inkjet printed Organic Field Effect Transistors

The fourth and last chapter of this thesis regards the employment of inkjet printing for the fabrication of *Organic Field Effect Transistors (OFETs)*. As in the previous chapter, in the first section a brief theoretical introduction to the working principle of this kind of device will be given; also, a review about the employment of printing techniques for the realization of OFETs will be reported. The second section reports the achieved experimental results that can be divided in four different subsections:

- Results about OFETs fabricated employing inkjet printing of PEDOT:PSS-based ink for the realization of the conductive electrodes;

- Results about OFETs fabricated employing inkjet printing of silver-based ink for the realization of the conductive electrodes;

- Experimental activity related to the ROBOSKIN project, consisting mainly in the fabrication and the electromechanical characterization of OFET-based systems working as tactile transducers for the realization of artificial electronic skin for robotic applications;

- Results in inkjet printing of TIPS-pentacene based solution as active layer of OFETs.

4.1 Organic Field Effect Transistors

Organic Field Effect Transistors (OFETs) were first described in 1987 by Koezuka and coworkers [1], who used electrochemically polymerized polythiophene as active layer of the device. So far, performances of OFETs have hugely improved year after year and field effect mobilities up to 18 cm^2/Vs have been reported for rubrene single crystal OFETs [2]. The typical structure of an OFET consists in two conductive electrodes, named source and drain, connected through an organic semiconductor layer, the channel, and a gate electrode, separated from the organic semiconductor by a thin insulating layer, called gate dielectric. In other words, an OFET has a structure similar to that of a parallel plate capacitor: the first plate is constituted by the organic semiconductor layer (the source and drain electrodes have the function of ohmic contacts for the channel), the second plate is the gate electrode, which is insulated from the first by the gate dielectric. Through this capacitive coupling the channel conductivity can be modulated by the gate electrode. It should be noted that the mandatory feature to define a transistor as an OFET is that the channel has to be made of an organic semiconducting material; gate, source and drain electrodes and the gate dielectric can be made both of inorganic and organic material. The first OFETs, in fact, were hybrid structures, assembled typically on highly doped silicon wafers, which constituted at the same time the gate electrode and the substrate of the whole structure. The gate dielectric was constituted by a thin layer of SiO_2 and the source and drain electrodes were metallic; the only organic material employed was thus the semiconductor. In recent years the fabrication of several all-organic and also all-polymeric devices has been reported; in such kind of devices the substrate is typically a polyester, the electrical contacts are made of conductive polymers and an organic dielectric is used instead of SiO_2.
Since the organic semiconductors are characterized by a low conductivity, OFETs adopt the architecture of the thin film transistor (TFT), which has proven its adaptability with low conductive materials [3]. From now onwards such devices will be indicated as OFETs or OTFTs indifferently. OFETs can be assembled in four different configurations, depending on the position of the organic semiconductor layer respect to the electrodes (see Figure 4.1):

a) bottom gate - bottom contact (BG - BC): the semiconductor layer is located above all the three electrodes;

b) bottom gate - top contact (BG - TC): the source and drain electrodes are located above the semiconductor layer while the gate lies below it;

c) top gate - bottom contact (TG - BC): the gate electrode is located above the semiconductor layer while the source and drain electrodes are below it;

d) top gate - top contact (TG - TC): all the three electrodes are above the semiconductor layer.

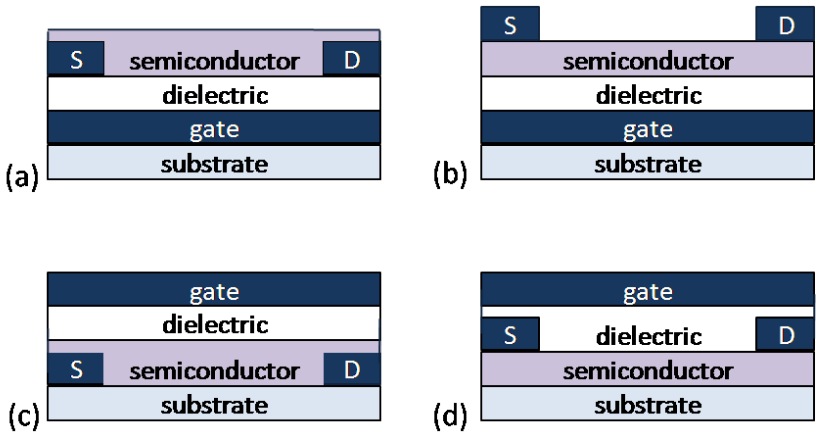

Figure 4.1: OFETs possible geometries: (a) bottom gate - bottom contact; (b) bottom gate - top contact; (c) top gate - bottom contact; (d) top gate - top contact.

The OFETs reported in this thesis are of three typologies: all-organic, all-polymer and hybrid. All of them were assembled in a bottom gate - bottom contact architecture.

4.1.1 OFETs working principle

Unlike the classical Metal Oxide Semiconductor Field Effect Transistors (MOSFETs), which typically work in inversion mode, OFETs always work in accumulation mode. When the gate electrode is unbiased a very low current flows through the channel between the source and drain electrodes and the transistor is in its OFF state. As a negative (positive) voltage is applied to the gate electrode, the electric field induced in the semiconductor layer attracts the positive (negative) charge carriers at the interface between the semiconductor and the dielectric in the channel; when a negative (positive) voltage is applied between source and drain electrodes, thus, the charge carriers

are driven across the channel area (ON state). Such a charge transport is substantially two-dimensional: charge carrier accumulation is highly localized at the semiconductor/insulator interface and the bulk of the material is hardly or not affected by gate induced field. Increasing the gate voltage to positive (negative) values, the number of charge carriers accumulated in the channel will reduce until the channel is fully depleted of free carriers. In principle, by applying a positive (negative) gate voltage allows negative (positive) charge carriers to accumulate in the channel so that the OFET should work in inversion regime; in practice, in fact, the current in inversion regime is negligible due to the high injection barrier at the interface between metal electrodes/semiconductor [4]. The gate voltage corresponding to the boundary between the accumulation and the inversion regime of an OFET is called *threshold voltage* and it will be indicated as V_T. So, when a voltage below V_T is applied to the gate electrode, the OFET is in its OFF state, i.e. no free charges are present in the channel and consequently no current flows through it. As the gate voltage becomes larger than V_T, a current begins to flow across the channel and two different operating regions can be identified:

Linear region

When $V_G < V_{DS} \ll (V_G - V_T)$ (small drain-source voltage applied), the electric field induced by the gate to the channel is uniformly distributed and thus a uniform charge distribution is induced in the channel, leading to a linear increase of the current in dependence to the applied source-drain voltage. This is therefore called *linear regime* and the equation governing the device behaviour is the following:

$$I_{DS} = \frac{Z}{L}\mu C_i \left[(V_G - V_T) V_{DS} - \frac{V_{DS}^2}{2} \right] \approx \frac{Z}{L}\mu C_i (V_G - V_T) V_{DS} \tag{4.1}$$

where Z is the channel width, L is the channel length, C_i is the capacitance of the gate dielectric and μ is the charge carrier mobility.

Saturation regime

When $V_{DS} > (V_G - V_T)$ the electric field induced by the gate at the drain contact is zero, and thus a depleted area with no induced free charge carriers is present in the channel: this phenomenon is called pinch-off. As a consequence the current flowing in

the channel saturates and a further increase of V_{DS} will no produce a current increase (*saturation regime*) according to the following equation:

$$I_{DS} = \frac{Z}{L}\mu C_i \left[\frac{(V_G - V_T)^2}{2}\right] \tag{4.2}$$

In Figure 4.2 a typical example of the output characteristic of an OFET working in accumulation mode is shown; both linear and saturation working regimes are indicated. Also another kind of electrical characteristic can be considered, the transfer character-

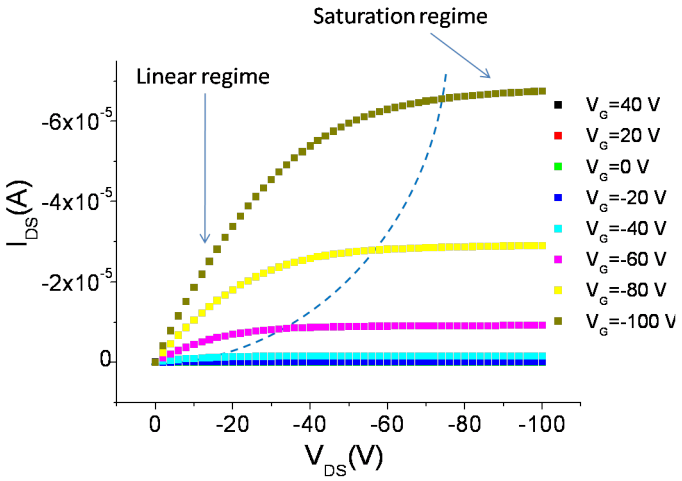

Figure 4.2: Typical output characteristic of an OFET; both linear and saturation working regimes are indicated.

istic, where the value of V_{DS} is fixed and the I_{DS} values are plotted as a function of V_G. From this plot it's easier to distinguish the two working regimes: in linear regime I_{DS} varies linearly with V_G, while in saturation regime it has a quadratic behaviour.

The main element of deviation from the ideal behaviour described above can be identified with the phenomena related to the intrinsic structural properties of the organic semiconductors. Typically, in fact, organic semiconductors are deposited in form of polycrystalline thin film, with a very high concentration of structural defects which act as scattering sites for charge carriers, causing a distortion in the, ideally, periodic lattice potential. Furthermore, if the defects induces one or more energy levels in the band gap of the organic *crystal*, they also act as trapping sites for charge carriers. Such

traps can be defined *shallow*, if their activation energy is in the order of k_BT, or *deep*, if their activation energy is outside the range of thermal excitation. The presence of traps in the semiconductor layer causes a temperature dependence of the charge carriers mobility and affects the threshold voltage of the device, since a additional voltage is required in order to fill all the bulk traps in the material before the conduction can occur.

4.1.2 Extraction of basic electrical parameters of OFETs.

The physical parameters which are usually considered in order to characterize the electrical performances of an OFET are the following:

- the field effect mobility μ, which indicates the charge carrier mobility inferred by the applied electric field;
- the threshold voltage V_T, already defined previously, corresponding to the minimum gate voltage value for the formation of the conductive layer at the interface between the semiconductor and the dielectric:
- the I_{ON}/I_{OFF} ratio, i.e. the ratio between the maximum and the minimum drain-source current values.

The procedure followed in this work in order to evaluate such parameters conforms the prescriptions provided by the Institute of Electrical and Electronic Engineers (IEEE) [5]: the field effect mobility and the threshold voltage, considered constants, are determined by a linear fit of the square root of the transfer characteristic acquired in saturation regime, and then using the equation 4.2 for the saturation regime; the I_{ON}/I_{OFF} ratio is calculated taking the ratio of the maximum and minimum I_{DS} values at a fixed V_{DS} value.

4.1.3 Printed Organic Thin Film Transistors

The high throughput, low cost, mechanical flexibility and light weight features which characterize printing manufactured devices, together with the solution-processability of most polymeric conductors, semiconductors and dielectrics, make the realization of printed OTFTs very attractive for low-end electronic applications as RFID tags and

display backplanes. In this section some examples of printed OFETs described in literature are reported, with a particular focus on inkjet printed devices and the critical issues related to the fabrication of such devices with such a technology. In 2009 Yan et al.[6] reported on several OTFTs where both p-type and n-type semiconductors were deposited by means of flexography, gravure and inkjet printing as active layer in bottom-contact/top-gate architecture devices. The schematic of the structure is reported in Figure 4.3(a) together with the chemical structures of the semiconducting polymers employed, while a photograph of gravure printed OTFTs on polyethylene terephthalate (PET) foil before top-gate contact deposition is shown in Figure 4.3(b). In such devices source and drain Au electrodes were fabricated by vacuum thermal evaporation on the plastic substrate, then the polymeric semiconductor layer was deposited on the substrate contacts by either spin coating or printing. The gate dielectric layer was either spin-coated or gravure-printed on top of the semiconducting polymer layer. Finally the gate electrode was deposited by vapour deposition over the whole structure. A comparison between spin-coated and printed devices is instead reported in

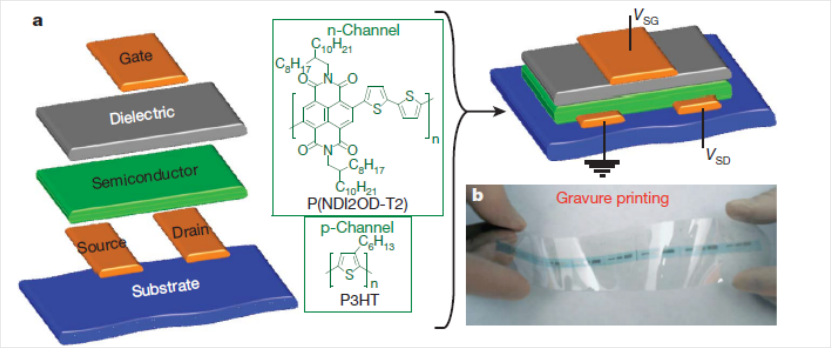

Figure 4.3: (a) Schematic of devices realized and chemical structure of semiconducting polymers used, (b) photo of gravure printed device. [6]

Figure 4.4 including: (a) optical images of devices with gravure printed semiconductor solution using printing disks with decreasing gravure cell depth/volume ratio, (b) AFM images of active layers deposited by spin coating, flexography, gravure and inkjet printing, (c) transfer plots of current versus carrier density of various printed devices and (d) transfer plot of OTFTs with gravure-printed semiconductor and dielectric layers. Also source, drain and gate electrodes of an OTFT can be patterned with different printing techniques. Cosseddu et al. reported several studies [7][8][9][10][11] on OTFTs

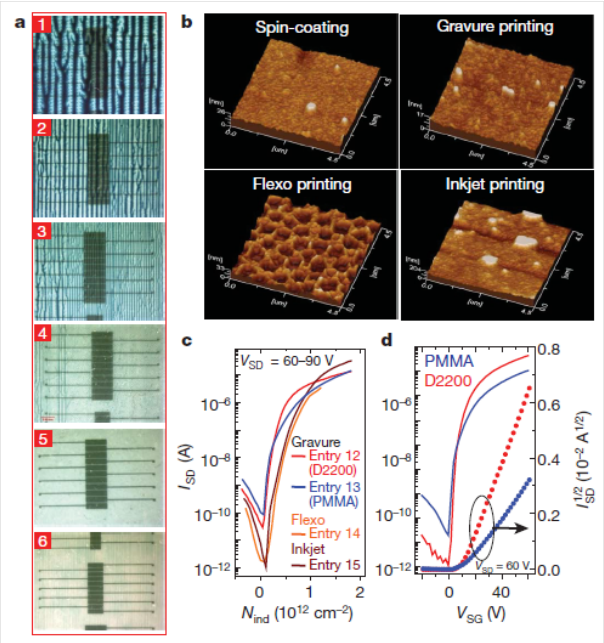

Figure 4.4: (a) Optical images of devices with gravure printed semiconductor using printing disks with decreasing gravure cell depth/volume ratio, (b) AFM images of active layers deposited by spin coating, flexography, gravure and inkjet printing, (c) transfer plots of current versus carrier density of various printed devices and (d) transfer plot of OTFTs with gravure-printed semiconductor and dielectric layers. [6]

where source and drain electrodes, made of the conductive polymer complex poly(3,4-ethylenedioxythiophene) poly(styrenesulfonate) (PEDOT:PSS), have been printed by means of soft lithography. They used a PDMS stamp, reproducing the pattern of source and drain electrodes, for both bottom contact and top contact devices fabrication, just by transferring the PEDOT:PSS contacts before or after the deposition of the semiconductor (thermally evaporated Pentacene in this case) respectively. Electrodes with channel width Z=5 mm and length L=25 μm were realized (but the technique is able to reproduce features in the order of 100 nm). The employment of inkjet printing as patterning technique for source and drain electrodes can be quite problematical. In fact, the minimum resolution achievable with most commonly used inkjet printers (typically around 20 μm) limits the smallest channel length that can be reached, thus affecting the circuiting design and limiting the switching speeds to 1-100 Hz. In Figure 4.5(a) an optical image of interdigitated source and drain OTFT electrodes (channel length of 100 μm and channel width of 2 mm), realized by inkjet printing of PEDOT:PSS-based ink, is shown. The output characteristics of a similar OTFT with L=50 μm and Z=2 mm, reported by Kawase et al.[12], is shown in Figure 4.5 (b): noticeably the channel is too large to obtain sufficient drain current at a lower voltage. In order to overcome

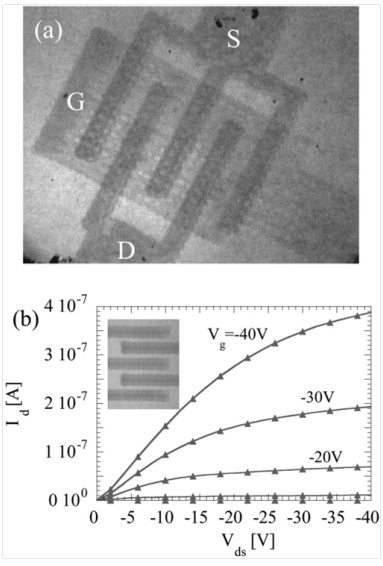

Figure 4.5: (a) Optical image of interdigitated source and drain electrodes realized by means of inkjet printing (L=100 μm and W=2 mm), (b) Output characteristics of an inkjet printed OTFT with L=50 μm and W=2 mm. [12]

this issue the same group demonstrated the use of an hybrid process to create channel lengths of 5 μm: the glass substrate is patterned, using lithography, with alternating hydrophilic glass and narrow hydrophobic polyimide regions. Thus when PEDOT:PSS-ink is printed, the patterned hydrophobic polyimide banks contain the spreading of the ink outside the source and drain electrodes regions (see Figure 4.6). In 2008 Sekitani

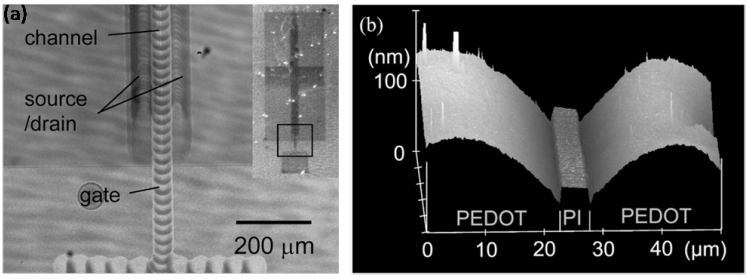

Figure 4.6: (a) Optical image of an inkjet printed OTFT with L=5 μm. In the inset a whole image of the device is shown. (b) AFM realized topographic image of source and drain electrodes. [12]

et al.[13] demonstrated the realization of short channel length (until 1 μm) OTFTs employing a sort of electrohydrodynamic jet sub-femtoliter printing technology. In their structure, shown in Figure 4.7(a), the source and drain electrodes were realized printing narrow silver lines with single-micrometer accuracy directly on top of the active layer (both vacuum-deposited pentacene and hexadecafluorocopperphthalocyanine (F16CuPc) were used) without any prior surface treatment or patterning technique. A self-aligning additive inkjet printing approach has been instead used in order to achieve sub-100 nm channel length OTFTs [14]. This method comprises three steps without employment of any lithography or precise relative alignment: first, a conductive layer of PEDOT:PSS is inkjet printed onto a glass substrate; secondly, the surface of this layer is modified in order to become a low energy surface through a carbon tetrafluoride (CF_4) plasma treatment; finally a second PEDOT:PSS electrode is inkjet printed partially overlapping the first conductive electrode. The ink of the second printed electrode is repelled from the first one before drying in the vicinity forming a sub-100 nm self-aligned channel between the two electrodes. Figure 4.8 shows the schematic of the process (a) and an AFM image of the self-aligned channel between the two PEDOT:PSS inkjet printed electrodes. Another limit of inkjet printed OTFTs concerns the structure

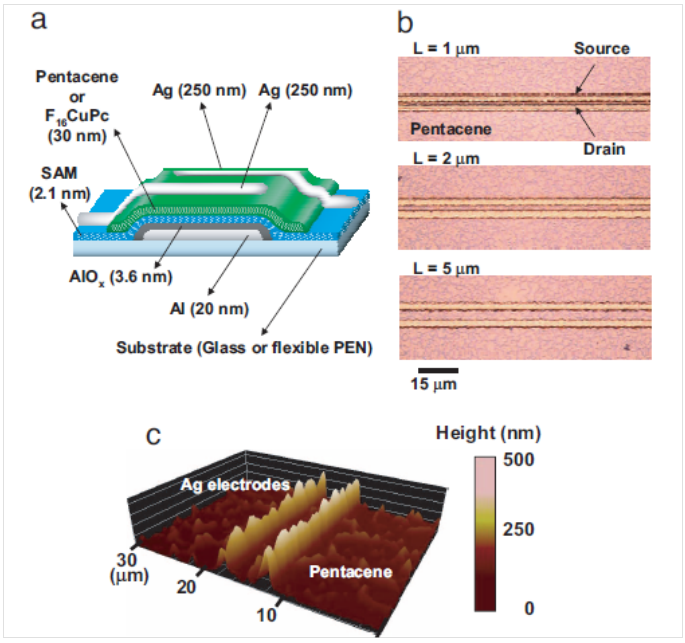

Figure 4.7: (a) Schematic of the short channel OTFTs structure. On the top of the active layer Ag nanoparticle source/drain contacts were printed by means of a subfemtoliter inkjet process. (b) Optical microscope images of pentacene OTFTs with channel length of 1 μm, 2 μm, and 5 μm. (c) AFM image of a pentacene OTFT with a channel length of 5 μm. [13]

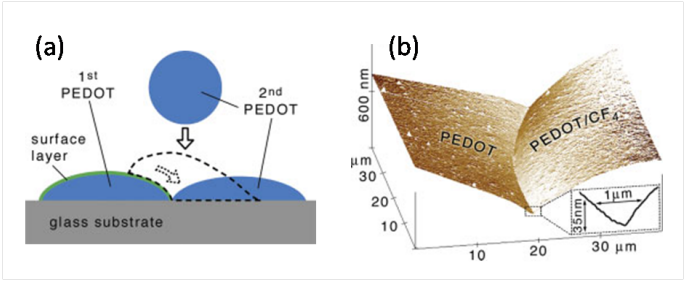

Figure 4.8: (a) Schematic of the additive self-aligned process, (b) AFM image of the short channel between source and drain PEDOT:PSS inkjet printed electrodes. [14]

of the devices, which are usually realized in bottom contact architecture with the aim of prevent the damage of the organic active layer from the ink solvent, and thus preserving the device performances [15]. For the same reason the gate electrode isn't generally printed in top position. However, some works [13][16] report attempts to print source and drain metallic electrodes above the semiconductor layer, reducing the volume of the deposited ink droplets, and thus limiting both the amount of solvent deposited and the sintering temperature of metallic nanoparticles which formed the electrodes, preventing damage to the underlying organic semiconductor. However, the reduction of the drop size is generally obtained by smaller jetting nozzles, which are easier to clog, thus reducing the reliability and repeatability of the process. Furthermore, machining small nozzles in inkjet cartridges is more complicated and thus involves the increasing of the process cost. The issue of solvent orthogonality, required in order to prevent dissolution of layers that have been previously printed, regards also the deposition by inkjet printing of dielectric and semiconducting layers. Even if such a condition could be quite difficult to guarantee, some groups reported about all-inkjet printed devices, e.g. using poly(vinyl pyrrolidone)K60 (PVP-K60) based ink as insulating material and polypyrrole (PPy) as the active layer [18], and soluble pentacene precursor and PVP [17]. However, the deposition of the insulating polymers by means of inkjet printing is generally avoided because they are generally insoluble or soluble but easily clog the printer nozzles. Furthermore, thin homogeneous dielectric inkjet printed layers are generally quite difficult to achieve [18]. Concerning the deposition through inkjet printing of the active layer, probably the most investigated inks are based on TIPS-pentacene, studied also during my research activity. However, it should be noticed that most papers reported the inkjet printing of such an ink by means of nozzles with a large orifice diameter (typically at least 50 μm); the process is thus more similar to a drop casting than an inkjet printing one, since one single inkjet printed droplet covers the whole channel region of the device (see Figure 4.9) [19][20]. More details about the inkjet printing methods applied to TIPS-pentacene based inks will be described in subsection 4.2.5. One of the goals of the work presented in this thesis is to show how the source and drain OTFT electrodes, in interdigitated configuration, can be patterned through the employment of a simple, piezoelectric, drop-on-demand printing technology, without the usage of lithographic techniques, chemical surface treatments or other processes, which could damage the devices and increase the fabrication time. Complex OTFT-

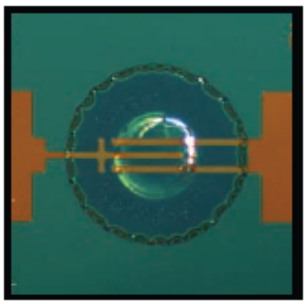

Figure 4.9: Optical microscope image (image size 350 μm $\times$ 350 μm) of inkjet printed TIPS-pentacene active layer reported by Kjellander et al.[19]. The channel region is covered by one printed droplet as a drop casting.

based systems have been realized with a good level of reliability and reproducibility. Also, a systematic study about inkjet printing process of TIPS-pentacene based ink as active layer was carried on, using the same cartridge employed for the realization of the electrodes, i.e. with nozzles with a diameter of 20 μm.

4.2 Results

In this section the main results achieved about the fabrication of OFETs by means of inkjet printing and their characterization both as transistors and strain sensors are reported. Despite the low mobility of organic materials (compared to crystalline semiconductors, it is about three orders of magnitude lower), there are applications, as the recently suggested electronic skin [21], in which the lower speed is tolerable and the use of organic materials seems to be more beneficial than detrimental. In fact, being able to obtain large sensing areas is certainly a benefit for a wide set of applications and using low cost fabrication techniques could widen the set of possible applications where sensing is required. OFET-based mechanical sensors are active devices: many different electronic parameters not only one, as for instance in piezoresistive sensors, can be extracted from their electrical characterization. Therefore, they are multiparametric sensors, offering the possibility of using a combination of variables in order to characterize their response to the parameter to be sensed. Finally, active sensors combine in the same device both switching and sensing functions and this allows to easily obtain a sensing device of limited size and good reliability. However, only a few ex-

amples of mechanical sensors have been reported so far [22][23]. Although mechanical flexibility is one of the main advantages of organic materials, the effect of strain on the mechanical and electrical properties of organic semiconductors have not yet been fully exploited and it is thus still an emerging research topic in fundamental physics and applications [24][25][26]. The results reported in this section involve, first of all, the electrical performances of the transistors realized, their electromechanical characterization as strain sensors and finally the development of more complex systems i.e. matrices and arrays of OTFTs, designed and fabricated by means of inkjet printing. In such systems each device acts as a mechanical sensor, so they will be employed as tactile transducers for the realization of artificial e-skin within the framework of the European project ROBOSKIN. As an activity of this project also the characterization of piezoelectric transducers for robotic tactile sensors realized by means of inkjet printing of silver electrodes on a PVDF thin film will be discussed. Finally, also the work carried out in inkjet printing of inks based on TIPS-pentacene as OFET active layer with the perspective of realizing a fully inkjet printed organic device will be reported.

4.2.1 Experimental summary

As in the case of OECTs, also for OFETs, the experimental details on the fabrication of OFETs by means of inkjet printing are fully reported in Chapter 2. Hereafter a brief summary will be given. All the OFETs reported in this work have been assembled in bottom gate - bottom contact architecture following the fabrication steps schematized in Figure 4.10. The substrate for the device consisted of a light, flexible and usually transparent plastic foil (PET, PEN or Kapton) onto which the gate electrode was inkjet printed. After the annealing and the consequent drying of the gate electrode, a thin layer (1.5 μm) of parylene C was deposited by means of chemical vapour deposition (see Appendix A for details). Then the source and drain electrodes were patterned in linear or in interdigitated configuration by means of inkjet printing. As already mentioned, two different conductive inks were employed as electrodes materials, a waterborne dispersion of the conducting polymer complex PEDOT:PSS and a silver-based ink containing silver nanoparticles dispersed in a liquid vehicle. Finally, an organic semiconductor was deposited. Several kinds of semiconductors were tested and deposited with various techniques: pentacene was deposited by means of thermal sublimation; TIPS-pentacene based inks were deposited by means of drop casting

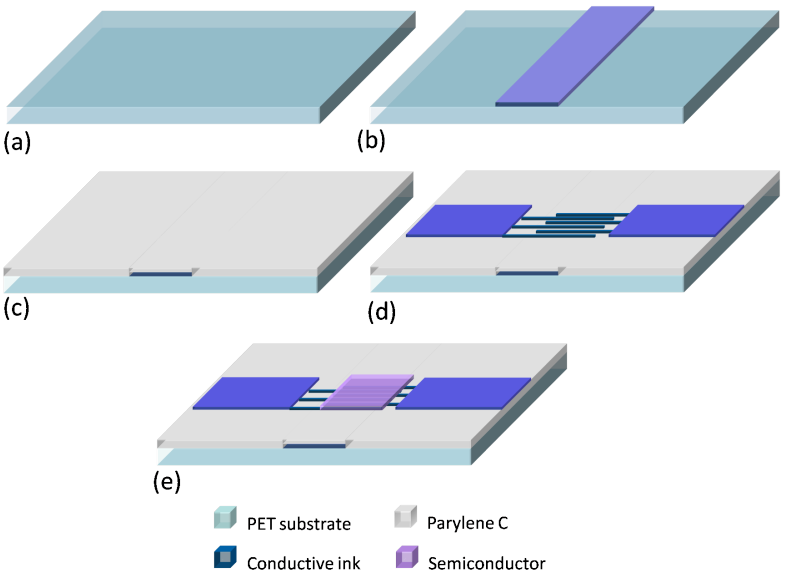

Figure 4.10: Fabrication steps for the realization of an inkjet printed OFET in bottom gate - bottom contact configuration: (a) the device was assembled onto a thin, lightweight, flexible and usually transparent plastic foil; (b) the gate electrode was printed on the substrate, then (c) the gate dielectric (parylene C) was deposited; (d) on the whole structure the source and drain electrodes were patterned by means of inkjet printing and finally (e) the semiconductor was deposited.

Semiconductor	*Form*	*Deposition Technique*
Pentacene	Solid	Thermal sublimation
TIPS-pentacene	Solution: 0.5% wt. in toluene	Drop Cast
	Solution: 5% wt. in toluene	Inkjet Printing
P3HT	Solution: blend P3HT:PS (20:80 w/w) 0.5% wt. in CB:CHN (80:20 v/v)	Drop Cast - Inkjet printing
N1400	Solution: 1% wt. in 1,2 dichlorobenzene	Spin Coating

Table 4.1: Semiconductors tested as active layer for inkjet printed OFETs.

and inkjet printing; P3HT based ink was spin-cast and inkjet printed on the sample; also an n-type semiconductor, named N1400, was tested, deposited by means of spin coating. In Table 4.1 the semiconductors and the corresponding deposition techniques used are summarized. Concerning the realization of the piezoelectric sensors, metallizations were patterned onto the two faces of PVDF 50 μm thick film employing the silver-based ink. All these devices have been tested both in their electrical and electromechanical performances; major details about the experimental set-up used to carry out such measurements will be given afterwards, when the achieved results will be discussed. Furthermore, concerning the activity for the optimization of the TIPS-pentacene deposition by means of inkjet printing, also AFM, XRD, photocurrent and optical absorption characterization were performed.

4.2.2 Fabrication of PEDOT:PSS electrodes for OFETs

The fabrication of the source, drain and gate electrodes of an OFET by means of the conductive polymer complex PEDOT:PSS, besides mechanical flexibility and easier processing, allows the realization of transparent, all-organic and all-polymer devices. Since Pentacene can be considered the organic semiconductor with the electric performances nearest to the ideal behaviour, the fist step in order to evaluate PEDOT:PSS based inkjet printed OFETs was to characterize them employing Pentacene itself as active organic layer. As can be clearly seen from Figure 4.11 all-organic devices realized using Pentacene gave rise to the typical unipolar p-type behaviour, with charge

carrier mobility up to 7×10^{-2}cm^2/Vs and I_{ON}/I_{OFF} ranging around 10^5 for devices with channel length and width of 150 μm and 4.5 cm respectively. Secondly, we tried to use a solution processable organic semiconductor with the aim to develop it as an ink for inkjet printing process. The first attempt was made with the polymeric semiconductor P3HT, which offers the advantage to realize an all-polymeric device. As expected, using P3HT instead of Pentacene as organic semiconductor led to a significant decrease in charge carrier mobility, nevertheless all the devices realized by means of spin coating showed nice electrical behaviour with mobility values similar to the previously reported ones [27][28]. In fact, even though P3HT is certainly one of the best performing solution processable polymers in terms of charge carriers mobility, it is well known from the literature that its average mobility is almost one order of magnitude lower than Pentacene based OTFTs [29]. For devices in which the P3HT based solution was deposited by spin coating, mobility values up to 6×10^{-3}cm^2/Vs were observed (the output and the transfer characteristics are reported in Figure 4.12a and b). Considering the electrical behaviour of inkjet printed P3HT devices, reported in Figure 4.12(c) and (d), despite a clear field effect behaviour can be noticed, these devices are characterized by a much lower charge carrier mobility, around 3×10^{-4}cm^2/Vs . The main reason for this behaviour is to ascribe to much poorer quality of the active layer deposited by inkjet printing, which is strongly correlated to the final deposited film morphology. This could be improved either by a proper optimization of the polymeric ink and/or by an accurate optimization of the deposition parameters. Because of

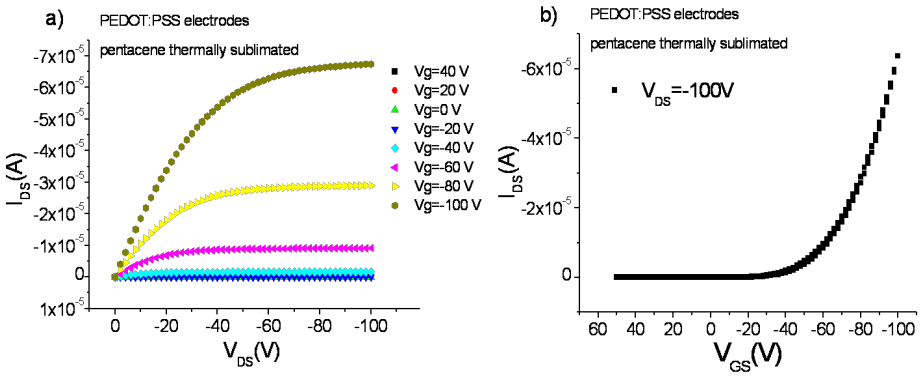

Figure 4.11: Output (a) and transfer (b) characteristics of an inkjet printed OFET with PEDOT:PSS electrodes and the active layer realized with thermal evaporated Pentacene.

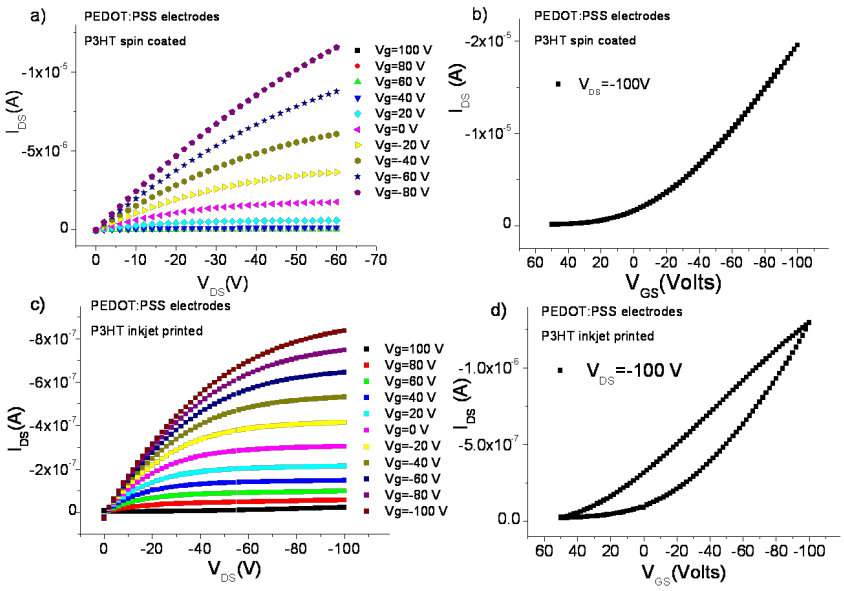

Figure 4.12: Output and transfer characteristics of OFETs with inkjet printed PEDOT:PSS electrodes and P3HT active layer deposited by means of spin coating (a, b) and inkjet printing (c, d).

such poor electrical performances observed, we tested other organic semiconductors as active layer for OFETs with PEDOT:PSS inkjet printed electrodes. Figure 4.14(a) and (b) reports the electrical characteristics of devices fabricated using N1400 and TIPS-pentacene (solution at 0.5 wt. % in toluene deposited by drop casting) used as active organic semiconductor layer respectively. As can be clearly seen both devices exhibited a unipolar behaviour. For n-type device we obtained electron mobilities up to 3.7×10^{-3} cm^2/Vs and on-off switching ratio (I_{ON}/I_{OFF}) of more than 10^3; on the other hand hole mobility values for p-type devices were up to 7.8×10^{-3} cm^2/Vs and the I_{ON}/I_{OFF} ratio up to 10^4. All the electrical parameters have been calculated from the transfer characteristics in saturation regime (V_{DD}=100 V for n-type and V_{DD}=−100 V for p-type device). The similar electrical performances of the two devices have suggested the idea of interconnecting the devices with the aim to implement a logic gate, namely an inverter. In Figure 4.13 the circuit configuration (a), the circuit symbol (b top), the truth table (b bottom) and the top view of the architecture (c) of the logic inverter realized are shown. Figure 4.14 (c) and (d) show the static characteristics V_{out} vs.

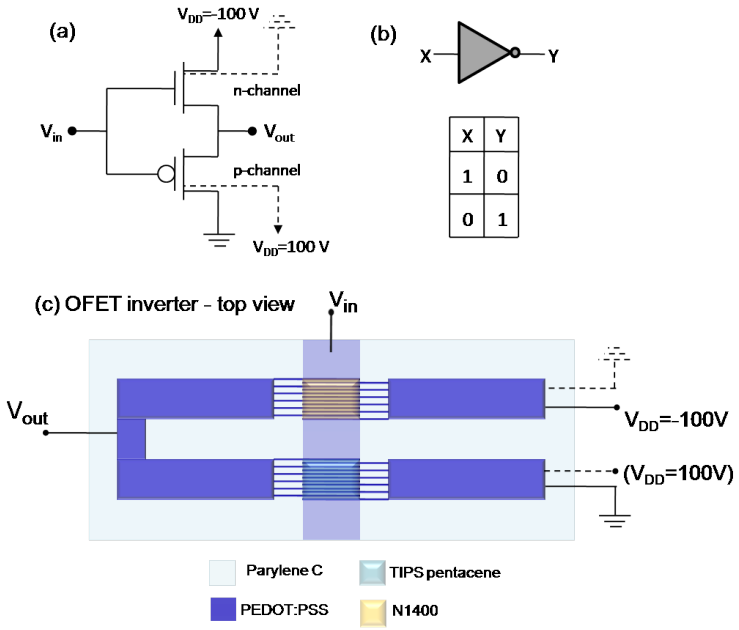

Figure 4.13: Circuit configuration (a), circuit symbol (b top), truth table (b bottom) and device schematic (c) of the logic inverter realized.

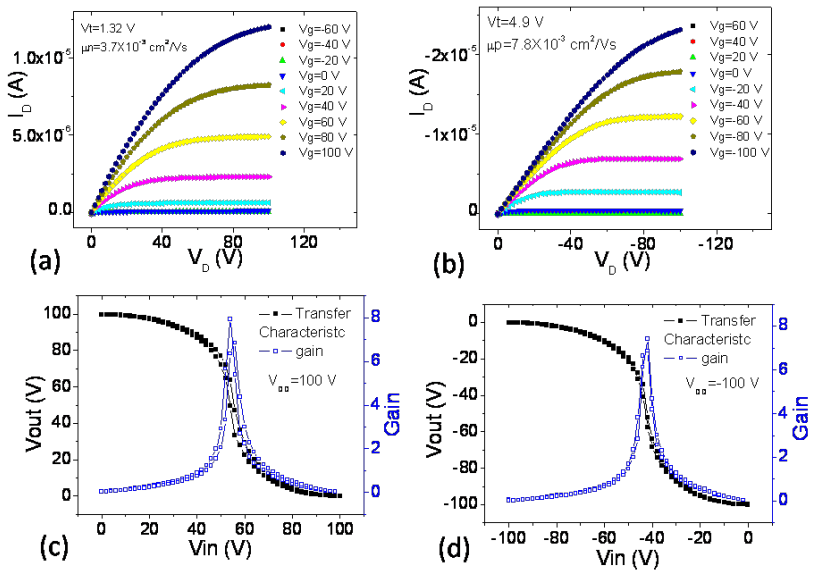

Figure 4.14: (a) Output characteristic ($I_D V_D$) of n-type OFET; (b) Output characteristic ($I_D V_D$) of p-type OFET; (c) and (d) output static characteristics of inverter logic gate for two different bias configurations of the devices.

V_{in} and the gain voltage (dV_{out}/dV_{in}) in two different configurations. In the first one (Figure 4.14c corresponding to dashed-line terminals in Figure 4.13c) the logic 0 corresponds to voltage level $V_{in/out}$=0 V and the logic 1 to voltage level $V_{in/out}$=100 V while in the second configuration (Figure 4.14d corresponding to solid-line terminals in Figure 4.13c) the 0 logic corresponds to $V_{in/out}$=−100 V and the 1 logic to $V_{in/out}$=0 V. It is noteworthy that the voltage gain dV_{out}/dV_{in} is around 8 and the response of the logic gate is balanced in both configurations thanks to the comparable electrical performances of n-type and p-type devices. However, for all devices the minimum channel length achievable, ensuring good reproducibility and the absence of short circuits between source and drain electrodes, was found to be 120 μm, as discussed in Chapter 2. The large channel length did not allow to reach high electrical performance of devices; therefore, with the aim to achieve shorter channel transistors, we decided to test a silver-based ink for the fabrication of inkjet printed electrodes.

4.2.3 Fabrication of OFET contacts by Silver ink

Employing silver-based ink as material for the electrodes of OFETs, an average channel length of 50 μm for interdigitated channel structures was achieved (Z=50 mm). The best electrical performances have been observed for devices realized employing TIPS-pentacene 0.5 wt.% in toluene solution deposited by means of drop casting as active layer, with charge carrier mobility up to 0.1 cm^2/Vs and I_{ON}/I_{OFF} ranging around 10^5 (electrical output (c) and transfer (d) characteristics are shown in Figure 4.15). In fact, even if the devices with thermally sublimated Pentacene exhibited a better field effect behaviour, their mobility values were more than one order of magnitude lower (up to 8×10^{-3} cm^2/Vs). Electrical characteristics of devices with Pentacene as active layer are reported in Figure 4.15 (a) and (b). The lower mobility values recorded for Pentacene-based samples is related to the morphology of the active layer itself. The crystal order of the thermally sublimated Pentacene layer, in fact, is contrasted by the roughness of the patterned substrate, which, on the contrary, does not affect the TIPS-pentacene active layer deposited from liquid phase, since it is formed by big self-assembled crystals. From the output characteristics, especially those of TIPS-pentacene based device, it's also clearly visible, in the linear region, the typical effect of the high injection barrier at the interface between the silver electrodes and p-type semiconductors [30].
Also the already mentioned n-type semiconductor N1400 was tested (electrical char-

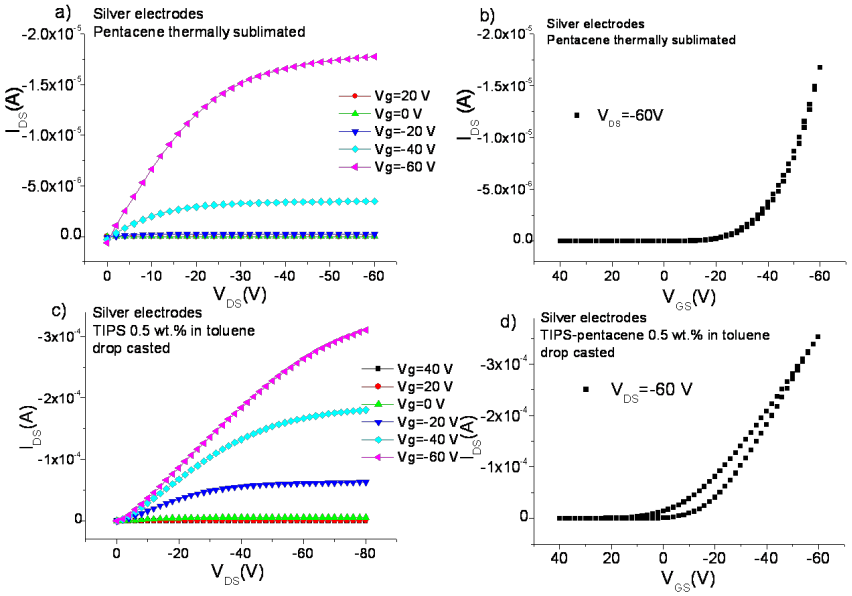

Figure 4.15: Electrical characteristics of inkjet printed OFETs with silver electrodes and the active layer realized with thermally sublimated Pentacene (a, b) and with TIPS-pentacene 0.5 wt.% in toluene deposited by means of drop casting (c, d).

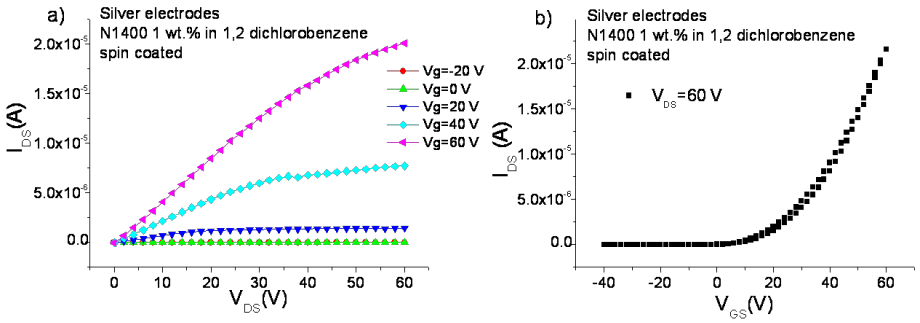

Figure 4.16: Output (a) and transfer (b) characteristics of an OFET with silver electrodes and the active layer realized with N1400-based solution deposited by means of spin coating.

acteristics shown in Figure 4.16). Although good electrical performances have been observed, with charge mobility values up to 4×10^{-3} cm^2/Vs and I_{ON}/I_{OFF} around 10^3, this semiconductor exhibited a huge sensitivity to the bias stress. In fact, in several tests, carried on by giving a pulsed gate voltage (frequency 100 Hz, duty cycle 0.3), the source-drain current degraded of one order of magnitude in about 5 hours. Conversely, the same test performed on devices with other semiconductors (Pentacene and TIPS-pentacene) did not show any degradation effect.

4.2.4 Activity related to ROBOSKIN project

ROBOSKIN [31] is a Collaborative Project funded by European Commission through its Cognitive Systems and Robotics Unit (E5) under the Information Society Technologies component of the Seventh Framework Programme (FP7). The project was launched on May 1^{st}, 2009, and will run for a total of 36 months. The consortium is composed of 6 research units:

1. University of Genova (Coordinator), Italy.
2. Ecole Polytechnique Federale Lausanne, Switzerland.
3. University of Hertfordshire, United Kingdom.
4. Italian Institute of Technology, Italy.
5. University of Wales, Newport, United Kingdom.
6. University of Cagliari, Italy.

Tactile sensing is a strategic issue for achieving safe interaction between robots and humans or objects, especially when operating in unstructured environments. As a matter of fact, tactile sensing provides the most important and direct feedback to control contact phenomena both in case of voluntary and reactive interaction tasks. Usually, tactile sensing is considered a basic perceptive strategy when objects are purposively manipulated or when it is important to control the effects of robot motion. ROBOSKIN is aimed at addressing tactile sensing from a different perspective, and in particular focusing on aspects related to sensing, perception and motion control. Therefore its main

objective is to enforce robot capabilities in efficiently and safely operating in unconstrained environments during tasks involving human-robot interaction. The project is scientifically organized in three main key research activities, which refer to:

1. Technological aspects of robot skin design and implementation: advanced semiconductor electronics, transduction devices and technologies, embedded electronics and system mechatronics.

2. Software and algorithmic aspects of tactile data processing: software engineering, robot control, embedded electronics and systems.

3. Cognitive issues related to skin-based behaviours and task level control: human-robot interaction, learning and assistive technologies.

The role of the University of Cagliari concerns the first point of the list above and in particular it is focussed on the development and optimization of devices that, being assembled on highly flexible substrates, can be employed as tactile transducers to be mounted on soft surfaces, as robot's face. The developed technology is based on Organic Field Effect Transistors employed as mechanical sensors. An important part of the activity, concerning this thesis and reported in the following subsections, was focused on the design of the devices and the selection of the materials in order to achieve, on the one hand, the best electrical performances and, on the other, a good and reproducible response to mechanical deformation. Also, we collaborated intensively with the Italian Institute of Technology and the University of Genova for the development of the technology to manufacture triangular prototypes for electronic robotic skin based on PVDF-sensors arrays. [32]

Single OFET electromechanical characterization

The first part of the activity was focused on the electromechanical characterization of single OFETs with thermally evaporated gold electrodes patterned by means of common photolithography with Pentacene and TIPS-pentacene as organic semiconductor. An interdigitated configuration was used for the source and drain electrodes, obtaining a channel length L=40 μm, and total channel width Z=64 mm. Good electrical performances have been obtained, with charge carrier mobility up to 0.1 cm^2/Vs and

7×10^{-2} cm^2/Vs for TIPS-pentacene and Pentacene respectively. In both cases we observed a I_{ON}/I_{OFF} ranging around 10^5. These devices have been employed for testing the electro-mechanical properties of the two different active layers. The devices have been deformed by bending the substrate onto different cylinders with known diameters in order to induce a tensile deformation on the active layer. The surface strain values induced in the active layers, corresponding to the bending radii, can be calculated using a known and already successfully used model [33]. Experiments were performed using bending radii in the range of 4 to 0.3 cm, corresponding to surface strain values in the range of 0.2 to 3%. Figure 4.17 reports transfer characteristics upon deformation and sensitivity vs surface strain plot for Pentacene (Figure 4.17 a and b) and TIPS-pentacene (Figure 4.17 c and d) devices. The reported transfer characteristics (Figure

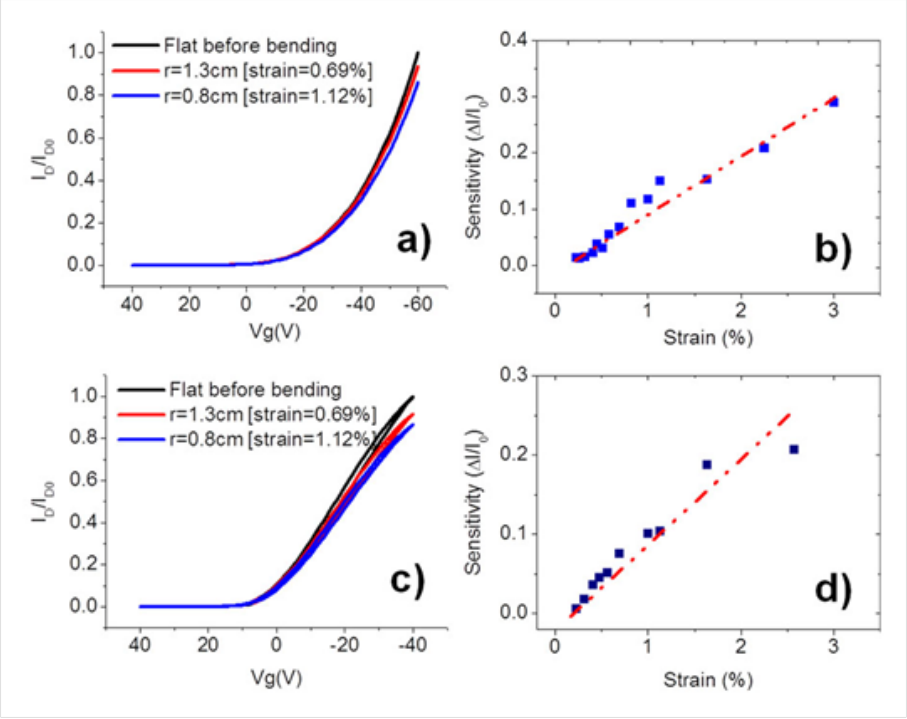

Figure 4.17: Electrical response of OTFTs mechanical sensors. Normalized transfer characteristics recorded at different bending radii (a and c) and sensitivity vs. surface strain plot (b and d) for Pentacene (upper graphs) and TIPS-pentacene (lower graphs).

4.17 a and c) have been normalized by dividing I_D values by I_{D0}, where I_{D0} is the maximum current recorded (at V_{GS} = -60 V) in the same device before bending its surface

for the first time. The sensitivity of the devices to strain was calculated as the variation of the current of the bent device, I_{Dn}, respect to the unbent status, I_{D0n}, normalized to the pristine value, i.e. $(I_{Dn}\text{-}I_{D0n})/I_{D0n}$. Both Pentacene and TIPS-pentacene based devices exhibited a marked response to the induced surface deformation. In particular we noticed that the sensitivities of the two different active layers are similar and, furthermore, the electrical response of the fabricated OTFTs was found to be linear within the range of deformation reported in the plots (the strain varying from 0.2 to 3%) (Figure 4.17 b and d). We assume that such a sensitivity to mechanical deformation can be related to changes taking place in the organic semiconductor thin films. In fact, a tensile stress could have a double effect on it: on one hand, Pentacene polycrystalline domains can get stretched, altering the molecule π-π stacking and thus affecting the charge transport within the same molecule (intra-chain) and between two close molecules (inter-chain); on the other hand the tensile stress could also cause the distance increase between the Pentacene crystals and reduce the tunnelling possibility of charge carriers from one crystal to another (inter-grain). The reduced charge mobility could be explained especially using the hopping transport model. Tensile stress leads to the increase of the potential barrier for thermal activated tunnelling, which reduces the charge carrier mobility in polycrystalline organic semiconductor films such as Pentacene and TIPS-pentacene [34]. These results are particularly important since they demonstrate that also a solution processable material, such as TIPS-pentacene, that can be deposited with easy and low cost technique over large areas, can be employed for the fabrication of mechanical sensors. Also, as preliminary measures, devices with inkjet printed PEDOT:PSS electrodes and thermally sublimated Pentacene were characterized. Such devices exhibited a good sensitivity to the tensile stress induced, as shown in Figure 4.18, where the sensitivity vs. strain plot in logarithmic scale for simple inkjet printed PEDOT:PSS stripes and for transistors with PEDOT:PSS inkjet printed electrodes and thermally sublimated Pentacene as active layer are reported. PEDOT:PSS stripes showed a low resistance variation with bending (lower than 1.5% for strain of 2%), while devices with Pentacene as active layer showed a marked and linear sensitivity with the deformation stress (higher than 5% for strain of 2%).

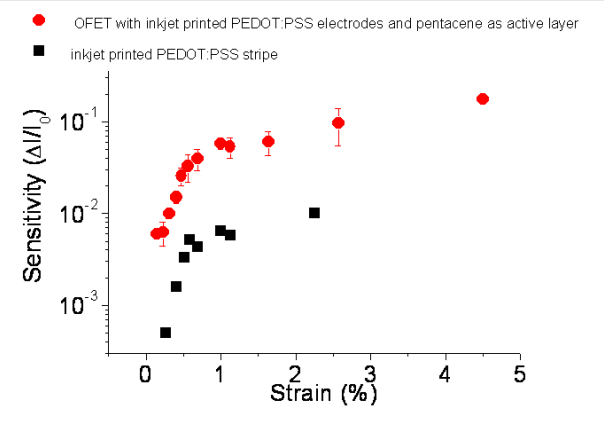

Figure 4.18: Sensitivity vs. strain plot in logarithmic scale for inkjet printed PEDOT:PSS stripe and for devices with PEDOT:PSS inkjet printed electrodes and thermally sublimated Pentacene as active layer.

Design and development of more complex OFET-based structures

Starting from these results, more complex OFET-based structures have been realized by means of inkjet printing. First, we developed arrays of OFETs with PEDOT:PSS inkjet printed electrodes. Figure 4.19 shows the simplest one: an array of 3 OFETs with a common gate electrode and independent source-drain contacts. The first matrix realized consisted instead of 7 interdigitated PEDOT:PSS-based OFETs into a 3 cm equilateral triangular PET substrate using a common source configuration. Devices have been placed into two different rows, as shown in Figure 4.20, each row with a common gate. The assembled devices have independent drain electrodes, in this way all the devices within the same matrix can be independently biased and measured. Each OFET had channel length and width of 150 μm and 4.5 cm respectively.
Because of our purpose of developing more complex systems containing many devices over large areas with optimal electrical performances, we decided to employ silver-based ink instead of PEDOT:PSS one in realizing OFETs printed electrodes in interdigitated configuration. In fact the silver-based ink, as already discussed, allows to realize transistors with shorter channels and, consequently, to reach both higher output current values and higher spatial density of devices. Thus we optimized the printing process for the realization of arrays of 8 elements with a common gate, a common source and independent drain contacts (see Figure 4.21) and finally we created the basic module

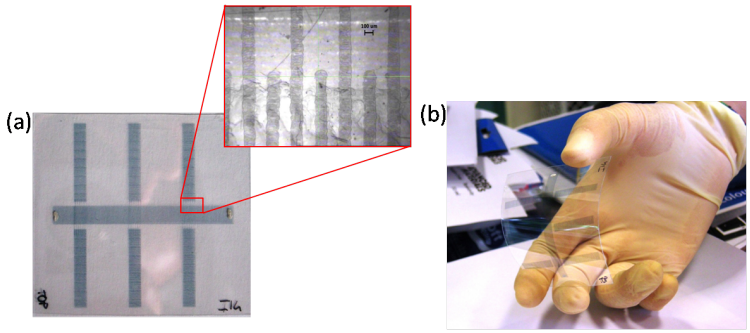

Figure 4.19: Photographs of an array containing 3 OFETs with the source, drain and gate electrodes patterned by inkjet printing of PEDOT:PSS based ink with a common source configuration. The inset shows a magnification of the source and drain interdigitated structure. (a) Top view; (b) photograph showing the transparency and flexibility of the structure.

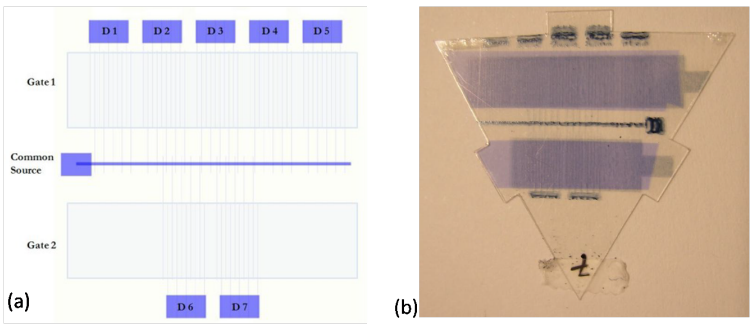

Figure 4.20: Schematic (a) and photograph (top view) (b) of the printed OFETs matrix realized with PEDOT:PSS electrodes.

of the robot skin realizing matrices of 8×8 OFET-based sensors, each with with L = 50 μm and Z = 50 mm, covering an area of 16 cm^2, with lateral pitch (in both x and y directions) of 5 mm. Every single element of the matrix can be independently addressed since devices are arranged in a common source configuration, with 8 independent gate electrodes, one per row, and 8 independent drain electrodes, one per column. A schematic of this layout and a photograph of the real device realized are depicted in Figure 4.22(a) and (b) respectively. The flexibility of such a system is shown in Figure 4.23, for matrices realized on PET (a and b) and Kapton (c) substrate.

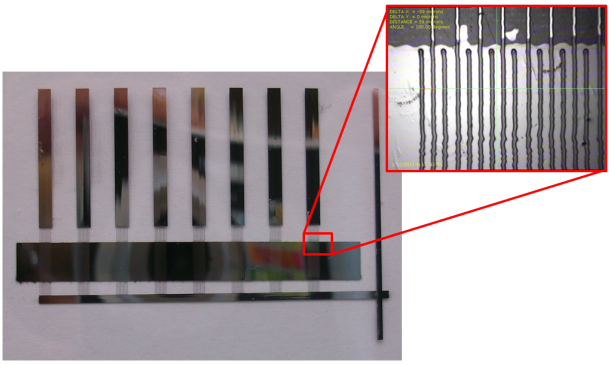

Figure 4.21: Photograph of an array containing 8 OFETs with the source, drain and gate electrodes patterned by inkjet printing of silver-based ink with a common source configuration. The inset shows a magnification of the source and drain interdigitated electrodes.

Matrix system electromechanical characterization

Since the results of the single OFET characterization showed that the sensitivities to mechanical deformation of Pentacene and TIPS-pentacene based devices were comparable, the latter, deposited from liquid phase (0.5 wt.% in toluene solution) by drop casting, has been used for the fabrication of matrices with 64 elements. The experimental set-up employed in order to evaluate the mechanical sensing of such systems consisted of a hemispheric indenter (4 mm radius) which exerted a vertical force on the matrix elements. As both vertical position (Δz) and force (F) of the indenter can be precisely controlled, in this way it was possible to proper calibrate the system, by measuring the electrical response of the tested devices induced by the applied external mechanical stimuli. With the aim to prevent the OTFTs from damages and also to

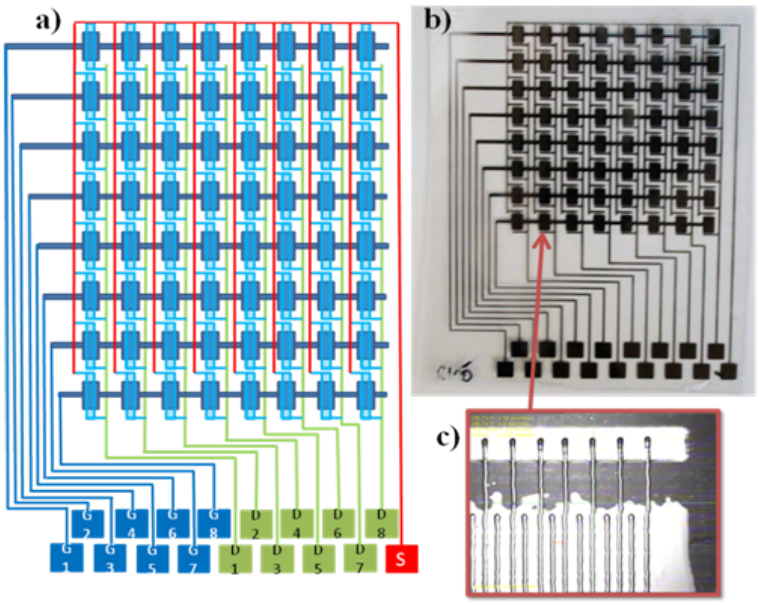

Figure 4.22: Schematic (a) and photograph (b) of OFETs in the matrix configuration on PET substrate; magnification of a single OFET device, showing the inkjet printed interdigitated source and drain electrodes (c).

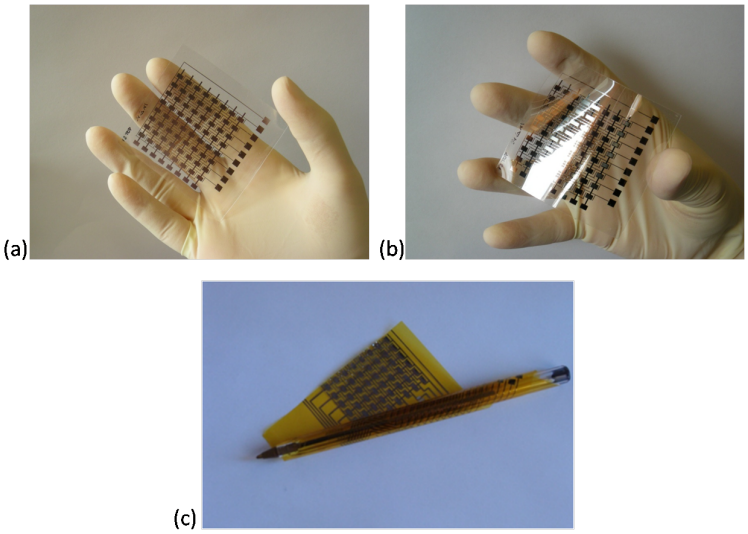

Figure 4.23: Photographs showing the size and the flexibility of the matrices realized on PET (a and b) and Kapton (c) substrates.

allow the PET substrate to get deformed by the vertical force applied, the PET substrates were embedded between two layers of a polydimethylsiloxane (PDMS) elastomer during the electrical characterization. The electrical response of the system to the applied mechanical stimuli and, consequently, to the induced surface strain is evaluated by recording the output current variation of each device within the matrix, as shown in Figure 4.24(a), where $\Delta I_D/I_{D0}$ vs F curve is plotted for 4 subsequent measurements cycle. The results can be summarized in three major points: 1) the reproducibility is good over the whole range of applied forces; 2) the response is linear for applied forces up to 1 N, which correspond to soft touches, while it saturates for higher forces; 3) the resolution (lowest detectable force) is around 0.05 N. Also, a dynamic test has been performed: an arbitrary pressure has been applied by moving a finger forward and backward across an entire row of sensors, and the response of each sensor has been recorded. Figure 4.24(c) reports I_D vs time curves of all the sensors of a row: the

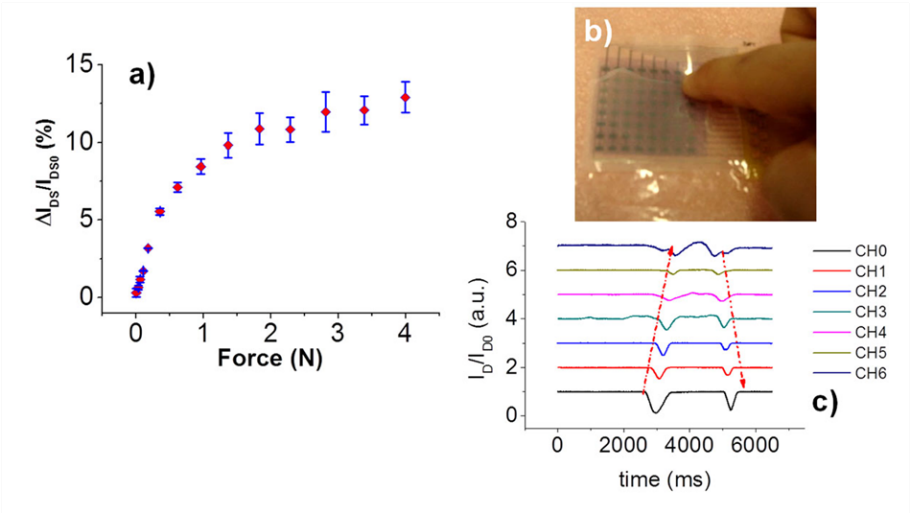

Figure 4.24: Calibration curve (Current vs Force) of inkjet printed OTFTs mechanical sensors (a). Picture of an inkjet printed matrix during a mechanical deformation test (b); electrical response of 8 different elements on the same row of the reported matrix during mechanical deformation (c).

responses are shifted in time since the stimulus propagates across them, nicely reproducing the movement of the finger (Figure 4.24 b). Moreover, since the dimension of the finger is comparable to the spatial resolution of the matrix (5 mm lateral pitch), a small cross talking can be observed: when the finger induces a deformation on one

element of the matrix, a small deformation is applied also to the adjacent elements. Summarizing we have demonstrated that OTFTs can be employed for the fabrication of mechanical sensors. In particular, it was shown that also solution-processable materials, such as TIPS-pentacene, can be employed for the same goal, giving rise to a pronounced, reproducible and linear (within a certain range) response to the applied mechanical stimulus. Moreover, matrices of 8×8 inkjet printed OTFTs have been fabricated and tested as tactile transducers, showing a reproducible, linear response for pressures up to 1 N, with a resolution of 0.05 N. These results represent a step forward for the fabrication, at low costs and over large areas, of flexible and compliant electronics for artificial skin applications.

Design, fabrication and test of arrays of piezoelectric transducers for robotic tactile sensors

Another kind of tactile transducers have been realized, in collaboration with the University of Genova and the Italian Institute of Technology, by inkjet printing of silver electrodes onto PVDF thin films in order to realize piezoelectric transducers. The experimental details concerning the printing process are reported in Chapter 2.
The complete system is composed of a large number of spatially distributed tactile elements (i.e. taxels), organized in a number of patches, which are surface compliant structures designed to cover large parts of a robot body. In the current implementation, taxels consist of piezoelectric transducers, which have to be integrated on a flexible PCB substrate. On top of the taxel layer, an elastomer was positioned as a protective layer. Patterned PVDF film triangles were glued on the PCB by the use of conductive Epoxy. The system has then been wired by soldering metal wires on the taxel terminations on the PCB back side. In order to optimize the thickness of the protective layer, freestanding PDMS films were prepared with different thicknesses. A 2.5 mm layer thickness has been finally chosen as optimally meeting the application requirements. The experimental set-up is constituted by a mechanical shaker, the triangular skin module (protective layer included) and a load cell. Controllable compressive forces were applied and the charge developed by the PVDF film was measured. A three-stage charge amplifier circuit with 3 orders of magnitude dynamics was fabricated. The objective of the tests was to validate the proposed approach and assess the performance of the skin module-interface electronics tactile sensing system. Different sets of triangular prototypes have

been manufactured and tested. A 4×4 mm square indenter has been mounted on the shaker to stimulate one taxel at a time. Figure 4.25 shows some preliminary results. By varying the amplitude of the applied stimulus at a fixed frequency, 3 different taxel responses can be compared as shown in Figure 4.25(a): the most similar behaviours are associated to taxels 4 and 7 belonging to the same triangle (T1), while the third one is associated to taxel 12 of another triangle (T2). The different sets of lines correspond to the 3 output stages of the electronics. The first set correspond to the charge amplifier (CA) output, the second one to the CA output voltage amplified 16× and the third one to the CA output voltage amplified 256×. Figure 4.25(b), on the other hand, shows the response of the same taxel for three different stimulus frequencies belonging to the range of interest for the present application. Again, the different sets are associated to the different output stages. As it can be seen, a good linearity is achieved over the whole explored range.

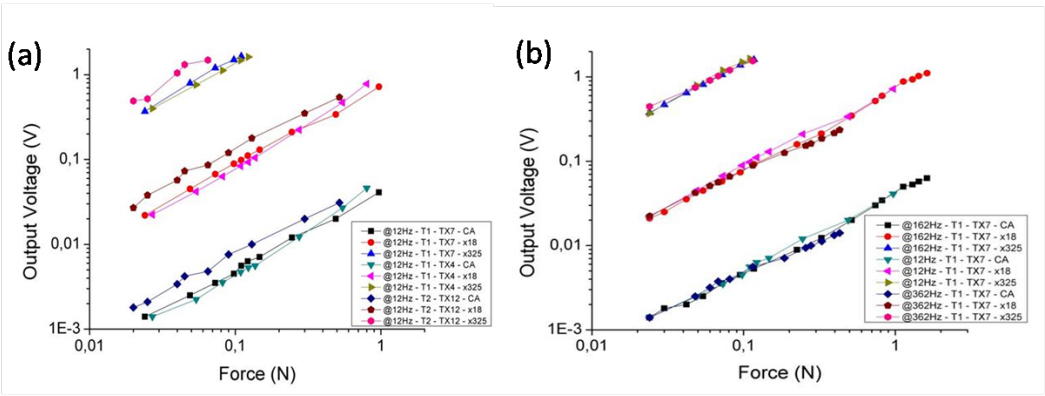

Figure 4.25: (a) Electrical response of 3 different taxels. (b) Response linearity: same taxel, different stimulus frequencies.

In summary, a large area tactile sensing system based on arrays of piezoelectric transducers has been designed, manufactured and tested. Metallic electrodes were patterned on PVDF films by means of inkjet printing. Preliminary results, showing the linearity and reproducibility of the system response to the applied mechanical stimuli, reveal the potentialities of the employed technology. Such results are intended as the first step towards the integration of different transducers on the same skin module. The presented manufacturing technology of skin patches can be scalable to cover large areas of the robot body.

4.2.5 Inkjet printing of TIPS-pentacene as active layer for OFETs

Two different approaches of inkjet printing TIPS-pentacene based inks were reported in literature. The first consists in single-droplet printing where each droplet acts as an individual functional deposit [20]; conversely, the second is based on printing multiple droplets which form a continuous film covering the whole area between the source and the drain electrodes in forming the OTFT channel [35][36]. Both methods present advantages and drawbacks. With the first, high crystal ordering is easily achievable controlling the hydrodynamic flows in the drying droplet which forms the channel (e.g. using a mixed solvent system or varying the surface energy of the substrate), leading to hole mobilities up to 0.2 cm^2/Vs for pure TIPS-pentacene inks and up to 1 cm^2/Vs for inks containing TIPS-pentacene blended with insulating or other semiconductive polymers [20]. On the other hand, printing multiple droplets could be more effective in forming an uniform thin film over a large area if the spot produced by one single droplet does not cover the channel region (e.g. if the channel length is greater than the droplet diameter); printing of several separate single drops in fact can lead to interfaces between droplets which negatively affect the uniformity of the printed active layer [36]. Employing this latter printing method mobilities up to 0.24 cm^2/Vs for pure TIPS-pentacene [36] and up to 0.11 cm^2/Vs in devices were TIPS blended with polystyrene was employed [35] were reported.

Both the inkjet printing approaches described above and drop casting were used for the realization of the TIPS-pentacene active layer of the OTFTs reported in this work. Two solutions with different TIPS-pentacene (provided by Sigma-Aldrich co.[37]) concentrations, i.e. 0.5 wt.% and 5 wt.% in toluene were prepared. Before deposition each solution was stirred for 1 h at 90 °C on a hot plate and, in case of inkjet printing, subjected to ultrasonic bath for 15 min before filling a DMP-11610 cartridge. The solutions were deposited without filtering. During deposition, the substrate (parylene C) was kept at a constant temperature of 90 °C for drop cast and of 60 °C for inkjet printed samples in order to promote fast solvent evaporation and subsequently to obtain a better crystallization of the semiconductor [38]. In Figure 4.26 the optical images with magnification of 5× for both TIPS-pentacene 5 wt.% (a) and 0.5 wt.% (b) solutions drop cast on parylene coated PET substrate are reported. Figure 4.27 instead reports the optical images of TIPS-pentacene 5 wt.% in toluene solution deposited by means

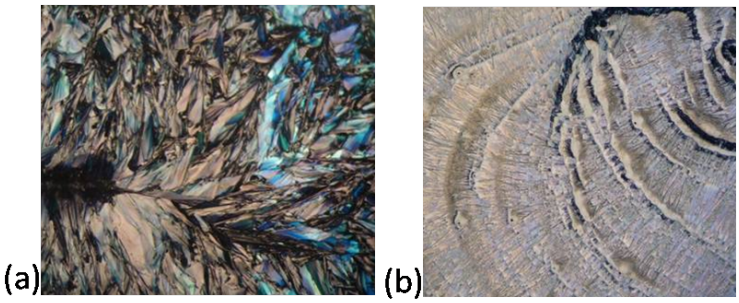

Figure 4.26: Optical images (magnification of 5×) of TIPS-pentacene 5 wt.% (a) and 0.5 wt.% (b) in toluene solutions drop cast onto parylene coated PET substrate.

of inkjet printing. The multiple-droplets and single-droplet approaches were developed employing small (≤90 μm) drop spacings for the first ((a) and (b)) and large (200 μm) drop spacing for the second (c). It can be clearly seen that multiple-droplets method led to superimposition between adjacent printed drops. The printing parameters used in both the approaches are listed in Table 4.2. It should be noted that single droplets patterns have to be printed with one single nozzle jetting at frequency of 1 kHz (the lowest limit of the printer); printing with higher frequency values in fact could lead to chaotic and uncontrolled droplets deposition. The optimal drop spacing which has to be used in order to obtain ordered separate droplets with a jetting frequency of 1 kHz is 150 μm. Although through the optimization of printing parameters it is possible to

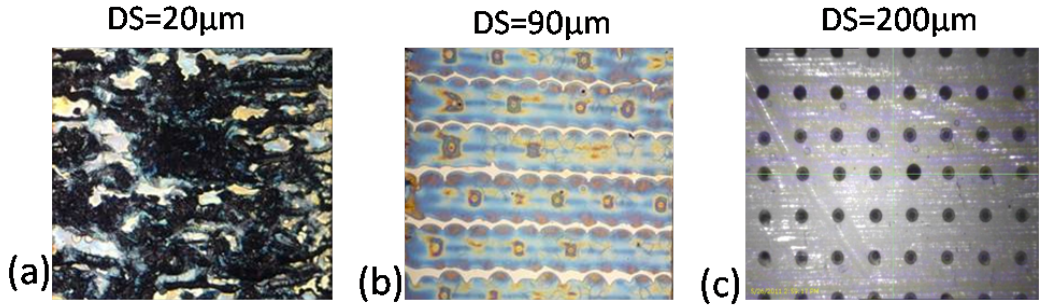

Figure 4.27: Optical images (magnification of 5×) of TIPS-pentacene 5 wt.% in toluene inkjet printed parylene coated PET substrate with a drop spacing of 20 μm (a) and 90 μm (b)(multiple-droplets approach). (c) Optical image taken by means of the Fiducial Camera of the same solution printed with a drop spacing of 200 μm.; the droplets diameter ranges between 40 and 60 μm (single-droplet approach).

Main Settings	multiple-droplets	single-drop
Firing Voltages range	20 - 25 V	12 - 15 V
Cartridge Print Heigh	1 mm	1 mm
Platen Temperature	60 °C	60 °C
Cartridge Temperature	RT	RT
Maximum Jetting Frequency range	25 kHz	1 kHz
Drop spacing	> 90 μm	> 120 μm
Number of jetting nozzles	2	1

Table 4.2: Main cartridge and printer settings used in printing TIPS-pentacene based ink with multiple-droplets and single-drop approach.

print ordered separate droplets in a controlled way, if the transistor has a channel larger than the drop diameter, one drop will not be able to cover the distance between source and drain electrode and, consequently, two or more partially superimposed droplets have to be printed anyway in order to form the active layer of the device. An example of such cases is depicted in Figure 4.28 where a comparison between the channel formed by two rows of partially superimposed drops (a) and by a single row of separate drops (b) is shown. In the first case the the drop diameter (around 50 μm) is smaller than the distance between source and drain electrodes (80 μm), while in the second case it is larger (since the distance between source and drain electrodes is 30 μm).

Electrical characterization

First, we tested the electrical performances of transistors with active layer realized by inkjet printing of TIPS-pentacene 0.5 wt.% in toluene solution with a multiple droplet approach. In Figure 4.29 are reported the output and transfer characteristics for OFETs with silver printed electrodes in interdigitated configuration (L=50 μm, Z=50 mm), with TIPS-pentacene 0.5 wt.% solution deposited by means of drop casting (a and b) and inkjet printing using a multiple droplets approach (using a drop spacing of 30 μm) (c and d). As already discussed in the previous paragraphs, the most diluted solution deposited by drop casting, led to good electrical performances with charge mobility values up to 0.1 cm^2/Vs; on the contrary for printed samples very low mobility values, i.e. up to 0.1×10^{-5} cm^2/Vs, were recorded. When the 0.5 wt. % ink is deposited

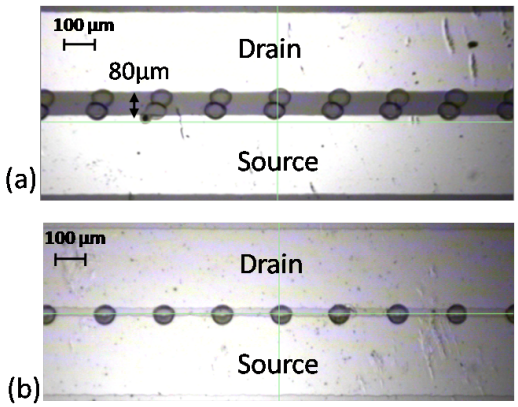

Figure 4.28: Transistor channel formed by two rows of partially superimposed TIPS drops (a) (the distance between source and drain electrode is 80 μm in this case) and by a single row of separate TIPS drops (b) (distance between source and drain electrodes of 30 μm).

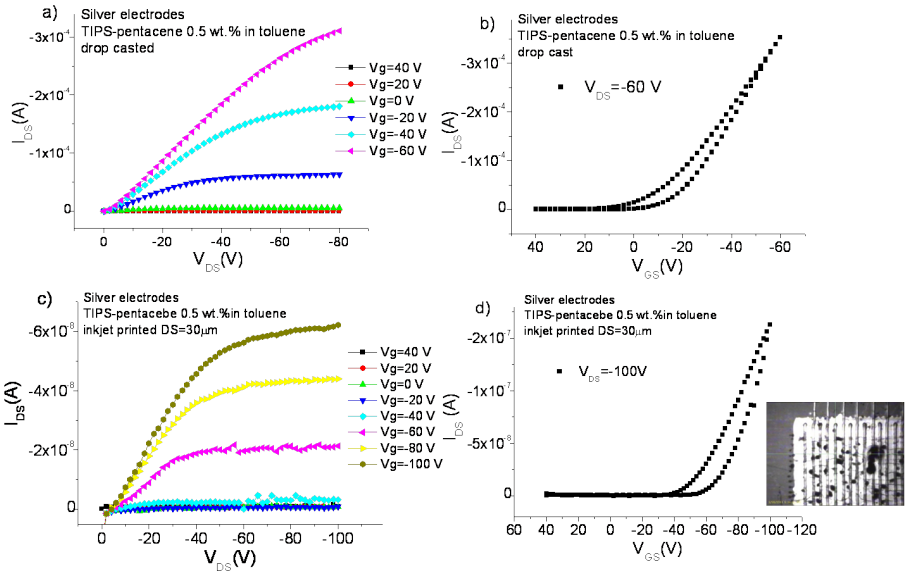

Figure 4.29: Electrical characteristics of devices with TIPS-pentacene 0.5 wt.% solution deposited by means of drop casting (a and b) and inkjet printing using a multiple droplets approach (c and d). The inset reports a photograph of the channel region after the deposition of the semiconductor solutions taken by means of the Fiducial Camera.

by means of inkjet printing (with 10 pL droplets), in fact, the amount of material which forms the channel results insufficient to guarantee good electrical performances, as confirmed by the AFM images reported in Figure 4.30 and by XRD spectra reported afterwards. Figure 4.30, in fact, reports a comparison between the AFM images taken analysing two samples, one with TIPS-pentacene 0.5 wt.% solution deposited by drop casting on the silver electrode (a) and in the channel region (b) and one with the same solution deposited by means of inkjet printing (c); the dashed lines roughly indicate the interfaces between the channel region and the silver electrodes. It can be clearly noticed that in inkjet printed samples a very small amount of material is located in the channel, with crystals which are insulated and bigger than in the drop cast samples.

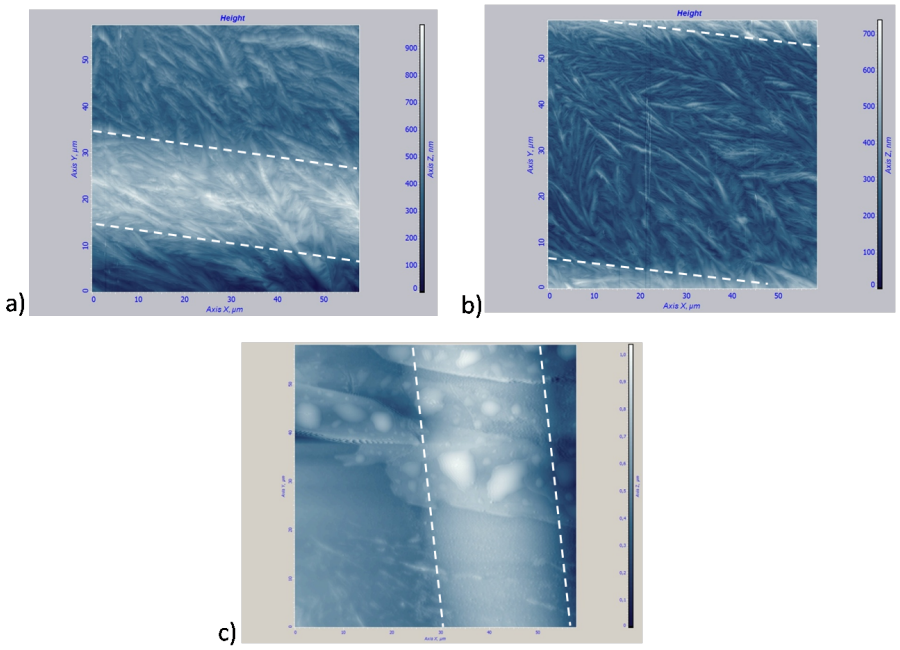

Figure 4.30: Comparison between the AFM images taken from a sample with TIPS-pentacene 0.5 wt.% solution deposited by drop casting on the silver electrode (a) and in the channel region (b) and by means of inkjet printing (c). The dashed lines indicate roughly the interfaces between the channel region and the silver electrodes.

In order to overcome this problem, for depositing a larger amount of material in the channel, a 10 times more concentrated solution, i.e. TIPS-pentacene 5 wt.% in toluene, was tested. The electrical characteristics for devices realized both by drop casting and inkjet printing (multiple droplets approach with drop spacing of 50 μm) are shown

in Figure 4.31. As it could be noticed, the device with the drop cast solution did not

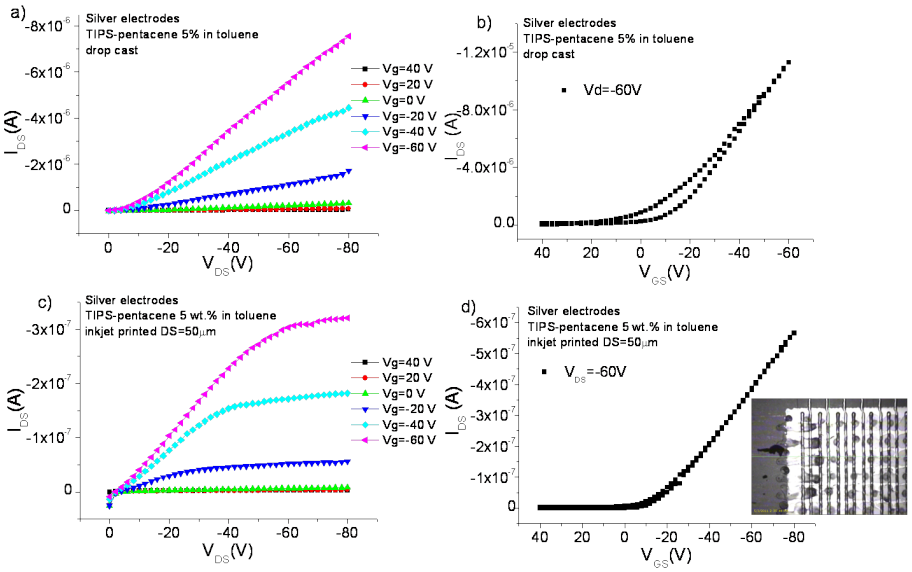

Figure 4.31: Electrical characteristics of devices with TIPS-pentacene 5 wt.% solution deposited by means of drop casting (a and b) and inkjet printing using a multiple droplets approach (c and d). The inset reports a photograph of the channel region after the deposition of the semiconductor solutions taken by means of the Fiducial Camera.

exhibit the saturation of the source-drain current, probably because of the large amount of material in the channel region. On the contrary, when printed, the most concentrated ink exhibited better electrical performances than the most diluted solution, with higher current values and higher mobility values, i.e. up to 8×10^{-5} cm^2/Vs. Both the solutions led however to low mobility and current values. For this reason, we decided to test the single droplet approach employing only the most concentrated ink. In order to better control the single droplet deposition, this approach was applied to OFETs with linear channel. It should be noticed that when transistors with inkjet printed silver electrodes were used, the minimum achieved distance between source and drain electrodes, in the range 60 - 50 μm, is larger than or, at least, equal to the average drop diameter, 50 μm. Thus, the deposition of one single drop doesn't allow the formation of the channel with a good overlapping between the semiconductor and the metallic electrodes. In this case, two or more rows of partially overlapping droplets had to be printed in order to form the channel. In such devices charge mobility values up to 2×10^{-3} cm^2/Vs were

observed, thus more than one order of magnitude higher than those obtained applying the multiple droplets method. Figure 4.32 reports the electrical characteristics of one of such devices, realized printing the 5 wt.% TIPS-pentacene solution with a drop spacing of 120 μm (in the inset a photograph of the device is shown). As discussed in Chapter

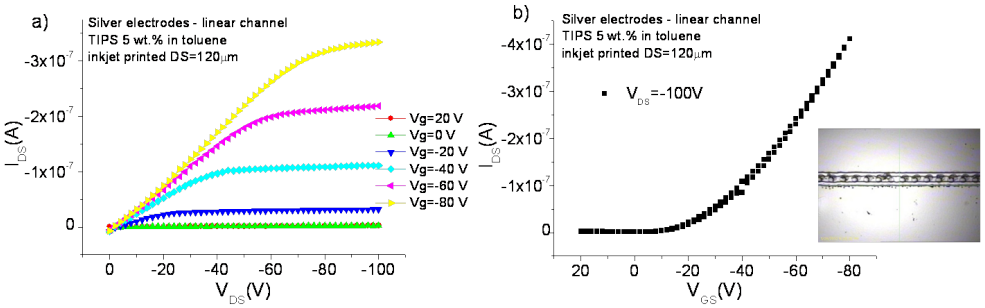

Figure 4.32: Electrical characteristics of an OTFT with silver inkjet printed electrodes (linear channel W=60 μm), realized printing the 5 wt.% TIPS-pentacene solution with a drop spacing of 120 μm. In the inset a photograph of the device, showing the partial superimposition of the droplets which form the channel is reported.

2, subsection 2.3.2, a procedure was developed also to realize short channel (L= 30 μm) devices with inkjet printed silver electrodes. Unfortunately for most of these transistors we measured a short circuit between source and drain electrodes; moreover, the thickness of the silver electrodes does not allow a good wettability of both source and drain electrodes with only one drop and the channel can be formed again by at least two partially overlapped drops. Therefore, devices with gold electrodes patterned through common photolitography with a channel length of 30 μm were realized in order to finally test the performances of TIPS-pentacene when actually one single droplet acts as an individual functional unit to form the channel, without discontinuity and grain boundaries in the active layer. The electrical characteristics of such devices are shown in Figure 4.33. Mobility values up to 8×10^{-3} cm^2/Vs have been recorded, even higher then the previous case.

XRD measurements

XRD measurements were performed in order to correlate crystal order of TIPS-pentacene samples both inkjet printed and drop cast with their electrical performances as active

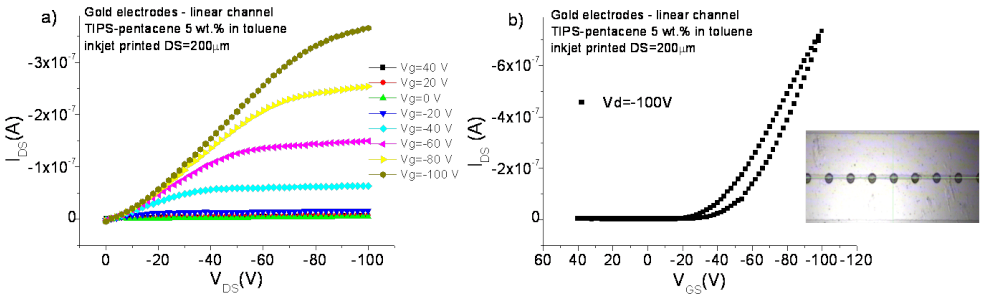

Figure 4.33: Electrical characteristics of a OTFT with gold electrodes (L= 30 μm) and TIPS-pentacene 5 wt.% solution inkjet printed with single drop approach as active layer. The inset report a photograph of the channel region where single droplets of TIPS-pentacene solution were deposited.

layer of OTFTs just discussed. In Figure 4.34 the comparison between the XRD spectra in specular geometry for samples consisting on TIPS-pentacene 5 wt.% in toluene solution, drop cast and inkjet printed on a substrate of 175 μm thick PET foil, coated with a 1.5 μm thick parylene layer, is reported. The inkjet printed samples were realized with a multiple droplets approach using drop spacings of 20 μm, 50 μm and 90 μm. Specular X-ray diffraction scans showed that both drop cast and inkjet printed samples were highly crystalline and had the molecular orientation ($\pi - \pi$ stacking perpendicular to the surface) requested for good horizontal charge transport. These observations agree with those reported by Sele et al.[38], for dip-coated TIPS-pentacene films onto silicon wafers from a toluene solution containing 1 wt.% TIPS-pentacene. However, we observed another peak (about 12.5°) which could be due either to the presence of crystallites with a different orientation or to material not completely dissolved in the solution. In the drop cast sample, the presence of some peaks (marked with apices in Figure 4.34) at lower 2Θ angles, indicates the coexistence of a thin film phase and a bulk phase which is not present or not measurable for inkjet printed samples. The integrated intensity of the inkjet printed samples is lower than that of the drop cast sample and decreases with increasing of drop spacing: this indicates a smaller amount of crystalline material due in turn to a lower amount of deposited material. Almost the same considerations can be done about the specular XRD spectra of samples realized employing the 0.5 wt.% solution, reported in Figure 4.35; the main difference is the absence of the peak at 12.5°. Analysing more in detail the XRD spectra for the two

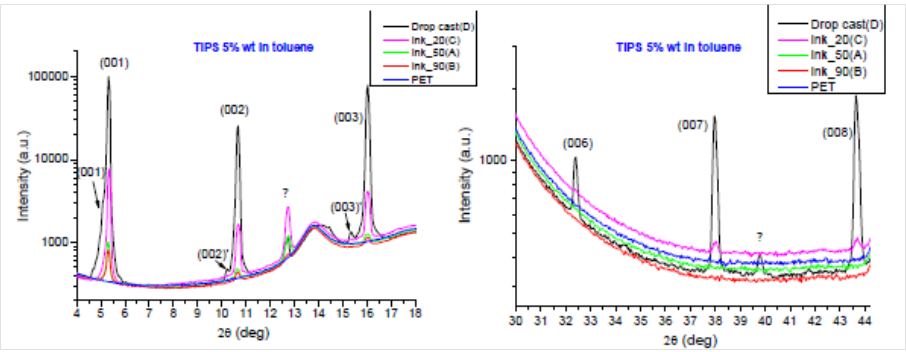

Figure 4.34: XRD spectra in specular geometry for samples of TIPS-pentacene 5 wt.% in toluene solution drop cast and inkjet printed on a substrate of 175 mum thick PET coated with a 1.5 μm thick parylene layer is reported. The inkjet printed samples were realized with a multiple droplets approach using drop spacings of 20 μm, 50 μm and 90 μm.

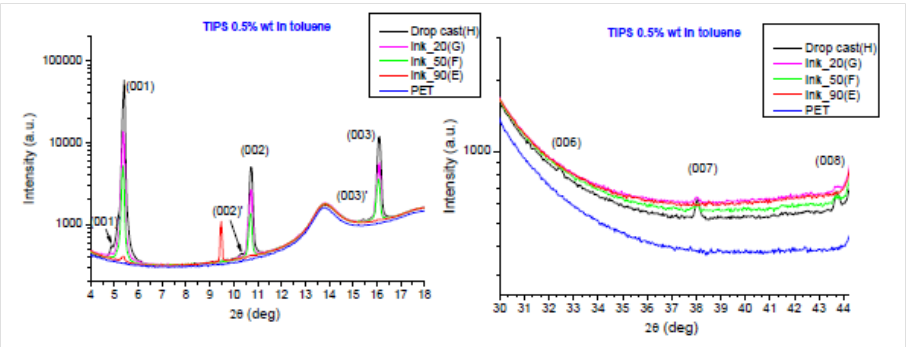

Figure 4.35: Comparison of the XRD spectra in specular geometry for samples of TIPS-pentacene 0.5 wt.% in toluene solution drop cast and inkjet printed on a substrate of 175 mum thick PET coated with a 1.5 μm thick parylene layer is reported. The inkjet printed samples were realized with a multiple droplets approach using drop spacings of 20 μm, 50 μm and 90 μm.

solutions deposited with the same method, the following considerations can also be done:

- Drop cast samples (Figure 4.36): both samples are highly crystalline but the most concentrated one have more intense peaks, caused by a larger amount of crystalline material per unit area;

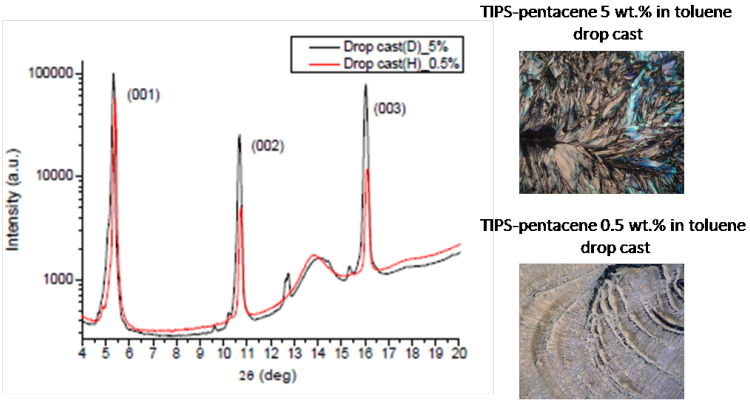

Figure 4.36: (Left) Comparison between the XRD spectra for TIPS-pentacene solution with concentration of 0.5 wt.% (red line) and 5 wt.% (black line) drop cast. (Right) Optical images (magnification of 5×) of the two samples.

- Inkjet printed samples - Drop spacing of 20 μm (Figure 4.37): The peaks have similar intensity for both samples, thus the crystal order and the amount of the deposited material are similar independently of the different morphologies (see optical images in Figure 4.37 left);
- Inkjet printed samples - Drop spacing of 50 μm (Figure 4.38): in this case the most intense peaks have been observed for the 0.5 wt.% sample, because material agglomerates in localized and probably crystalline regions, as can be clearly observed in the optical images (Figure 4.38 left);
- Inkjet printed samples - Drop spacing of 90 μm (4.39): the low intense XRD peaks of the 0.5 wt.% TIPS-pentacene sample show that a very low amount of material was deposited.

It should be noted that also the XRD spectra of TIPS-pentacene 5 wt.% in toluene solution deposited with single drop approach were collected. The samples consisted of

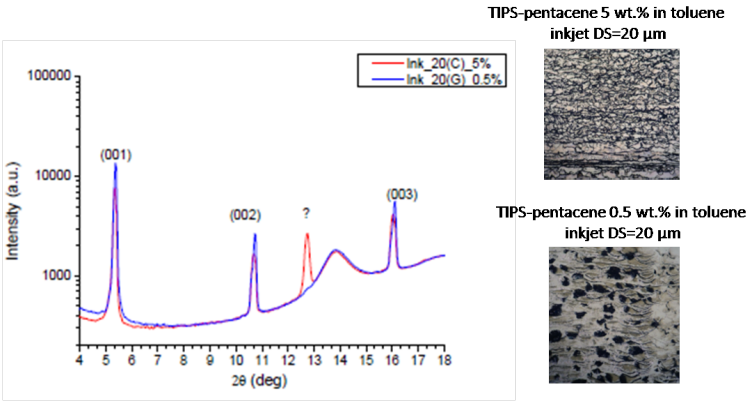

Figure 4.37: (Left) Comparison between the XRD spectra for TIPS-pentacene solution with concentration of 0.5 wt.% (blue line) and 5 wt.% (red line) inkjet printed using a drop spacing of 20 μm. (Right) Optical images (magnification of 5×) of the two samples.

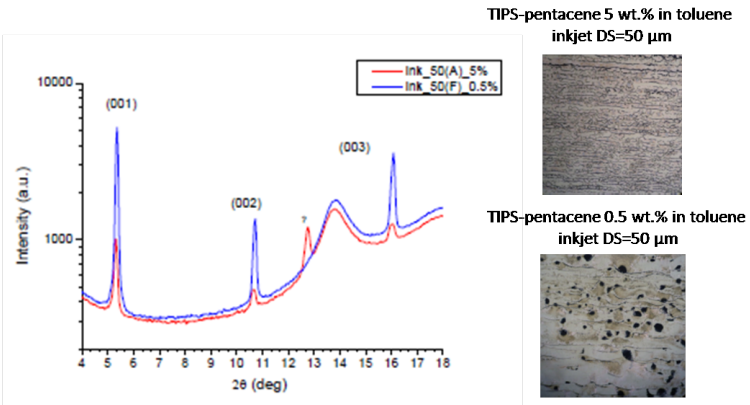

Figure 4.38: (Left) Comparison between the XRD spectra for TIPS-pentacene solution with concentration of 0.5 wt.% (blue line) and 5 wt.% (red line) inkjet printed using a drop spacing of 50 μm. (Right) Optical images (magnification of 5×) of the two samples.

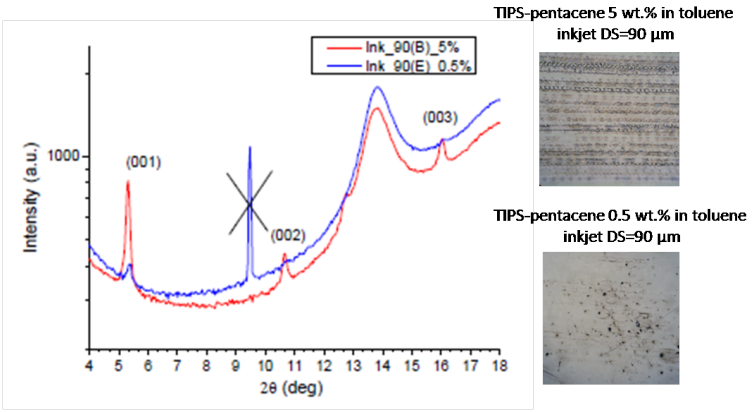

Figure 4.39: (Left) Comparison between the XRD spectra for TIPS-pentacene solution with concentration of 0.5 wt.% (blue line) and 5 wt.% (red line) inkjet printed using a drop spacing of 90 μm. (Right) Optical images (magnification of 5×) of the two samples.

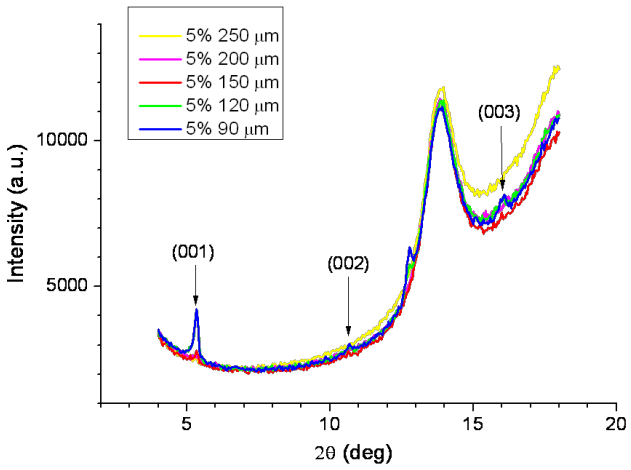

Figure 4.40: XRD spectra for samples of TIPS-pentacene 5 wt.% in toluene solution inkjet printed on a substrate of 175 mum thick PET coated with a 1.5 μm thick parylene layer is reported. The samples were realized with a single drop approach using drop spacings of 250 μm, 200 μm, 150 μm, 120 μm. Also the spectrum of the sample realized with a drop spacing of 90 μm is reported.

Deposition technique	*Solution and drop spacing*	*Approach*	*Mobility (cm^2/Vs)*
Drop casting	TIPS-pentacene 0.5 wt.%	-	9.63×10^{-2}
	TIPS-pentacene 5 wt.%		1.32×10^{-2}
Inkjet printing	TIPS-pentacene 5 wt.% DS=50 μm	multiple droplets	7.9×10^{-5}
	TIPS-pentacene 5 wt.% DS=90 μm		–
	TIPS-pentacene 5 wt.% DS=120 μm	single drop	sample A: 1.45×10^{-3}
			sample B: 2.38×10^{-3}
	TIPS-pentacene 5 wt.% DS=150 μm		1.82×10^{-3}
	TIPS-pentacene 5 wt.% DS=200 μm		sample A: 1.22×10^{-3}
			sample B: 1.11×10^{-3}
			sample C: 5.88×10^{-3}

Table 4.3: Transistors characterized by means of photocurrent spectroscopy technique.

square patterns filled with several separated inkjet printed spots. Figure 4.40 shows the spectra referred to different drop spacings: 250 μm, 200 μm, 150 μm, 120 μm and 90 μm. The signal began to be observed for drop spacing of 150 μm, while for higher drop spacings there was not signal maybe because of the low density, and consequently the low amount, of material deposited. The peaks of samples with drop spacings of 120 μm and 90 μm have equal intensity.

Photocurrent measurements

The photocurrent measurements were performed on devices with the active layer deposited by drop casting (both TIPS-pentacene 0.5 wt.% and 5 wt.% solutions), inkjet printing with multiple droplets approach and inkjet printing with single drop approach. All samples were previously electrically characterized as transistors and the respective charge mobilities values were calculated from their transfer characteristics. In Table 4.3 a summary of the samples analysed is reported. The PC collected spectra have been compared with the absorbance spectra reported in literature. First of all, we noticed that only some of our samples show a spectrum with peaks position similar to the characteristic absorption peaks at 600, 650 and 700 nm of TIPS-pentacene crystalline thin

film [39], while all of them present a marked peak around 400 nm always with an intensity higher that the other peaks. Figure 4.41(top) shows the normalized photocurrent spectra of samples deposited by drop casting and inkjet printing with a multiple droplets approach, while in Figure 4.42(bottom) the spectra referred to samples inkjet printed with a single drop approach are reported; the peak around 400 nm is indicated with a red arrow. A similar feature was observed by Davis et al.[39] in the comparison be-

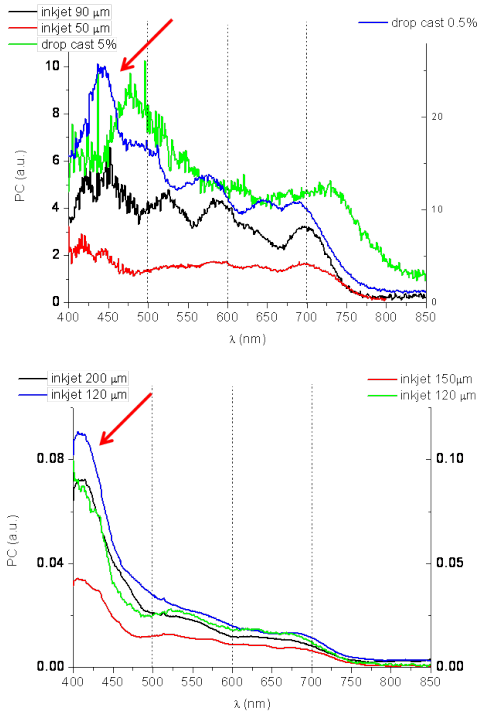

Figure 4.41: Normalized photocurrent spectra for samples of TIPS-pentacene deposited by drop casting, inkjet printing with multiple droplets approach (top) and inkjet printing with single drop approach (bottom). The red arrows indicates the peak around 400 nm observed for all the characterized samples.

tween the optical absorption spectra of TIPS-pentacene deposited by drop-casting and spin casting: they observed that sharp peaks appeared at 425 and 450 nm in the more disordered spin-cast film, along with a change in the relative intensities of the peaks at 600, 650 and 700 nm; moreover the onset of absorption for spin-cast TIPS-pentacene films was very slightly blue shifted compared to that for the drop-cast film (see Figure 4.42). These changes in the absorption characteristics of the spin-cast TIPS-pentacene

film were related to a lower degree of molecular order and thus a lower crystallinity of the spin-cast sample. The correlation between the crystal ordering and the photo-

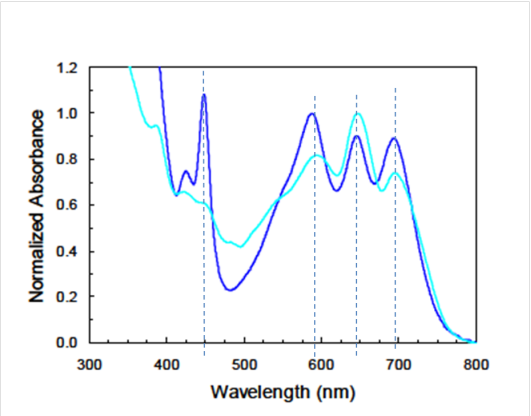

Figure 4.42: Normalized UV/Vis spectra for drop cast (light blue) and spun cast (dark blue) thin films of TIPS-pentacene on ZnO reported by Davis et al.[39].

conductive properties of TIPS-pentacene thin films was also studied by Ostroverkhova et al.[40], who observed a red shift in the spectra of highly crystalline TIPS-pentacene samples i.e. drop cast and thermal evaporated (sample FPc 1b, solid line in Figure 4.43), respect to the samples in liquid phase (sample FPc in tetrahydrofuran, dash-dotted line in Figure 4.43) which have an amorphous structure. All our samples did not exhibit spectra comparable with that of the liquid solution, indicating thus that none of them seemed to have a completely amorphous structure. Also, referring to

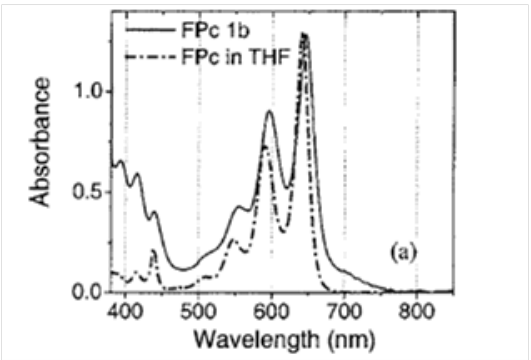

Figure 4.43: Optical-absorption spectra of TIPS-pentacene in tetrahydrofuran solution (dash-dotted line) and TIPS-pentacene thin film evaporated on glass (solid line)[40].

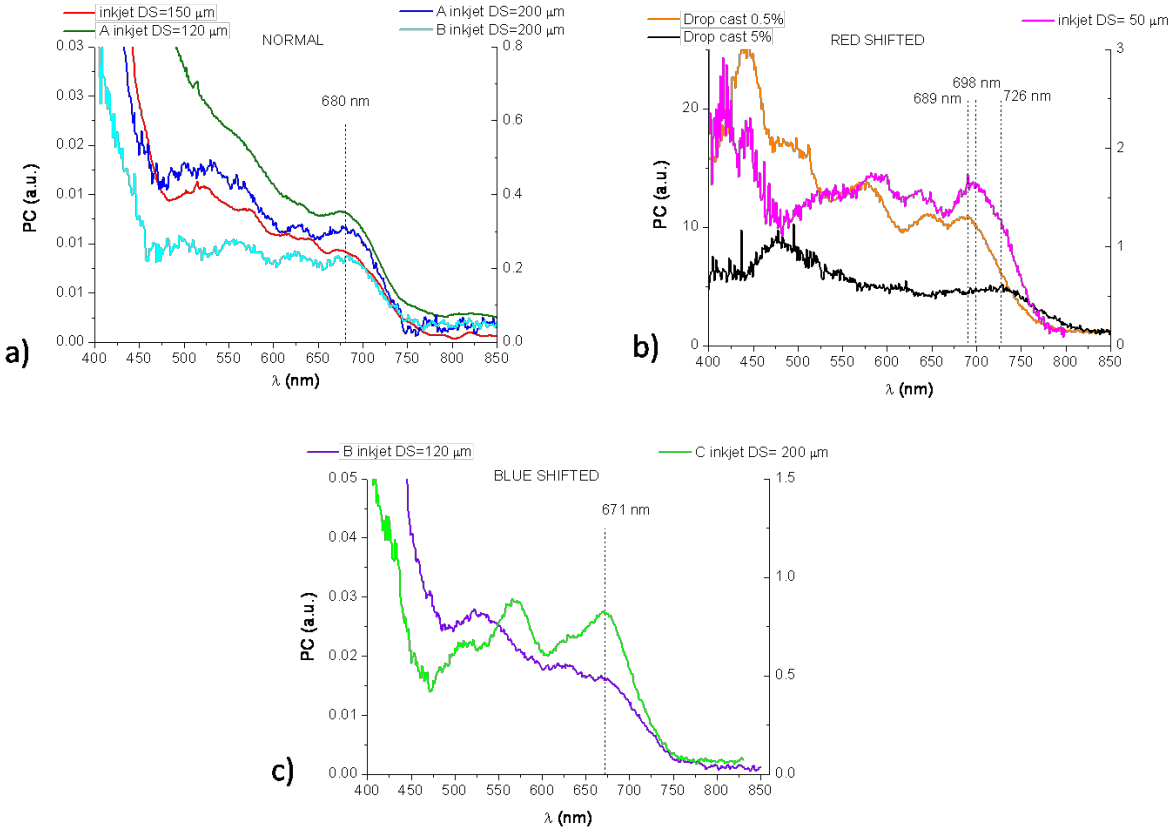

Figure 4.44: Photocurrent spectra of the inkjet printed samples with mobility values in the range $1.1 \times 10^{-3} \div 1.8 \times 10^{-3}$ cm^2/Vs which showed the first peak at 680 nm (a). The inkjet printed samples with a higher mobility values showed a blue-shift in the spectrum (c) while for lower mobility values a red-shift occurred (b). The drop cast samples which have the highest mobility values, showed a red-shift exhibiting thus an opposite behaviour respect to the inkjet printed samples.

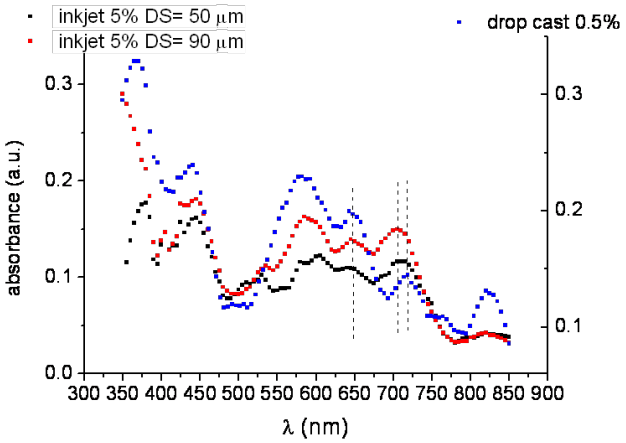

Figure 4.45: Absorption spectra of samples realized by drop casting of TIPS-pentacene 0.5 wt.% in toluene solution and inkjet printing with multiple droplets approach of 5 wt.% TIPS-pentacene in toluene solution.

the first peak of the spectra, i.e. the peak at higher wavelength, we observed a correlation, for the inkjet printed samples, between the peak position and the corresponding mobility of the device. Almost all the inkjet printed samples spectra had the first peak at 680 nm corresponding to mobilities in the range $1.1 \times 10^{-3} \div 1.8 \times 10^{-3}$ cm^2/Vs; the spectra of these samples are reported in Figure 4.44(a). The photocurrent spectra of inkjet printed samples with higher mobility values (around 6×10^{-3} cm^2/Vs), showed a blue-shift of the first peak at wavelength of 671 nm (Figure 4.44(c)); while the inkjet printed samples which exhibited lower mobility values (around 8×10^{-5} cm^2/Vs) i.e. those realized with a multiple droplets approach, exhibited a red-shift of the first peak at 698 nm (Figure 4.44(b)). The drop cast samples, which have the highest mobility values, showed a red-shift exhibiting thus an opposite behaviour respect to the inkjet printed samples. These results were confirmed by the optical absorption measures performed on the sample realized by drop casting of TIPS-pentacene 0.5 wt.% solution and by inkjet printing with multiple droplets approach of 5 wt.% TIPS-pentacene solution i.e. the samples with the highest and the lowest recorded mobility values respectively (see Figure 4.45).

Comparing the results obtained in the electrical characteristics, the XRD scans and

the PC and optical absorption measurements on the samples realized by inkjet printing of TIPS-pentacene based solution, we may conclude that the electrical performances of the devices seems to be correlated more with the morphology than with the crystal order of the active layer. The main cause for the limited mobility values in the inkjet printed samples, in fact, seems to be the presence of grain boundaries between extended highly crystalline regions, which limit the hopping transport of the charge carriers, instead of the lack of crystalline order of the whole active layer. The effect of such grain boundaries is more pronounced in the samples realized by inkjet printing with multiple droplets approach, where very low mobility values were founded even if all the spectra collected (XRD, photocurrent and optical absorption) showed a high crystal order. Conversely, the samples inkjet printed with a single drop approach, although exhibiting higher mobility values, showed less intense peaks in the XRD spectra and a blue-shift of the PC spectra, both indicating a lower crystal order. These features, in fact, may be due to the presence of crystalline micro-domains with different orientations which affects the XRD and PC spectra but still allow the charge transport, with consequent higher values of the charge carriers mobility.

Bibliography

[1] H. Koezuka, A. Tsumura, T. Ando, *Synth. Met.*, **1987**, 18, 699. 116

[2] J. Takeya, M. Yamagishi, Y. Tominari, R. Hirahara, Y. Nakazawa, T. Nishikawa, T. Kawase, T. Shimoda, S. Ogawa, *Appl. Phys. Lett.*, **2007**, 90, 10 , 2120-2123. 116

[3] G. Horowitz, *Adv. Mater.*, **1998**, 10, 5, 365-777. 116

[4] P. Cosseddu, *Correlation between interface-dependent properties and electrical performances in OFETs*, PhD Thesis, University of Cagliari, **2006**. 118

[5] IEEE, *Standard test methods for the characterisation of organic transistors and materials*, New York, **2008**, ISBN: 9780738160139. 120

[6] H. Yan, Z. Chen, Y. Zheng, C. Newman, J. R. Quinn, F. Dötz, M. Kastler, A. Facchetti, *Nature*, **2009**, 457, 679-687. 121, 122

[7] P. Cosseddu, A. Bonfiglio, *Appl. Phys. Lett.*, **2006** 88, 023506. 121

[8] P. Cosseddu, A. Bonfiglio, *Thin Solid Films*, **2007**, 515, 7551-7555. 121

[9] P. Cosseddu, A. Bonfiglio, I. Salzmann, J. P. Rabe, N. Koch, *Org. Electron.*, **2008**, 9, 191-197. 121

[10] P. Cosseddu, J.-O. Vogel, B. Fraboni, J. P. Rabe, N. Koch, A. Bonfiglio, *Adv. Mater.*, **2009**, 21, 3, 344-348. 121

[11] P. Cosseddu, A. Bonfiglio, *Appl. Phys. Lett.*, **2010**, 97, 203305. 121

[12] T. Kawase, T. Shimoda, C. Newsome, H. Sirringhaus, R. H. Friend, *Thin Solid Films*, **2003**, 438-439, 279-287. 123, 124

[13] T. Sekitani, Y. Noguchi, U. Zschieschang, H. Klauk, T. Someya, *Proceedings of the National Academy of Sciences*, **2008**, 105, 4976-4980. 124, 125, 126

[14] C. W. Sele, T. Werne, R. H. Friend, H. Sirringhaus, *Adv. Mater.*, **2005**, 17, 997. 124, 125

[15] M. Singh, H. M. Haverinen, P. Dhagat, G. E. Jabbour, *Adv. Mater.*, **2010**, 22, 673-685. 126

[16] Y. Noguchi, T. Sekitani, T. Yokota, T. Someya, *Appl. Phys. Lett.*, **2008**, 93, 043303. 126

BIBLIOGRAPHY

[17] S. E. Molesa, S. K. Volkman, D. R. Redinger, A. de la Fuente Vornbrock, V. Subramanian, *IEEE Int. Electron Device Meeting Tech. Digest*, **2004**, 1072. 126

[18] Y. Liu, K. Varahramyan, T. Cui, *Macromol. Rapid Commun.*, **2005**, 26, 1955-1959. 126

[19] B. K. C. Kjellander, W. T. T. Smaal, J. E. Anthony, G. H. Gelinck, *Adv. Mater.*, **2010**, 22, 4612-4616. 126, 127

[20] X. Li, W. T. T. Smaal, C. Kjellander, B. van der Putten, K. Gualandris, E. C. P. Smits, J. Anthony, D. J. Broer, P. W. M. Blom, J. Genoe, G. Gelinck, *Org. El.*, **2011**, 12, 1319-1327. 126, 147

[21] T. Someya, Y. Kato, T. Sekitani, S. Iba, Y. Noguchi, Y. Murase, H. Kawaguchi, T. Sakurai, *PNAS*, **2005**, 102, 35, 12321-12325. 127

[22] H. Kawaguchi, T. Someya, T. Sekitani, T. Sakurai, *IEEE J. Solid State Circuits*, **2005**, 40, 1, 177-185. 128

[23] G. Darlinski, U. Bottger, R. Waser, H. Klauk, M. Halik, U. Zschieschang, G. Schmidt, C. Dehm, *J. Appl. Phys.*, **2005**, 97, 93708. 128

[24] T. Sekitani, Y. Kato, S. Iba, H. Shinaoka, T. Someya, T. Sakurai, S. Takagi, *Appl. Phys. Lett.*, **2005**, 86, 073511. 128

[25] C. Yang, J. Yoon, S. H. Kim, K. Hong, D. S. Chung, K. Heo, C. E. Park, M. Ree, *Appl. Phys. Lett.*, **2008**, 92, 243305. 128

[26] P. Cosseddu, A. Piras, A. Bonfiglio, *IEEE Transaction on Electron Devices*, **2011**, 58, 3416. 128

[27] J. A. Lim, J. H. Cho, Y. D. Park, D. H. Kim, M. Hwang, K. Cho, *Appl. Phys. Lett.*, **2006**, 88, 082102. 131

[28] Z. Bao, A. Dodabalapur, A. J. Lovinger, *Appl. Phys. Lett.*, **1996** 69, 26, 4108 75, 76, 131

[29] S. K. Park, Y. H. Kim, J. I. Han, D. G. Moon, W. K. Kim, M. G. Kwak, *Synthetic Metals*, **2003**, 139, 377-384. 131

[30] J-P. Hong, A-Y. Park, S. Lee, J. Kang, N. Shin, D. Y. Yoon, *Appl. Phys. Lett.*, **2008**, 92, 143311. 134

[31] http://www.roboskin.eu/ 136

[32] Second year annual report of ROBOSKIN project. Available on-line: http://www.roboskin.eu/images/report/pubsummary_ last.pdf 137

[33] J. K. F. Yau, N. Savvider, C. Sorrell, *Physica C*, **1996**, 266, 223. 138

[34] C. S. Kim, S. Lee, E. D. Gomez, J. E. Anthony, Y.-Lin Loo, *Appl. Phys. Lett.*, **2008**, 93, 103302. 139

[35] M-B. Madec, P. J. Smith, A. Malandraki, N. Wang, J. G. Korvink, S. G. Yeates, *J. Mater. Chem.*, **2010**, 20, 9155-9160. 147

[36] S. H. Lee, M. H. Choi, S. H. Han, D. J. Choo, J. Jang, S. K. Kwon, *Org. El.*, **2008**, 9, 721-726. 147

[37] http://www.sigmaaldrich.com/italy.html 147

[38] C. W. Sele, B. K. C. Kjellander, B. Niesen, M. J. Thornton, J. Bas P. H. van der Putten, K. Myny, H. J. Wondergem, A. Moser, R. Resel, A. J. J. M. van Breemen, N. van Aerle, P. Heremans, J. E. Anthony, G. H. Gelinck, *Adv. Mater.*, **2009**, 21, 4926-4931. 147, 154

[39] R. J. Davis, M. T. Lloyd, S. R. Ferreira, M. J. Bruzek, S. E. Watkins, L. Lindell, P. Sehati, M. Fahlman, J. E. Anthony, J. W. P. Hsu, *Supplementary Material (ESI) for J. Mater. Chem.*, **2011**, 21, 1721-1729. 160, 161

[40] O. Ostroverkhova, S. Shcherbyna, D. G. Cooke, R. F. Egerton, F. A. Hegmann, R. R. Tykwinski, S. R. Parkin, J. E. Anthony, *J. Appl. Phys.*, **2005**, 98, 033701. 161

Conclusions

In conclusion, in this thesis we demonstrated how inkjet printing can be employed for the realization of Organic Thin Film Transistors (OTFTs) assembled on flexible and transparent substrates. A deep study about the optimization of printing process for the deposition of several kinds of materials, in order to realize different pattern shapes have been done and reported. Mainly, two kinds of of OTFTs were fabricated and characterized: Organic ElectroChemical Transistors (OECTs) and Organic Field Effect Transistors (OFETs).

Concerning OECTs, we demonstrated the possibility of using inkjet printing to fabricate all-PEDOT:PSS devices, that are reproducible and robust enough for the realization of biosensors and low-cost circuitry. The robustness of the devices was achieved thanks to a treatment of the printed structures with Ethylene Glycol, that can be done as a final fabrication step after the printing. In this way, several runs of measurements can be performed on the same device without problems of delamination, which are typical for PEDOT:PSS devices when measured in liquid environment. We also demonstrated that the working range of such devices can be controlled by varying the device geometry (i.e. the ratio between the gate and the channel areas) as in the case of structures with the gate acting as a polarizable electrode.

After the preliminary fabrication process optimization, material tests and electrical characterization, the realization of inkjet printed OFETs developed in two complementary activities. On the one hand we have demonstrated that such devices can be employed for the fabrication of mechanical sensors. In particular, it was shown that the solution-processable organic semiconductor TIPS-pentacene can be employed as active layer, giving rise to a pronounced, reproducible and linear (within a certain range) response to the applied mechanical stimulus. Moreover, matrices of 64 inkjet printed OTFTs have been fabricated and tested as tactile transducers, showing a re-

producible, linear response for pressures up to 1 N, with a resolution of 0.05 N. These results represent a step forward for the fabrication, at low costs and over large areas, of flexible and compliant electronics for artificial skin applications. On the other hand, with the aim of realizing a full-printed device, part of the research activity was focussed on the investigation of samples with not only the conducting electrodes, but also the semiconductor layer deposited by means of inkjet printing. In particular the organic semiconductor TIPS-pentacene was employed and characterized by means of both electrical characterization and spectroscopic techniques as XRD, photocurrent and absorption measurements. We attested that the electrical performances of the devices seems to be correlated more with the morphology than with the crystal order of the active layer. The main cause for the limited mobility values in the inkjet printed samples, in fact, seems to be the presence of grain boundaries between extended highly crystalline regions, which limit the hopping transport of the charge carriers, instead of the lack of crystalline order of the whole active layer. In order to overcome this issue, inkjet printing of the semiconductor with a single droplet approach, i.e. with one single droplet acting as a individual functional unit to form the channel, should be advisable. The comparison between the spectroscopic and the electrical measures, in fact, suggested that active layers realized with this kind of deposition are characterized by the presence of crystalline micro-domains with different orientations, which lowers the overall crystal order but allows the charge transport, with consequent higher values of the charge carriers mobility.

Appendix A

Other fabrication techniques

Organic semiconductor deposition

Thermal sublimation

Thermal sublimation system has been used in this thesis for the deposition of the not-soluble pentacene small molecules (sublimation temperature $\sim 145\,^{\circ}\mathrm{C}$) as the active layer of inkjet printed OFETs. A schematic of the system is reported in Figure A.1. The process consists of thermal sublimation of material, placed in a small glass container, the *crucible*, which is heated by means of *Joule effect*: a current is passed through a resistive filament (typically Tungsten) surrounding the crucible. The evaporation

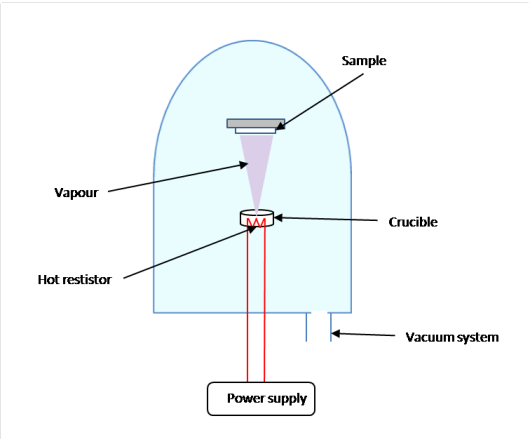

Figure A.1: Schematic of thermal evaporation system.

takes place in a *High Vacuum Chamber*, with a pressure range between 5×10^{-5} and

5×10^{-8} mbar. These low pressures are requested to avoid interaction between vapour-phase material and the residual atmosphere. Such kind of system can be also used for deposition of metallic layers (e. g. gold and aluminium) and generally permits the deposition of materials in form of thin films.

Spin coating

Spin Coating is a very simple technique used to deposit liquid phase material onto a flat substrate. In Figure A.2 the different phases involved in the process are shown:

a) Once the substrate is fixed on the spinning plate, a certain amount of liquid phase material is placed on it.

b) The substrate is spun round at high speed.

c) The fluid is spread on the substrate by centrifugal force and the excess material is expelled.

d) After the rotation is stopped, the solvent evaporation leads to the dried, uniformly distributed, spin coated film.

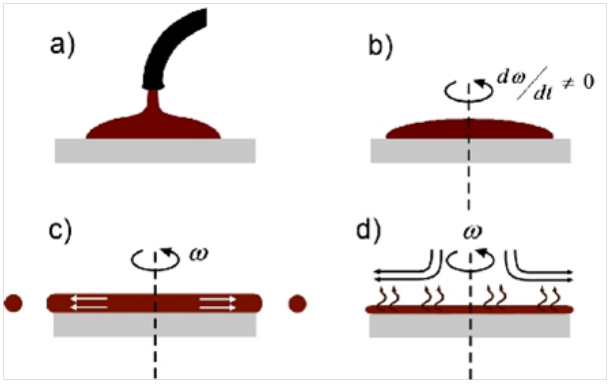

Figure A.2: Schematic of the spin coating process phases. [2]

The thickness of the material layer deposited by means of this procedure depends mainly on the rotation speed and time, and on the chemical and physical properties of the solvent contained in the deposited fluid [3][1]. In present work spin coating has been used to deposit some semiconductor-based solution on inkjet printed OFETs and to treat PEDOT:PSS-based OECTs with Ethylene Glycol.

Dielectric deposition

Chemical Vapour Deposition (CVD) of parylene

The dielectric layer of all OFETs presented in this thesis has been realized by means of Chemical Vapour Deposition (CVD) of parylene C. A schematic of the CVD system used for the deposition of parylene is reported in Figure A.3. Before the process starting samples are located in the polymerization chamber and a small amount of material (generally a few grams) in form of solid dimer is placed inside the vaporisation chamber where a pressure of 1 torr is reached. As the temperature in the vaporisation chamber is increased to 175 °C, the dimer starts to sublimate reaching the pyrolysis chamber, in which a pressure of 0.5 torr and a temperature of 680 °C are kept. This high temperature converts the dimer to monomer phase. Once reached the polymerization chamber (kept at RT and 0.1 torr), the monomers begins the process of polymerization by means of the formation of covalent bonds between each other. When the polymeric chains become long enough, they deposit on the substrate under the action of gravity. The result of the process is a conformal coating of parylene on the samples, whose thickness essentially depends on the amount of dimer used.

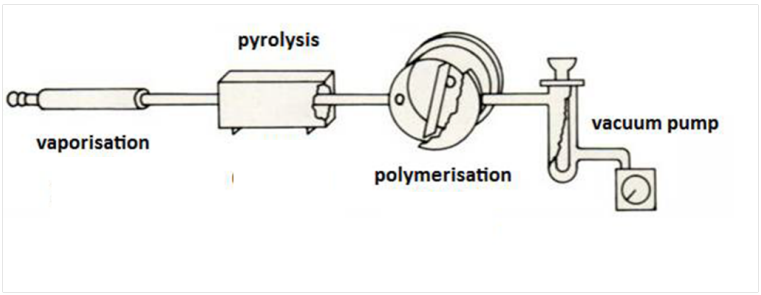

Figure A.3: Schematic of the CVD system for the deposition of parylene.

Bibliography

[1] W. S. Wong, A. Salleo, *Electronic materials: science & technology*, Springer,**2009**. ISBN:0387743626. 172

[2] S. L. Hellstrom *Basic Models of Spin Coating*, **2007**, coursework for Physics 210, Stanford University. 172

[3] R.W. Kelsall, I.W. Hamley, M. Geoghegan, *Nanoscale science and technology*, JohnWiley & Sons, **2005**. ISBN: 0470850868. 172

Acknowledgements

First of all, I'd like to thank my advisor Prof. Annalisa Bonfiglio for giving to me the possibility to live the hard but exciting and unforgettable experience of getting a doctorate and for all the things she taught me over these three years.
I'm very grateful to my co-advisor Dr. Piero Cosseddu, who has supervised my work each single day and who has been able to be my boss and my friend at the same time.
I would also like to thank all my colleagues: Giorgio, Stefano, Alberto, Andrea, Monia and Giulia, for the support, encouragement, care, love they gave to me.
A special thanks to Prof. Beatrice Fraboni, for her important support to my research activity and her kindness.
A big thank you to all other people with which I collaborated during these years: Dr. Silvia Milita, who performed the XRD measurement, Prof. George Malliaras for his fruitful advices and discussions in the field of organic electrochemical transistors, Prof. Giorgio Cannata and Prof. Maurizio Valle for the work done together concerning the ROBOSKIN project.
Thanks to Laura, Daniela and Omar, my dearest friends here in Sardinia, I will miss them so much!
Thanks to Nicola, which has made my life better by the day that I met him.
Last but not least, thanks to my Mum, my Dad, and my sister Chiara, without whom I would never become who I am today.